Methodological Developments towards Quantitative Short TE *in vivo* ^{1}H NMR Spectroscopy without Water Suppression

DISSERTATION
Zur
Erlangung des Grades eines
Doktors der Naturwissenschaften
- Dr. rer. nat. -

dem Fachbereich 2, Biologie/Chemie
der Universität Bremen
vorgelegt von

Zhengchao Dong

Juli 2002

Gutachter der Dissertation:	Prof. Dr. Dieter Leibfritz Prof. Dr. Wolf-Dieter Stohrer
Tag des öffentlichen Kolloquiums:	15.08. 2002
Beisitzer der Prüfung:	Prof. Dr. Franz-Peter Montforts Dr. Wolfgang Dreher

Contents

Abbreviations and Symbols

Abbreviations

ADC: Analog-to-digital converter

ACQ: Acquisition

AMARES: Advanced method for accurate, robust and efficient spectral fitting

Asp: Aspartate

a.u.: Arbitrary unit

CHESS: Chemical selective saturation

Cho: Choline

Cr: Creatine

CRLB: Cramer Rao lower bound

CV: Coefficient of variation

CWT: Continuous wavelet transformation

dB: Decibel

DWT: Discrete wavelet transformation

FFT: Fast Fourier transformation

FID: Free induction decay

FWHM: Full width at half maximum

FM: Frequency modulation

GABA: γ-aminobutyric acid

Glc: Glucose

Gln: Glutamine

Glu: Glutamate

Glx: Glu + Gln

GSH: Glutathione

Ins: Myo-inositol

ISIS: Image-selected *in vivo* spectroscopy

IWT: Inverse wavelet transformation

LCModel: Linear combination model

LPSVD: Linear prediction singular value decomposition

MC: Monte Carlo study

mM: Millimole

MPM: Matrix pencil method

MRI: Magnetic resonance imaging

MRS: Magnetic resonance spectroscopy

MRSI: Magnetic resonance spectroscopic imaging

NA: Number of accumulations

NAA: N-acetylaspatate

NAAG: N-acetylaspartylglutamate

NMR: Nuclear magnetic resonance

PCr: Phosphocreatine

PE: Phosphorylethanolamine

PPM: Parts per million

PRESS: Point resolved spectroscopy

QUALTY: Quantification improvement by converting lineshapes to the Lorentzian type

RF: Radio frequency

SD: Standard deviation

SNR: Signal-to-noise ratio = 20log(Signal amplitude/SD of noise) (in dB)

STEAM: Stimulated echo acquisition mode

SVD: Singular value decomposition

SW: Spectral width

T: Tesla

Tau: Taurine

TE: Echo time

TR: Repetition time

VARPRO: VARiable PROjection method

WS: Water suppression

WT: Wavelet transform

WTC: Wavelet transform coefficient

w.w.: Wet weight

Symbols

A, a: Signal amplitude

$B_m(t)$: Time domain model signal of metabolite m

B_0: External magnetic field

C: Concentration

M: Macroscopic magnetization

N, n: Number of spins in the group or in the compound

$\Re$: Real number

S: NMR signal

T_1, T_2: Spin-lattice and spin-spin relaxation times

$\Delta\alpha$: Difference of Lorentzian decay rates between the model signal and the *in vivo* signal

$\Delta\beta$: Difference of Gaussian decay rates between the model signal and the *in vivo* signal

$\Delta\omega$: Frequency difference between the model signal and the *in vivo* signal

$\Delta\varphi$: Zero order phase difference between the model signal and the *in vivo* signal

γ: Gyromagnetic ratio

σ: Standard deviation of noise; shielding constant of orbiting electrons

ω_0: Larmor frequency

ψ: Mother wavelet

Introduction

Since the first *in vivo* magnetic resonance (MR) spectroscopy (MRS) performed some two decades ago, *in vivo* MRS has proven to be a unique versatile and non-invasive technique in biochemical and biomedical studies and clinic diagnosis. The first *in vivo* MRS was performed on ^{31}P [Gord80] [Grif80], but now the technique is used for ^{1}H, ^{31}P, ^{13}C, ^{19}F, ^{23}Na and other nuclei, among which ^{1}H MRS predominates because of the highest natural abundance of protons in human body and the highest NMR detectability, and also due to the wealthy amount of information contained in ^{1}H MRS.

Different from MRI [Laut73], which provides an anatomical map of the normal and pathological distribution of water and fat, MRS provides spectra of compounds in the humans and animals. The potential of *in vivo* MRS is that it can non-invasively detect the concentration of metabolites in the subject. Therefore, accurate and reliable quantification of the MRS is crucially important for the developments and the applications of *in vivo* MRS.

In the past decade or so, various methods have been developed to quantify *in vivo* MRS, with algorithms ranging from simple spectral peak integration to sophisticated parametric non-linear spectral fits, and with different degrees of success. Some of the methods are the Maximum Likelihood method (ML) [Prie81], the Linear Prediction Singular Value Decomposition method (LPSVD) [Bark85a][Kölb92], the Variable Projection method (VARPRO) [Veen88] and the Advanced Method for Accurate, Robust and Efficient Spectral fitting (AMARES) [Vanh97], Linear Combination of Model spectra (LCModel) method [Prov93], and the Wavelet Transform (WT) based method [Serr97], to name just a few. Some recent review articles are found in [Krei97], [Mier01] and [Vanh01].

Although proton MRS is the most popular, widely used and extensively investigated *in vivo* NMR technique, it is also the most difficult to quantify because of the intrinsic complexities associated with it. The *in vivo* proton MRS have all the common problems of *in vivo* MRS, such as low signal-to-noise ratio, lineshape distortion, spectral overlapping and baseline distortion, among which the latter two are more pronounced with short TE (echo time) ^{1}H

MRS. For instance, the ^{1}H MR spectra of human brain consist of more than 20 NMR detectable compounds crowded in a spectral region of about 4 ppm. Short TE *in vivo* ^{1}H MRS features a well structured baseline from macromolecules and lipids. The unique feature of *in vivo* ^{1}H MRS is the dominant water signal which is 3 to 5 orders of magnitude larger than metabolite signals. The dominant water signal constitutes serious problems to *in vivo* ^{1}H MRS: (i) it is the source of strong artifacts severely distorting the baseline, which can be larger than the metabolite signals, making reliable spectral analysis and estimation impossible; (ii) its broad resonance line extends far into the spectral region of interest making the spectral post-processing a challenging task; (iii) the large dynamic range of the signal means demanding requirements both for hardware data acquisition and software signal quantification. Therefore, water suppression (WS) technique, which saturates water signal prior to data acquisition, is traditionally used as a routine in *in vivo* ^{1}H MRS to avoid these problems.

However, WS has several disadvantages [Hurd98] [Dong00a]: (i) Signals with small chemical shift differences to water are also partially suppressed; (ii) Some WS methods may cause magnetization transfer effects to metabolites and thus cause systematic quantification errors; (iii) RF pulses used for WS increase the total RF power deposition and require additional adjustments; (iv) Additional measurements are necessary, if water is used as an internal reference for absolute quantification; (v) Spoiler gradients pulses increase the acoustic noise level.

Because of this, *in vivo* proton MRS acquired without WS has attracted increasing attention in recent years. Efforts have been made to address these difficulties in order to measure and quantify *in vivo* ^{1}H MRS acquired without WS [Hurd98] [Veen00] [Dong00a,b, 02][Clay01][Serr01a]. However, to the best knowledge of the author, until now only 3 metabolites with prominent singlets, namely NAA (3.01 ppm), tCr (3.04 ppm) and tCho (3.24 ppm), could be quantified by Matrix Pencil (MPM) based method (Dong00b), singular value decomposition (SVD) based method [Clay01] and wavelet transform (WT) based method [Sarr01], performed on spectra acquired at TE's > 40 ms [Dong00b] and TE = 288 ms [Clay01], [Serr01a].

The objective of this thesis is the methodological developments to quantify short TE *in vivo* ^{1}H MRS acquired without WS. A fast, automatic, robust and accurate quantification method was developed, which combines experimental approaches, prior knowledge and sophisticated software algorithm to tackle the common problems of *in vivo* ^{1}H MRS and the special

problems associated with MRS acquired without WS. The method is able to quantify more than 10 metabolites from signals acquired on a 4.7 Tesla spectrometer and with TE = 20 ms. This method can also be used to quantify signals acquired with WS.

The thesis is structured as follows:

Chapter 1 gives a brief introduction to the basics of NMR and *in vivo* proton MRS, in which the topics closely related to the present work, such as the basic principle of localization and the metabolite MR spectra, are introduced and reviewed.

Chapter 2 describes the general aspects of spectral quantification including the common problems, preprocessing approaches and quantification strategies. Some of the well established and widely used quantification methods are also briefly reviewed. This chapter sets the direction and the goal, the reference and the benchmark for the new method developed in chapter 3.

Chapter 3 is devoted to the methodology developments towards quantitative short TE *in vivo* ^{1}H NMR spectroscopy without WS. The main scheme of the method is to integrate the metabolite spectral prior knowledge, experimental techniques and software approaches in the quantification to treat the difficulties associated with the short TE *in vivo* ^{1}H MRS acquired without WS. Full prior knowledge of chemical shifts and J-coupling constants of the metabolites are used to obtain the model signals, which are incorporated in the spectral fitting. The experimental approaches eliminate the first order phase errors and the frequency modulation artifacts caused by gradient pulses. The software approaches employ sophisticated water signal extraction technique, spectral simulation technique, WT technique and non-linear least squares technique to overcome the problems of large signal dynamic range, severe spectral overlapping and heavy baseline distortion, and to accurately fit the signal. This method can be represented by the acronym of "metabolite **S**ignal **P**rior knowledge and **E**xperimental approaches **C**ombined spectral **F**itting **I**n the **T**ime domain (**SPECFIT**)".

After an introduction to this chapter, Section 3.2 describes the MPM based parametric spectral fitting scheme including water signal extraction, spectral zoom and lineshape transformation. This method is shown to have a high frequency resolution, to be good at signal separation and to be able to accurately estimate signals with large dynamic range. It can be used as an independent method to quantify metabolites with prominent singlets from *in vivo* MRS acquired at medium and long TE's [Dong00b][Alth02]. In this thesis its advantages with respect to water signal extraction and lineshape transform are used as a part of SPECFIT for quantification of short TE *in vivo* ^{1}H MRS in Section 3.7.

Sections 3.3 and 3.4 describe the experimental approaches to eliminate first order phase errors and frequency modulation (FM) artifacts caused by gradient pulses. The former can limit the first order phase errors to within 0.5 degree in the spectral range of interest, while the latter can perfectly eliminate the FM artifacts associated with ^{1}H MRS without WS, resulting in virtually artifact-free spectrum comparable to the intrinsically artifact-free one with WS. These approaches greatly improve the quality of the spectra and improve the performance of the spectral fitting.

Model spectra of the metabolites are used in the spectral fitting, which are obtained by spectral simulation instead of phantom measurements. Section 3.5 describes the simulation technique using the GAMMA (General Approach to Magnetic resonance Mathematical Analysis) [Smith94], a C++ library facilitating the simulation of NMR experiments.

Baseline characterization is performed by WT technique with a scheme initiated by Young et al [Youn98]. In section 3.6 the discrete WT (DWT) is briefly introduced as it is relatively new to the NMR community and the basic properties of DWT and the principles behind the DWT based baseline characterization and signal denoising are exploited.

Section 3.7 is devoted to the SPECFIT spectral fitting scheme. In the first three subsections the model function, the spectral fitting algorithm and its implementation are introduced. The SPECFIT method is evaluated and validated in the next two subsections by Monte Carlo studies and phantom experimental data under various conditions. Applications of the method to *in vivo* ^{1}H MRS acquired from rat brains at short TE without WS are given in Section 3.7.6. Intra-individual and inter-individual results are presented and compared with the literature values. Factors affecting the performances of the method are discussed.

Chapter 4 contains the discussions and an outlook.

1 Basics of *in vivo* ^{1}H MRS

The *in vivo* MR spectra provide wealthy information on the metabolites of the subject, including the structures and the concentrations of the metabolites and their interactions with the environments. This property of the *in vivo* MRS makes it a versatile and unique technique of *in vivo* biochemical and biomedical studies and a potential non-invasive tool of clinical diagnosis.

The information of *in vivo* MRS is reflected by the parameters of *in vivo* MR spectra: the amplitudes, frequencies and relaxation rates of the resonance lines. The objective of quantification of *in vivo* MRS is to determine the concentrations of metabolites from the amplitudes of the corresponding components of MR signal. Other parameters also influence the accuracy of the quantification. In this chapter, the basic aspects concerning the characteristics and quantification of *in vivo* ^{1}H MRS are reviewed.

1.1 Bloch equation and relaxation

The object of NMR is nuclear macromagnetic momentum ***M,*** which is the vector sum of the micromagnetic momentums of nuclear spins in the sample volume. Bloch [Bloc46] proposed an equation, the Bloch Equation, which is the basic equation of NMR, to describe the motion of magnetic momentum in a magnetic field. The Bloch equation is given as,

$$\frac{d}{dt}\boldsymbol{M} = \gamma \boldsymbol{M}\times\boldsymbol{B} - \frac{(M_x - M_x^0)}{T_2}\boldsymbol{i} - \frac{(M_y - M_y^0)}{T_2}\boldsymbol{j} - \frac{(M_z - M_z^0)}{T_1}\boldsymbol{k} \qquad \text{Eq. 1.1-1}$$

The first term of the equation describes the action of magnetic fields on the magnetic momentum. If the magnetic field is static, that is $\boldsymbol{B} = \boldsymbol{B}_0$, which is in the z direction, the above equation has an analytical solution, called the stationary solution. Suppose, the system is initially in the thermal equilibrium state, that is, $M_{x,y}^0 = 0, M_z^0 = M_0$, then Eq.1.1-1 gives

$$M_{x,y} = 0, M_z = M_0 . \qquad \text{Eq. 1.1-2}$$

When an RF field $2\boldsymbol{B}_1\cos(\omega t)$ is applied along the x direction superimposed on $\boldsymbol{B}_0$, the linearly polarized RF field can be decomposed into two circularly polarized RF fields with opposite angular frequencies ω and -ω. Given that $\omega \approx \omega_0$, where ω_0 is the Larmor frequency, it is shown that only the right hand circular polarized field has significant effects on the magnetic momentum. The total effective field is given by,

$$\begin{aligned} \boldsymbol{B} &= \boldsymbol{B}_0 + 2\boldsymbol{B}_1\cos\omega t \\ &= (\boldsymbol{B}_1\cos\omega t, \boldsymbol{B}_1\sin\omega t, \boldsymbol{B}_0). \end{aligned} \qquad \text{Eq. 1.1-3}$$

The effect of RF field is best illustrated in the rotating frame of reference with angular frequency ω around z. In this case, the total effective field reads,

$$\boldsymbol{B} = (B_1, 0, B_0 - \frac{\omega}{\gamma_I}) \qquad \text{Eq. 1.1-4}$$

Fig.1.1-1 illustrates the effective total field $\mathbf{B}_{eff}$ and its effect on the magnetic momentum: **M** rotates around B_{eff}. On resonance, i.e. $\omega = \omega_0$, $B_{eff} = B_1$, M rotates around B_1 with angular frequency $\omega_1 = \gamma_I B_1$. If the duration of RF field B_1 is t_p, termed the RF pulse width, the flip angle is given by,

$$\alpha = \gamma B_1 t_p . \qquad \text{Eq. 1.1-5}$$

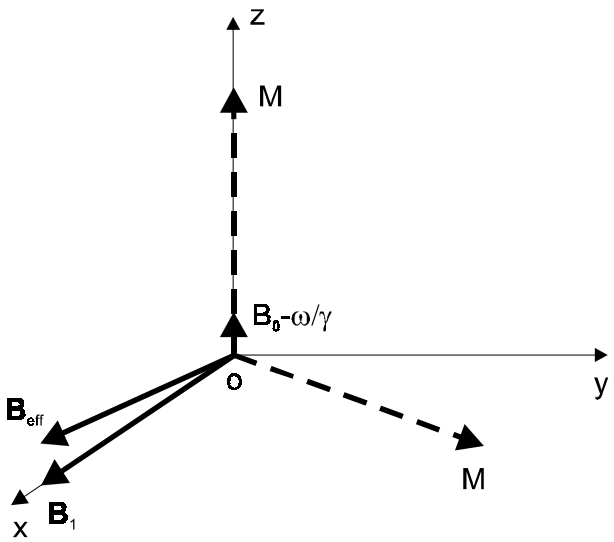

Fig.1.1-1 Effects of total magnetic field B_{eff} in the presence of RF field B_1.

A 90^0 pulse ($\alpha = 90^0$) turns the magnetization to the x-y plane, and a 180^0 pulse tilts M to –z. This equation holds true for $B_1 >> (B_0 - \omega/\gamma)$. A square RF pulse with central frequency ω_0 and width t_p will effectively excite spins in the frequency range of $\omega_0 \pm 1/t_p$. Usually RF pulses with specially designed shapes are needed to obtain desired excitation profiles.

T_1 and T_2 in Eq.1.1-1 represent two different relaxation mechanisms termed spin-lattice relaxation time or longitudinal relaxation time and spin-spin relaxation time or transversal relaxation time, respectively. The spin-lattice relaxation returns the magnetization to the thermal equilibrium state through energy exchange between spins and their environments. While the spin-spin relaxation dephases the coherence between the spins established by the RF pulse, causing the transverse component M_{xy} to vanish. Field inhomogeneity also contributes to the transverse relaxation, causing the effective transversal relaxation time T_2^*. Relaxation rates are important parameters of MRS, as they reflect the interaction of spins with their environment and the dynamic characteristics of the molecules, and influence the amplitudes and decays of the time domain signals or equivalently determine the linewidths and the intensities of the spectra.

1.2 Chemical shifts and spin–spin coupling

The nuclear resonance frequency is determined by the gyromagnetic ratio γ of the nucleus and the magnetic field that the nucleus experiences. Shortly after the discovery of NMR, it was found [Proc50] that a nucleus experiences not the external magnetic field only, but the combination of the external field and the internal field, which is induced by the external field and is related to the electron density around the nucleus. It is this property that makes NMR the unique technique that detects the local and microscopic properties of a molecule.

The field experienced by the nuclear spins inside the molecule is [Call93] [Abra60],

$$B = B_0(1-\sigma), \qquad \text{Eq. 1.2-1}$$

where σ is the shielding constant of the orbiting electrons, which is a scalar for liquid state sample and for *in vivo* MRS. The Larmor frequency of a spin j in a multispin system is then given by,

$$\omega_j = \omega_0(1-\sigma_j)\,. \qquad \text{Eq. 1.2-2}$$

This frequency is referred to as chemical shift of the spin. In practice, chemical shift is conventionally expressed in a scale that is independent of the external field and is defined, in the unit of parts per million (ppm), as,

$$\delta = \frac{\omega_j - \omega_r}{\omega_r} \times 10^6 \qquad \text{Eq. 1.2-3}$$

where ω_r is the reference frequency. In ^{1}H and ^{13}C NMR, the compound tetramethylsilane (TMS) is conventionally used as a reference, whose chemical shift is assigned 0. In *in vivo* proton MRS, the spectral range is typically from 0 to 4 ppm.

Another important phenomenon in liquid state and in *in vivo* proton MRS is the splitting of resonances caused by the indirect spin coupling, commonly referred to as spin-spin coupling or J-coupling [Erns87]. The J-coupling is the interaction between spins I and S conveyed by the electrons around the nuclei. The Hamiltonian of a two-spin system with J-coupling reads [Erns87],

$$H = -\gamma B I_z - \gamma B S_z + J_{IS}\vec{I}\cdot\vec{S} \qquad \text{Eq. 1.2-4}$$

The J-coupling constant is independent of the external field and therefore given in Hz. Typical values of ^{1}H-^{1}H J-coupling constants are in the range of 1 – 20 Hz. The effect of J-coupling is to cause the resonance line to split. For the simplest case, where two 1/2 spins are weakly coupled, i.e. $|\omega_I - \omega_S| >> J_{IS}$, both singlets of the non-coupled spins at ω_I and ω_S are split into doublets of equal amplitude at $\omega_I \pm J_{IS}/2$ and $\omega_S \pm J_{IS}/2$. In multispin system, scalar coupling may occur between each pair of spins. Take a three-spin system AMX as an example, where there are J-couplings between AM and MX, but no coupling between AX. In this case, resonances of A and X are both doublets and resonances of M are "doublets of doublets". For strong coupling, where $|\omega_I - \omega_S| \sim J_{IS}$, and multispin system, the splitting of resonance lines is more complicated. This is just the case of most *in vivo* proton MR spectra. In spin echo experiments the spectra of J-coupled system are more complicated because of the evolution of transverse magnetization under the scalar coupling interaction. Fig.1.2-1 shows the spectral patterns of Glu at different TE's. J-coupling induced line splitting and J-evolution make the quantification of MRS a challenging task. For some parametric spectral estimation methods, only uncoupled lines can be fitted. Some J-coupled lines, such as those of GABA and lactate, can be separated from uncoupled lines, by using the J-difference spectral editing

and multiple-quantum coherences based spectral editing techniques [Graa01], but this technique only benefits the detection and quantification of the specific metabolites concerned. A more general solution to the problem of resolving the J-coupled and overlapping spectral lines is utilizing the *in vitro* model spectra of pure metabolite solutions acquired under the same conditions as the *in vivo* spectra to be quantified, as used in LCModel [Prov93] and in [Bart99]. In the present work, instead of by measuring the *in vitro* spectra, the model spectra are obtained by spectral simulation with the help of an object-oriented C/C++ library GAMMA [Smit94], which was designed to simulate NMR spectra.

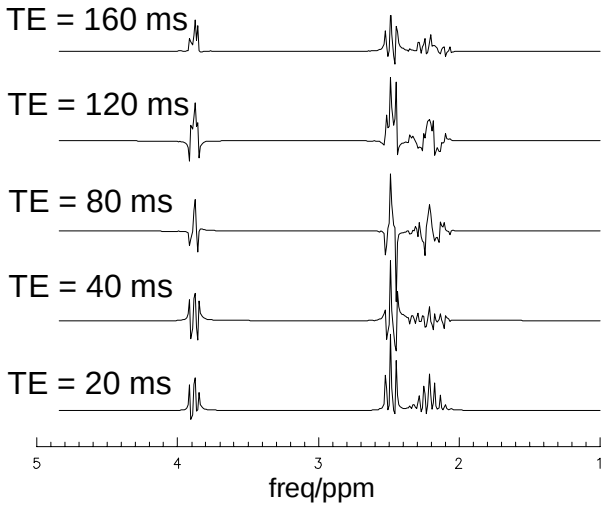

Fig.1.2-1 Glutamate spectra at different TE's, simulated with the help of GAMMA [Smit94], a C++ library for NMR spectral simulation. Note the different patterns of the spectra at different echo times due to the J-coupling.

1.3 Localized NMR

Non-localized NMR is inappropriate for *in vivo* biochemical and biomedical applications due to several reasons. (i) Non-localized NMR spectra are mixtures of signals stemming from the whole object under investigation, which is spatially inhomogeneous in terms of metabolite composition and biological structures. Therefore, it is impossible to assign resonance lines to their spatial origins and/or to interpret the lines from the non-localized spectrum. (ii) The non-localized NMR spectral lines are broad due to inhomogeneous biological structures and the metabolite composition of the objects. The spectrum suffers from severe line-shape and baseline distortions, and much information is lost due to spectral overlapping. (iii) Inhomogeneity of B_0 over a large volume further broadens the line-width, thereby reducing

the spectral resolution. (iv) In the case of ^{1}H NMR, broad water resonance lines are difficult to suppress and large spectral residues will cause spectral distortion and contamination.

On the other hand, localized NMR can offer high quality spectra from a selected location or tissue that resemble most the high resolution liquid state NMR spectra, thus facilitating *in vivo* biochemical and biomedical studies.

1.3.1 Principle of localization

Localized NMR or spatially encoded NMR is achieved by superimposing magnetic gradient fields on the static field $\mathbf{B}_0$.

Consider a superposition of B_0 and a gradient field $\mathbf{G}_x$ in x direction. The resultant magnetic field **B** is thereby spatially dependent and is given by

$$\mathbf{B}(x) = \mathbf{B}_0 + x\,\mathbf{G}_x \qquad \text{Eq. 1.3-1}$$

Correspondingly, the Larmor frequency is also spatially dependent and reads,

$$\omega = \gamma(\mathbf{B}_0 + x\,\mathbf{G}_x) \qquad \text{Eq. 1.3-2}$$

Let the gradient field be constant over the sample, and the signals from the sample are hence spatially encoded, in x direction, in this case, by

$$\Delta\omega = \Delta x \cdot G_x \qquad \text{Eq. 1.3-3}$$

or

$$\Delta x = \Delta\omega / G_x \qquad \text{Eq. 1.3-4}$$

where $\Delta\omega$ denotes the frequency difference of resonance from the two volume elements and Δx represents the spatial separation of the two volume elements in x direction.

To encode the signal in 3D space, the following gradient is needed,

$$\mathbf{G} = \mathbf{G}_x + \mathbf{G}_y + \mathbf{G}_z \qquad \text{Eq. 1.3-5}$$

where

$$\mathbf{G}_n = \partial \mathbf{B}_z / \partial n \cdot \mathbf{n} \qquad \text{Eq. 1.3-6}$$

and **n = i, j, k** are unit vectors in x, y, and z directions, respectively.

The total magnetic field and Larmor frequency are given, respectively, by

$$\mathbf{B}(\mathbf{r}) = \mathbf{B}_0 + \mathbf{r} \cdot \mathbf{G} \qquad \text{Eq. 1.3-7}$$

and

$$\omega(\mathbf{r}) = \gamma(B_0 + \mathbf{r} \cdot \mathbf{G})$$

$$= \gamma(\mathbf{B_0} + \mathbf{xG_x} + \mathbf{yG_y} + \mathbf{zG_z}). \qquad \text{Eq. 1.3-8}$$

For a given gradient field **G**, Eq.1.4-7 in principle determines the relation between a volume element located in (x, y, z) and the resonance frequency of the volume element $\omega(\mathbf{r})$. However, a close examination of the equation reveals that $\omega(\mathbf{r})$ is determined by the combination of xG_x, yG_y, and zG_z, therefore, $\omega(\mathbf{r})$ may correspond to more than one volume elements. In order to establish a unique relation between the location of a volume element and the resonance frequency, special localization schemes are developed based on the principle outlined above, frequency selective RF pulses and the time encoding technique as used in the 2D NMR. Many localization methods have been developed in recent years, such as PRESS (**P**oint **RES**olved **S**pectroscopy) [Bott84] [Ordi85], STEAM (**ST**imulated **E**cho **A**cquisition **M**ode) [Frah87] and ISIS (**I**magine **S**elected ***In vivo*** **S**pectroscopy) [Ordi86]. In the next sections, slice selection method and PRESS localization sequence, which is used in the present work, are described in some detail.

1.3.2 Selective excitation

Selective excitation is important with respect to MRS, MRSI and MRI, as it allows localization in combination with magnetic field gradients. Selective excitation refers to applying shaped RF pulses to excite only a specific frequency region. In other words, only those spins whose Larmor frequencies fall in the profile of the RF pulse spectrum are affected with a selective excitation. The principle of selective excitation by RF pulses can be understood by Fourier transform theory: a time domain RF pulse and its frequency domain excitation profile constitute a Fourier transform pair. The shapes and durations of RF pulses determine the excitation profiles and bandwidths. An ideal δ function like infinite RF pulse has excitation profile covering the whole frequency range. In conventional NMR, hard RF pulses with very strong intensities and very short durations are used commonly, in order to obtain sufficiently wide excitation profiles so that all spins in the sample can be stimulated as uniformly as possible. These RF pulses are referred to as non-selective RF pulses. Soft RF pulses with smaller intensities and longer durations are also used to selectively excite certain chemical shift range, as used in the solvent suppression. In MRS and MRI, soft RF pulses are used both to excite only a specific chemical shift range, as used in water suppression (WS) [Haas85] [Dodd86], and to stimulate some narrow slices in the sample in combination with

the magnetic field gradients which are strong enough to spread the Larmor frequencies of the sample to a width larger than the excitation bandwidth. The soft RF pulse, however, has a narrow and shaped central excitation profile with side lobes, which have several disadvantages: (i) The side lobes will induce unwanted signals from outside of the selected chemical shift region or from outside of the desired slice; (ii) Spins whose resonance frequencies corresponding to the main lobe are not uniformly excited. To obtain better excitation profiles, specially designed shaped RF pulses are used instead of the simple soft RF pulse. Two of these RF pulses, namely Gaussian pulse and sinc pulse, are commonly used.

1.3.3 Slice selection

The basic procedure in the localized NMR is to selectively excite a thin slice in the sample by applying a magnetic field gradient, which is normal to the slice, together with a frequency selective RF pulse. In doing so, two parameters should be considered: the position of the slice and the thickness of the slice. The former is determined by the magnetic field gradient strength and the frequency of the RF pulse. The latter is determined by the magnetic field gradient strength and the excitation bandwidth of the RF pulse.

Consider a magnetic field gradient in the Z direction, superimposing on the static field $\mathbf{B}_0$. The Larmor frequency is given by,

$$\omega(z) = \gamma(B_0 + z \cdot G_z) \qquad \text{Eq. 1.3-9}$$

which is a function of z position. If an RF pulse with infinite duration, which has infinite excitation spectral range, is applied, the whole sample will be excited. To excite a slice centered on $z = z_0$, a specially designed frequency selective RF pulse must be applied in the presence of the magnetic field gradient. In general, a square RF pulse with finite duration has a finite excitation band in frequency domain and the longer the duration of the RF pulse, the narrower of the excitation bands. To achieve a desired excitation profile, shaped RF pulse should be used. According to Fourier transform theory, a squared excitation profile can be achieved by applying a sinc-shaped RF pulse. Fig.1.3-1 shows schematically the principle of slice selection scheme.

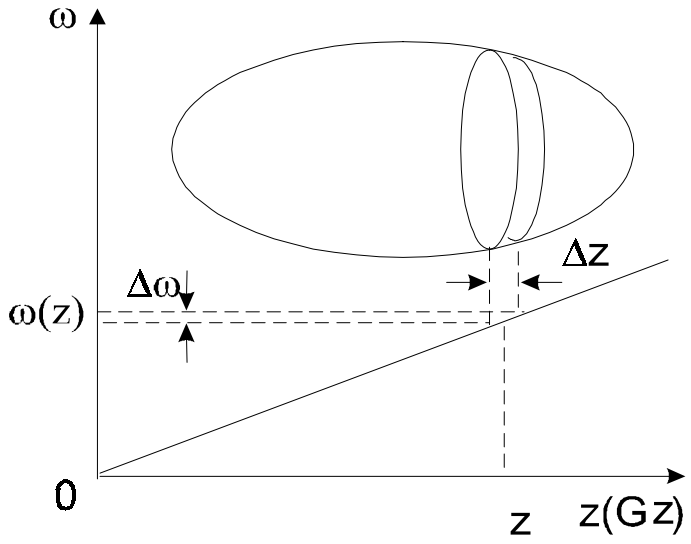

Fig.1.3-1 The principle of slice selection scheme. In the presence of the magnetic filed gradient a RF field with a narrow frequency range $\Delta\omega$ around $\omega(z_0)$ is applied. According to Eq.1.3-2, only a slice of thickness of Δz around z_0 satisfies the resonance condition and thereby is excited. In the figure, the slice is perpendicular to the magnetic field gradient which is in Z direction. As a matter of fact, with a combination of field gradients in three independent directions, a slice with any orientation can be selected.

As can be seen from Fig.1.3-1, for a given strength of magnetic gradient field, the thickness of the slice is proportional to the excitation band width of the RF pulse. On the other hand, according to Eq.1.3-4, for a given RF pulse with excitation band width of $\Delta\omega$, the slice thickness is inversely proportional to the strength of the magnetic field gradient.

The slice selection scheme plays an important role in localized NMR and MRI in shortening the total measurement time. Suppose, one wants to image a 3D object with n^3 voxels. If each voxel is measured independently, n^3 measurements are needed which is very time consuming. With slice selection scheme, it is possible to measure all n^2 voxels in the slice simultaneously achieving the so called “planer imaging”[Mans77][Mans78].

1.3.4 Point resolved spectroscopy (PRESS)

The PRESS localization sequence [Bott84] is shown in Fig.1.3-2.

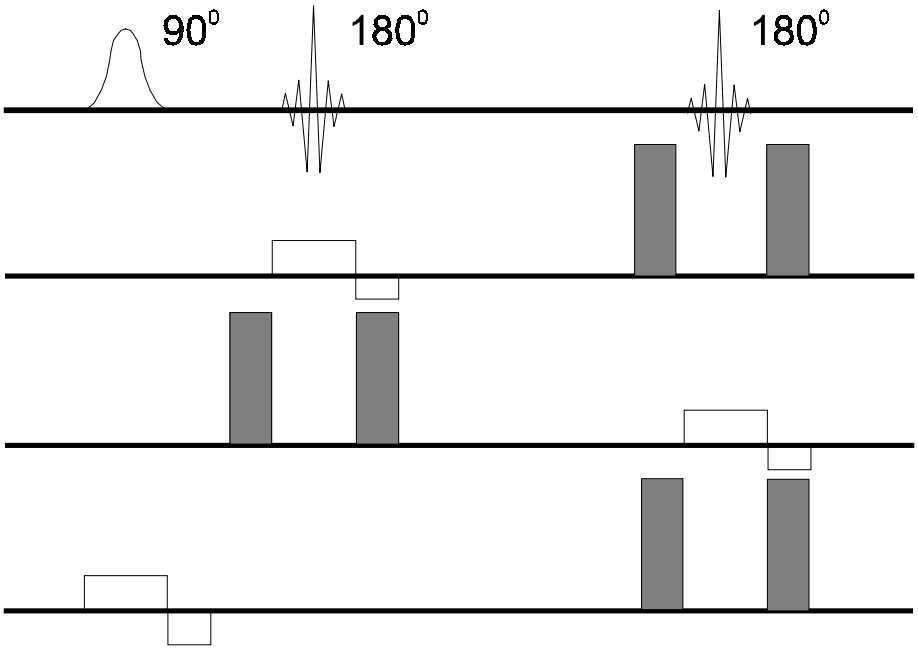

Fig.1.3-2 PRESS sequence. The gradients in shade are spoilers and the in solid lines are the slice selective and the refocusing gradients.

The slice selective 90^0 excitation pulse in the presence of the G_z gradient tilts the magnetization into the transverse plane and two slice selective 180^0 pulses refocus the transverse magnetization at TE. Each slice selective gradient pulse is followed by a refocusing gradient pulse to cancel the dephasing effect of the slice selective gradients. In short TE experiment, acquisition starts at the maximum of the echo and samples the second half of the echo as FID. In long TE experiment, the whole echo can be sampled.

Spoiler gradients are used to crush the unwanted signal coherences, i.e. the coherence pathways of spins from outside of the voxel selected by the three slice selective pulses, by dephasing the spin magnetization. Spoiler gradients, on the other hand, are the main sources of acoustic noises, eddy current effects and time variant magnetic field modulations [Wu00], which can cause lineshape and baseline distortions or sideband artifacts if water is not suppressed. It is therefore desirable to adjust the strength and duration of the spoiler gradients and to optimize the waveform of the spoiler gradients [Henn99] to effectively suppress the "ghost" signals from outside of the voxel and produce minimum side effects at the same time. Some approaches to optimize PRESS pulse sequence are discussed in Chapter 3 in connection with the removal of the so-called frequency modulation sidebands of unsuppressed water signal caused by gradient pulses [Clay99, Dong02].

The echo time (TE) is an important parameter of PRESS sequence with respect to quantitative ^{1}H MRS. Short TE gives rise to higher SNR and less information loss of the spectrum than the long TE. However, the short TE spectra suffer from severe baseline distortion which makes spectral quantification more difficult. Also stronger spoiler gradients are required for shorter duration, which will lead to more pronounced lineshape and baseline distortions. For standard PRESS sequence the shortest possible TE is around 20 ms. But with asymmetric RF pulses, very short TE of some 6 ms has been achieved in our laboratory [Gepp01]. Defined TE's are often chosen to refocus some specific J splitting lines or to separate some overlapping spectra as used in J-difference spectral editing [Camp79]. For instance, TE = 144 ms is often used to refocus the doublet of lactate at 1.3 ppm.

The advantage of PRESS is its high SNR because signal losses are only caused by T_2 relaxation and J-modulation. To reach a sufficient SNR, signal accumulations are usually performed, accompanied by an 8 or a 16-step RF phase cycling to further suppress signals from outside of the voxel. Theoretically, an 8 or 16-step RF phase cycling can eliminate completely the unwanted signal from outside of the voxel [Henn84, Roel01]. In the present work, a 16-step phase cycling is used instead of spoiler gradients to reduce the frequency modulation artifacts caused by gradient pulses.

1.4 Proton MR spectroscopy

In the *in vivo* MR spectroscopy, proton is the most widely used nucleus for biomedical researches, clinical researches and clinical diagnostic routines. This is because that proton is the most sensitive nucleus for MRS and the most abundant nucleus in the human body. For example, the relative sensitivity of the proton signal of NAA is about 5000 times higher than the natural abundant C-13 signal of NAA [Lenk01]. However, on the other hand, short TE *in vivo* ^{1}H MR spectra is very complicated. This creates tough difficulties for the accurate quantification of ^{1}H MRS, which is mandatory for the application of MRS. To overcome these difficulties prior knowledge of metabolite MR spectra have been deduced and incorporated into variety of quantification methods. The quantification method developed in the present thesis makes use of the simulated model spectra that are based on the prior knowledge of spectral properties of the metabolites, such as the chemical shifts and J-coupling constants, and spectral multiplicities. In this section, the chemical properties and the NMR spectral

characteristics of pure compounds of main metabolites in brain are presented together with their clinical significance. The chemical shifts and J-coupling constants [Govi00] are given in the Appendix.

- Choline (Cho) and Phosphorylcholine (PCh)

The structures and MR spectral properties of Cho and PCh are given as follows:

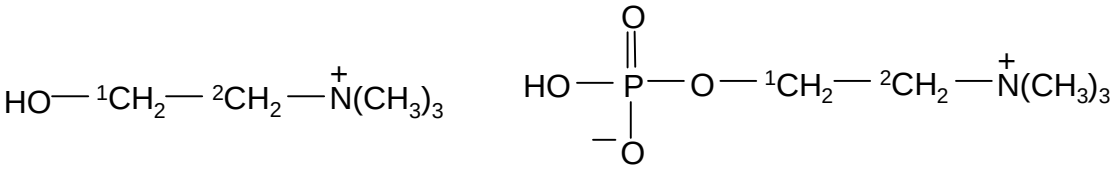

Cho and PCh have prominent singlets at about 3.20 ppm, which are difficult to resolve at a field strength of 4.7 T or lower. Therefore, both metabolites, together with acetylcholine, glycerophosphocholine, are referred to as choline containing compounds or total choline (tCh). Choline containing compounds have longer T_2 compared to other metabolites and can be observed and quantified at long TE. tCh resonances overlap partially with Tau. Even at TE = 144 ms, the overlapping at 3.20 ppm can still be observed in rat brain spectra, due to the high concentration of Tan (~ 6 mM) [Pfeu99]. Thus tCh may be overestimated if the quantification method can not resolve the overlapping lines. For human brain, the Tau levels are much lower (~ 1.5 mM) [Govi00], and the overlapping is less observable, but an overestimation can still result. Cho levels are increased in many tumor types.

- Creatine (Cr) and Phosphocreatine (PCr)

The structures and MRS properties of are given as:

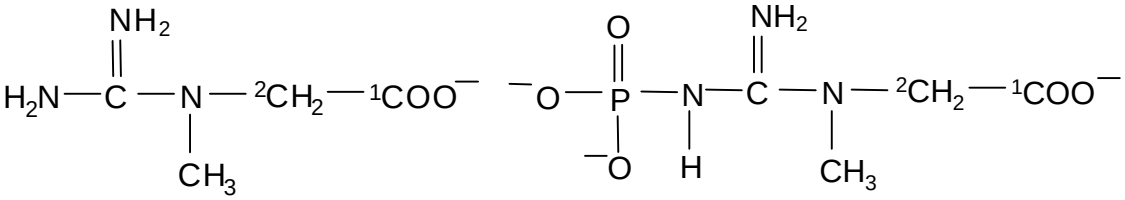

Both compounds are found in high concentrations in human brain and animal brain. They show prominent singlets in the high field region with respect to water and with very close chemical shifts. In high field *in vivo* MR spectra, resonances of Cr and PCr can be resolved [Pfeu99]. At a field strength lower than 7 T, Cr and PCr resonances cannot be resolved *in vivo.* Therefore, the sum of their concentrations is often interpreted and is denoted as total

creatine (tCr). Due to its high concentration and its prominent singlet at 3.03 ppm, tCr can be observed at long TE and is among the most widely investigated metabolites. For the same reason, tCr is often used as an internal reference for relative quantification. However, tCr levels have been shown to decrease in stroke, trauma and all tumor types [Ceci01] [Smit02]. In these pathological conditions, the relative concentration of the other metabolite with respective to tCr may lead to misinterpretation as an increase of the ratio may result from either a decrease of tCr or an increase of the other metabolite, or both.

- γ-Amino (GABA)

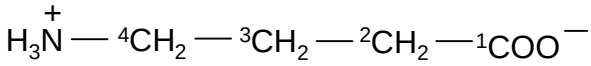

GABA is the reaction product of glutamate and the primary inhibitory neurotransmitter in the cerebral cortex [Roth00]. GABA concentration is relatively low, ~ 1.6 mM, and its spectra are J-split and overlap with the spectra of several metabolites such as NAA, and creatine, at 1.89, 2.38 and 3.01 ppm, respectively. Thereby, GABA is difficult to observe and to quantify *in vivo* with standard ^{1}H MRS. However, its spectra are refocused at TE about 100 ms, therefore, with spectral editing techniques it is possible to detect GABA [Graa01 and therein].

- Glutamate (Glu):

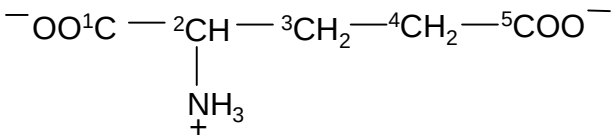

Glutamate has a high concentration in animal and human brains of about 10 mM, comparable to that of NAA. However, due to J-coupling, its resonance lines are split, making glutamate difficult to observe and to quantify, especially at low field, when spectra of glutamate, glutamine and NAA strongly overlapped. Pfeuffer et. al. [Pfeu99] showed that at high field and with short TE, glutamate and glutamine can be separated and thereby reliably quantified. At TE = 100 ms, the resonances at 2.35 ppm are refocused [Graa98], therefore it may be possible to observe them by means of spectral editing. Glutamate is a neurotransmitter in the central nervous system and is the most abundant amino acid in the human brain.

- Glutamine (Gln):

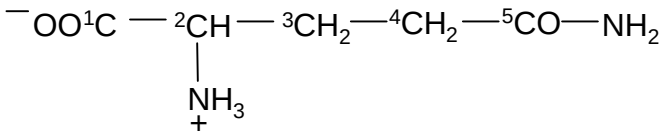

Glutamine has resonances from 2.13 ppm to 2.45 ppm and a relatively high concentration of 3 to 6 mM in human brain. For the same reason as Glu, Gln is difficult to detect and quantify and therefore Gln and Glu are usually referred to as Glx. In the present work, with the use of full prior knowledge, it is found that Glu and Gln can be resolved and quantified under the condition of good shim.

- Lactate (Lac)

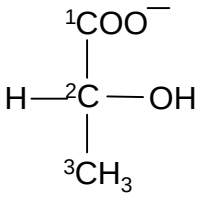

The signal of CH_3 group of Lac consists of a doublet located at about 1.31 ppm overlapping with lipid signals. To distinguish Lac from lipids, TE = 144 ms (1/J) in PRESS sequence is often used because Lac is fully inverted. In normal brain tissue Lac levels are typically very low and any detectable increase of Lac can be considered abnormal. Proton MRS indicated [Kama94] that lactate increased in cerebral edema, ischemic stroke or in tumors. Lactate levels were also found increased in regions peripheral to the infracted tissue [Gill96]. In tumors, Lactate levels are different in individual spectra, but do not correlate with tumor types or degree of malignancy [Smit02].

- Myo-Inositol (Ins)

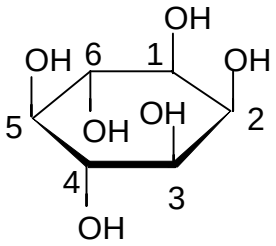

Ins has a high concentration in human brain. However, due to its short T_2 it is difficult to be observed at long TE. Ins is a glial marker and shows different concentration levels in diseases. Proton MRS indicates increased myo-Inositol in renal failure, diabetes mellitus, chronic

hypoxic encephalopathy and hypernatremia, and decreased in hepatic encephalopathy and hyponatremia [Graa97]

- N-acetylaspatate (NAA)

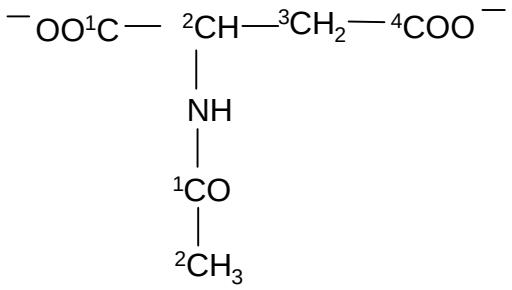

NAA is one of the most important metabolites in brain ^{1}H MR spectroscopy. In normal brain tissue, NAA concentration is about 10 mM, one of the highest in brain metabolites, and has a prominent singlet resonance at 2.01 ppm. This resonance, together with the singlets of Cr at 3.0 ppm and Cho at 3.24 ppm, can be measured at long echo time when most J-coupled resonances decay out. It can be estimated easily by different spectral quantification methods. In fact, the singlets of NAA , tCr (3.0 ppm) and Cho have been used recently to quantify *in vivo* ^{1}H MRS acquired without WS [Dong00b][Clay01][Serr01a]. However, at short echo times, the singlet of NAA overlaps with resonance lines of Glutamate at 2.04 ppm and GABA at 1.91 ppm, and also with the background originating from macromolecules, making it difficult to quantify accurately. Another important spectral property of this resonance is that its chemical shift is largely temperature independent[1][Corb95]. Therefore, the prominent NAA chemical shift is often used to calibrate *in vivo* MR spectrum. In the present work, this property of the NAA resonance is used to determine frequency offsets of the measured and the simulated metabolite spectra and then to determine the initial values of frequencies for spectral fitting (See Section 3.7). Furthermore, the chemical shift difference between NAA and water can be used as a measure of brain temperature *in vivo* [Corb95].

Though the exact function of NAA remains unknown, it is commonly regarded as a neuronal marker, as it is found in neurons only. NAA can provide abundant diagnostic information. NAA is reduced or absent in stroke, brain tumor, ischemia, degenerative disease [Smit02]. Reduced NAA is found to be an common and possibly an early chemical abnormality of

[1] In the temperature range of 14 ^{o}C and 44 ^{o}C and pH value range of 5.5 and 7.1, the temperature coefficient of NAA chemical shifts is $7 \cdot 10^{-4}$ ppm/^{o}C [Corb95]

chronically epileptogenic brain tissue [Smit02]. However, NAA is found to increase in Canavans' disease [Ceci01].

- Taurine (Tau)

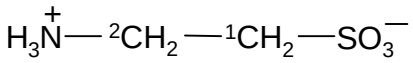

Tau has two triplets at 3.2 and 3.4 ppm. It overlaps with part of Glc multiplets and partially overlaps with Ins and with tCh. Tau levels are in general higher in animal brain than in human brain. A concentration of 2.30 mM in cat brain was reported [Zijl97] and an even higher concentration (~ 6.0 mM) was given for rat brain [Pfeu99], while the average value is 1.5 mM in human brain [Govi00]. At TE = 144 ms, Tau can still be observed in rat spectrum overlapping with tCh at 3.20 ppm, due to its high concentration.

2 Quantification of MR Spectroscopy

2.1 Introduction

The last decade witnessed an increasing research interest in the *in vivo* MR spectroscopy in the field of biochemical and biomedical studies, because MR spectroscopy offers a unique non-invasive tool for these purposes. Although significant progresses have been made, much work needs to be done to improve the quantification of MRS.

The conventional analytical method in NMR is Fourier transformation, with which the spectral information can be obtained and the structures of the compounds can be determined. In the *in vivo* MR spectroscopy, the components of the sample and their structures are usually known as prior knowledge, but the quantities or concentrations are unknown and need to be determined. Therefore the main task of the *in vivo* MR spectroscopy is spectral quantification. Although FT analysis and the simple spectral fitting techniques can be used in some cases, their results are usually not satisfactory due to the special features of *in vivo* MRS. First, the concentration of metabolites in the brain are only in the order of millimole (mM), while the concentration of water in the brain is about 40 moles. Second, signal contamination from unwanted substances is hard to avoid. For example, in the case of proton MRS of the brain, the metabolite signals are superimposed by macromolecule signals and lipid signals. Third, the spectra are very complicated. This is especially true for proton MRS in brain where spectra of more than 20 metabolites are crowded preferentially in a frequency range of about 4 ppm. Fourth, *in vivo* signals may be distorted by unwanted artificial effects, such as eddy current effects caused by gradient pulses. Fifth, the measuring time is limited, and time consuming data accumulations are not allowed.

As consequences of the aforementioned reasons, *in vivo* proton MR spectra are associated with severe spectral overlapping, heavy baseline distortion, low signal-to-noise ratio and strong line shape distortion, making it difficult to distinguish peak from peak, peak from noise and peak from baseline. Even some isolated singlets can not be reliably quantified by conventional methods, such as peak height measurement and area integration, simply due to one or more of the problems outlined above.

The complexity of the *in vivo* proton MR spectroscopy requires sophisticated and systematic data processing approaches, which may involve software and hardware, time domain and frequency domain, pre-acquisition and post-acquisition treatments, and also prior knowledge. Different methods have been developed to tackle these tough problems.

2.2 Spectral preprocessing

Spectral fitting is very important for quantification. However, it is only one step in MRS quantification, which involves improvements of hardware, acquisition technique developments and post-procession optimizations. In this section the common preprocessing procedure used *in vivo* proton MRS quantification are introduced.

2.2.1 Windowing and filtering

Window functions are commonly used on time domain raw data to improve either the SNR or the spectral resolution, or to remove truncation effects in the frequency domain. A number of window functions are commonly used in routine spectral processing for different purposes [Cane96] [Fuku81]. Rectangular window function or zoom technique in the frequency domain are also used for selecting a spectral region of interest to reduce the number of data points or to remove disturbing signal components. However, this technique should be used with care if the subsequent quantification is carried out in the time domain, since signal truncation in one domain will induce artifacts in the other domain.

2.2.2 Zero filling

Zero filling means to add zeros to the measured data series prior to FT to extend the number of data points in order to improve the digital resolution of the frequency domain signal. In the present work, spectral fitting is performed in the time domain with limited number of data points. For a better visualization, the original data are zero filled and the estimated signals are reconstructed with a larger number of points.

2.2.3 Lineshape correction and transform

The lineshape of *in vivo* MRS is distorted by eddy currents caused by switched magnetic gradients as well as B_0 field inhomogeneities. Lineshape correction and lineshape transform are necessary to ensure reliable spectral estimation. These lineshape imperfections can be corrected by using a reference signal, which should be a singlet and is equally distorted

[Klos90][Graa90b]. In water unsuppressed ^{1}H MRS, the water signal can be extracted and used as a reference [Dong00a, b]. Otherwise, a separate measurement without WS must be performed or a self-deconvolution method for lineshape correction proposed by Maudsley [Maud95] should be used. The extracted water signal should be as complete as possible but should not contain any lipid and metabolite signals. Otherwise, serious problems such as baseline and/or phase distortions in the spectral region near water will result.

Some spectral estimation methods, such as SVD based and MPM based methods, require certain types of model functions. Thus a lineshape transformation from the measured lineshape to the ideal lineshape is necessary.

2.2.4 Phase correction

In the quadrature detection scheme, NMR signal is measured in two quadrature channels, x and y, as complex data. In an ideal case, one channel receives the real part and the other the imaginary part. However, in practice, each channel may receive the mixture of real and imaginary parts of the signal due to phase errors. For most of the quantification methods, phase errors need to be carefully corrected to avoid quantification errors.

One kind of phase error is independent of the signal frequencies and is termed zero order phase error. Zero order phase error can be easily detected and corrected in the time domain. At t = 0, the quadrature components of the signal is given by

$$S_0 = \sum_{k=1}^{K} a_k e^{i\varphi_0} \ . \qquad \text{Eq. 2.2-1}$$

and φ_0 is determined by

$$\varphi_0 = tg^{-1}\frac{S_{0y}}{S_{0x}}. \qquad \text{Eq. 2.2-2}$$

Zero order phase error is corrected by multiplying the signal with the factor $e^{-i\varphi_0}$.

Another kind of phase error is caused by the hardware imperfections or the pulse sequence timing error. For instance, the first point of the FID is not acquired instantaneously after the pulse because of the “dead time” of the receiver, or the first point of data is not acquired exactly at the top of echo due to timing errors of the pulse sequence. The resulting errors develop linearly with frequency and can be expressed as

$$\varphi(\omega) \ = \ \varepsilon + \kappa(\omega). \qquad \text{Eq. 2.2-3}$$

First order phase errors can be corrected manually or automatically. The aim is to obtain a pure absorption mode for real components and a pure dispersion mode for imaginary

components. However, judging whether a complex spectrum is in pure absorption mode or not is rather subjective, time consuming and expertise demanding. This is especially true when the spectrum has severe baseline distortion and/or spectral overlapping.

2.2.5 Baseline correction

If a spectrum consists of sharp peaks superimposed upon broad and slowly varying background, the former are referred to as spectral lines and the latter is termed baseline.

The spectral lines originate from the sample under investigation and carry information of interest, while the baseline often stems from various sources and constitutes interference to the desired signal. Baseline needs to be corrected, i.e., removed to ensure reliable and accurate spectral analysis and, especially, spectral quantification.

There are different sources for a non-flat baseline. First, it may originate from the sample itself. In *in vivo* proton MRS, the spins from macromolecules and lipids have spin-spin relaxation times that are much shorter than those of low molecular weight metabolites, and thereby their signals decay very rapidly in the time domain and contribute signals with broad features in the frequency domain. Second, baseline may originate from experimental operations on the sample. For instance, complete WS is rare to realize and the residual water signal may induce baseline and phase distortions. Third, some post-processing procedure may also cause baseline distortion. In proton MRS without WS, water components usually need to be modeled and extracted in order to separate them from the metabolite signals. If the water signal is not correctly modeled, the resultant spectrum will suffer from baseline and phase distortions after removal of the water components. Another example is that dropping the first few data points in the FID will cause the so-called baseline rolling.

The baseline problem is more pronounced in short TE *in vivo* proton MRS, where all the above mentioned sources of baseline distortions may exist.

Baseline correction is the most important step in the quantification of short TE *in vivo* proton MRS and is probably by far the most difficult task. Baseline correction can be performed as a preprocessing step before spectral fitting, or can be incorporated in the fitting procedure, or can be performed iteratively together with spectral fitting. A plain and simple baseline correction method is to choose some points in the spectrum that are supposed to characterize the features of baseline and then either connect them by straight lines or better fit them with a spline. While for spectra with minor baseline problem, this method might work to some extent, it is rather problematic for spectra with severe baseline problems as in typical short TE *in vivo* ^{1}H MR spectra. This method is rather subjective and would lead to bad reproducibility

among different operators. Even the method is used in an automatic way, the deviation would be rather large for different measurements of the same subject. The baseline fitting with a polynomial function has largely the same problem in that one might choose the degree of the polynomial rather subjectively.

2.3 Quantification strategies

The quantification of MRS is to acquire the metabolite concentrations of the subject under investigation from the spectral parameters, e.g. amplitudes or peak areas, obtained by various of spectral estimation methods. Therefore, signal parameters must be calibrated against a standard of reference whose concentration is known or whose concentration is taken as the unit. The standards of reference can be the internal standard or the external standard.

2.3.1 External standard

With this method, the measured metabolite signal is compared with the signal obtained by a measurement on a standard sample with known concentration. The sample can be a phantom placed near the subject or a phantom mounted after the subject is removed from the scanner. In the former case, a reference scan acquires reference signal after sampling the subject is finished. In doing so, only the voxel position is changed, while other experimental parameters are kept unchanged. This approach is time saving compared to the second one. However, RF field may be significantly different between voxels in the subject and in the reference phantom, thus RF inhomogeneity may cause errors in the signal calibration. In addition, the spatially dependent eddy currents will also induce calibration errors for the same reason. The reported error range extends from a few percent [Henn92] to 40% [Henr95]. The second approach eliminates the errors caused by RF field inhomogeneity by measuring the standard signal from the same location in the phantom, assuming that the RF field distribution remains unchanged in the *in vivo* case and in the phantom case. However, the filling factor and the loading of the RF coil may change when the *in vivo* subject is replaced by the phantom, thus introducing calibration errors. Compared with the former approach, this approach needs more time. In general, the advantages of external references are that the concentration of the external standard sample is known and that the signal can be measured with high SNR.

2.3.2 Internal standard

In this case, the calibration signal is obtained from inside of the subject, usually from the same voxel. The signal may be extracted from the same scan or may be collected from a separate scan. The obvious advantages of this method over the external standard method are that the errors caused by RF field inhomogeneity and eddy currents spatial dependency can be avoided, and that the errors caused by filling factor and loading differences are also eliminated. With these, the internal standard is more preferable and attractive than the external standard. The major problems associated with the internal standard are that the concentration of standard is unknown or unstable and that the standard may not be fully NMR visible.

The tissue water signal has been used as an internal standard [Krei97] [Erns93] [Chri93] [Bark93], because of several reasons. The water concentration in tissue is well known and is relatively stable[Chri94][Gide99]. The water signal can be measured accurately with high SNR and very fast due to the high concentration of tissue water. As WS is a common protocol in conventional proton MRS, separate measurements are necessary if water is used as a standard of absolute quantification.

In human brain studies the water contents differ considerably between gray and white matter. The water composition is 75% for gray matter and 62% for white matter [Erns93]. Compared with the biochemical findings of 0.82 and 0.73 [Lent81], the values determined by NMR method is about 10% lower, which indicates that about 10% of water in brain tissue may be MR invisible in proton spectroscopy with TE's of 15 ms or longer. Another study [Chri94] showed that the ratio of MR invisible water to MR visible water is about 5%. The invisibility of MR water signal suggests the existence of short T_2 component of tissue water. Compartmentation effects may also lead to a reduced water content as discussed in [Erns93]. Corrections should be introduced to compensate the signal losses caused by short T_2 and the compartmentation effects in order to reach close agreement of water contents determined by MRS and biochemical method. A precision of 1.5% of the water content was reported [Erns93].

A more important issue concerning the water content as a reference is whether the water content varies in pathological brain tissue or not. Several studies [MacK94] [Bess89] [Chri94] [Helm00] have come to the general conclusion that the water content is rather stable and the error limits would be within 10%.

The total creatine is also often used as an internal relative standard for quantification[Gyng91] [Frah89] [Mier98]. The reasons, among others, for choosing total creatine as a relative standard are that creatine signals are prominent and are less overlapping compared to other

prominent metabolites. The shortcoming of using creatine (or any other metabolite) as the internal standard is that the concentration of creatine may change during pathological conditions. When the concentration ratio changes, one can not easily determine whether it is caused by changes of creatine only, or of the other metabolite, or even of both. Absolute values of concentration are occasionally given, assuming a certain value of creatine concentration, such as 10 mM [Frah89] or 6.0 mM [Mier98]. One should keep in mind that in this case the concentrations are still relative.

In comparing the quantification results of different methodologies and different application studies, one should be aware that several factors can affect the values of the estimated concentrations, such as which standards were used, which standard concentration was assumed, what parts of the tissues were measured and what relaxation time values were used for the corrections. Omitting these factors may lead to errors or wrong conclusions. For example, the T_2 values are about 60 ms for water and about 300 ms for NAA *in vivo* at 4.7 T. Without T_2 correction NAA concentration will be overestimated by more than 20% even for short TE = 20 ms.

2.4 Quantification methods

This section introduces some of the MRS quantification methods developed in recent years. These methods are classified into two categories, namely the time domain methods and the frequency domain methods. Examples of their application results are given to indicate their advantages and disadvantages, their most suitable application areas and their limitations.

2.4.1 Time domain and frequency domain

Although the NMR signal is measured in the time domain as FIDs or spin echoes, traditionally NMR spectral analyses were almost uniquely carried out in the frequency domain, because the spectral information such as spectral components and their characteristics are not so easily visualized in the time domain, and the signal transformation from time domain to frequency domain can be easily and efficiently carried out by the fast Fourier transformation (FFT). In recent years, many time domain [Dijk92][Boog94] and new frequency domain methods [Stan95] [Prov93] [Slot98] have been developed. In fact, time domain signal and its frequency counterpart contain exactly the same information and are in this sense equivalent. If performed correctly, both frequency domain and time domain spectral analytic methods can give the same results [Boog94] [Joli91]. However, either method has its

own advantages and disadvantages, and each has its own pre-condition requirements and limitations.

The advantages of frequency domain are:

1. Working in frequency domain offers easy approaches for baseline correction and first order phase correction.
2. Frequency domain analysis can be carried out in a selected spectral region of interest, thus reducing the number of data points in the processing and consequently the computing time.
3. Frequency selection can eliminate some signal contaminations from macromolecules and spectral corruptions by incomplete WS.

The disadvantages of frequency domain are:

1. Complex lineshapes other than Lorentzian type, such as that described by Voigt function in time domain, may be difficult to be incorporated into the frequency domain spectral fitting, as no frequency domain analytical functions of the lineshapes are available.
2. Truncated time domain signal may cause artifacts, such as baseline rolling in the frequency domain.

The advantages of time domain are:

1. Truncation effects can be avoided.
2. It is easy to incorporate complex lineshape function into the model functions of time domain fitting.
3. Time domain model functions can be easily adapted to changes in the data sets, such as non-uniform sampling.
4. As far as model function based methods are concerned, time domain methods have simpler model functions and are more efficient to compute.

The disadvantages of time domain are:

1. It is difficult to perform baseline correction in time domain.
2. The whole spectrum is processed even though the spectral region of interest is much smaller. For the same spectral resolution, this means more data points and longer computing time. However under certain conditions frequency selective quantification is also possible in time domain [Knij92].

2.4.2 Frequency domain methods

The frequency signal is characterized by the peak areas (corresponding to amplitudes in time domain), peak positions or chemical shifts (frequencies), linewidths (damping factors) and phases.

Spectral integration is the classical way to estimate the peaks areas. This method works well as long as the SNR is high, the peaks are well separated and the baseline is flat. These prerequisites pose severe difficulties for *in vivo* spectral quantification, especially for ^{1}H MRS, as *in vivo* spectra usually feature severe spectral overlapping, low SNR and baseline distortion. In some case, spectral integration may still be reasonable. For example, at long TE (= 288 ms), the ^{1}H MRS reveals only three prominent singlets from NAA (2.01 ppm), Cr (3.24 ppm) and Cho (3.02 ppm) and a flat baseline. Simple spectral integration or spectral fitting can be used for quantification [Veen00]. The drawbacks of this approach are that the signal suffers from severe information and SNR losses, the accuracy of this approach is usually low and it requires appropriate phasing. In general, more advanced and sophisticated frequency spectral fitting methods should be employed.

2.4.2.1 Model function fitting

The FID is a sum of exponentially decaying sinusoids in the ideal case. Fourier transformation of this FID gives frequency domain MR spectrum with group of Lorentzian lines. Suppose that the FID is expressed as,

$$y(t) = \sum_{k=1}^{K} a_k e^{i\varphi_k} e^{i\omega_k t - \alpha_k t} \qquad \text{Eq. 2.4-1}$$

Performing Fourier transformation gives the frequency domain signal [Boog94],

$$S(\omega) = \int_0^\infty y(t) e^{-i\omega t} dt$$

$$= \sum_{k=1}^{K} \left\{ \frac{\alpha_k^2 a_k^2}{\alpha_k^2 + 4(\omega_k - \omega)^2} \cos\varphi_k - \frac{2\alpha_k a_k (\omega_k - \omega)}{\alpha_k^2 + 4(\omega_k - \omega)^2} \sin\varphi_k \right\}$$

$$+ i \sum_{k=1}^{K} \left\{ \frac{\alpha_k^2 a_k^2}{\alpha_k^2 + 4(\omega_k - \omega)^2} \sin\varphi_k - \frac{2\alpha_k a_k (\omega_k - \omega)}{\alpha_k^2 + 4(\omega_k - \omega)^2} \cos\varphi_k \right\} \qquad \text{Eq. 2.4-2}$$

where the first summation is the real part of the spectrum (pure absorption spectrum) and the second part is the imaginary part of the spectrum (pure dispersion spectrum).

The principle of spectral fitting is to adjust the parameters of the model function, namely, a_k, α_k, ω_k, φ_k, so that the distance χ^2 between the measured and the fitted spectra is minimized in the least squares sense [Marq63],

$$\chi^2 = \sum_{i=0}^{N-1} \{ \frac{1}{\sigma_i} [S_{meas}(\omega_i) - S(\omega_i)] \}^2 \rightarrow 0 \qquad \text{Eq. 2.4-3}$$

where σ_i is the standard deviation of each data points, and the summation is carried out over all complex data points.

It should be noted that the model function given above is the ideal one. Field inhomogeneity and susceptibility of the living object make the lineshape deviate from pure Lorentzian or pure Gaussian types, and signal contamination of macromolecules and lipids forms a baseline underlying the metabolite signal. These lineshape and baseline distortions should be taken into account. The actual decay of time domain signal can be described by the Voigt function, $e^{-\alpha t} e^{-\beta t^2}$, which is the multiplication of Lorentzian and Gaussian decay functions. As no analytical expression of the Voigt lineshape is not available, it is often approximated by a combination of Lorentzian and Gaussian lineshapes: $c_L\ S_L(\omega) + c_G\ S_G(\omega)$, where S_L and S_G are Lorentzian and Gaussian lineshape signals and c_L and c_G are their weighting factors. A polynomial is usually used to model the baseline and incorporated into the model function,

$$B(\omega) = \sum_{q=1}^{Q} c_q \omega^q \qquad \text{Eq. 2.4-4}$$

where Q is the degree of the polynomial which should be decided prior to the spectral fitting and c_q is the parameter to be fitted. The determination of Q is rather empirical, and a too large or a too small number can lead to poor fitting.

Although many frequency domain methods have been developed [Mier01], most of them are not successful or appropriate for quantification of short TE *in vivo* ^{1}H MRS, except LCModel and the one in [Stan95]. The former will be reviewed in the following subsection and the time domain version of the latter will be reviewed in the section devoted to time domain methods.

2.4.2.2 Linear combination of model spectra

The above frequency domain spectral fitting scheme fits the spectrum by a series of single resonance. It has no intrinsic mechanism to resolve the contributions from different sources of the overlapping peaks, and no prior knowledge other than the lineshapes are used. Improvement would be achieved, if prior knowledge is incorporated in the fitting. De Graaf and Bovee [Graa90a] proposed to implement prior knowledge of chemical shifts, J-coupling, relative amplitudes and line widths derived from *in vitro* measurements of pure metabolite solutions to quantify *in vivo* spectra. Prior knowledge is also used in the LCModel by incorporating the model signals of metabolite solutions *in vitro*, as introduced by Provencher [Prov93], which fits the *in vivo* ^{1}H MR spectra as a linear combination of the model spectra. This method assumes that the chemical properties, i.e. the chemical shifts and J-couplings, are the same for the metabolites *in vitro* and *in vivo*. The model function for spectral fitting is given as follows.

$$Y(\omega_k) = \exp[-i(\varphi_0 + \omega_k \phi_1)]\{\sum_{j=1}^{N_B} \beta_j B_j(\omega_k) + \sum_{l=1}^{N_M} C_l \sum_{n=-N_S}^{N_S} S_n M_l(\omega_{k-n}; \gamma_l, \varepsilon_l)\} \quad \text{Eq. 2.4-5}$$

where $C_l \geq 0$ is the concentration of the metabolite, $\gamma_l \geq 0$ is the linebroadening factor, and S_n is the lineshape coefficient, and M_l is the model spectrum measured *in vitro*. Zero and first order phase corrections are represented by ϕ_0 and ϕ_1. Baseline is represented by N_B cubic B-splines, $B_j(\omega)$. N_B and N_S are the numbers of degrees of freedom in determining the baseline and lineshape. As can be seen from the model function, phase correction and baseline correction are incorporated into the LCModel, which can reduce tasks of preprocessing and user interference.

Typically, the spectral region from 1.0 ppm to 4.0 ppm is used by the LCModel in spectral evaluation. With full prior knowledge incorporated into the spectral fitting, overlapping spectra can be better resolved because most metabolites do not completely overlap and the J-coupled lines are automatically accounted for. This makes LCModel especially suitable for short TE spectral estimation. Usually, about 10 metabolites can be estimated from short TE spectra with this method [Haje00] [Prov01].

Presently, LCModel is the most widely used commercial metabolite quantification method in *in vivo* proton MRS.

Although the LCModel is robust, accurate and automatic, it also has some shortcomings. In order to apply LCModel, it is necessary to measure model spectra of all metabolites *in vitro*, with the same experimental conditions and parameters as those of *in vivo* experiments. Whenever experimental conditions and/or parameters change, new model spectra must be

measured and calibrated. This can be rather time consuming. The phantoms of the model solutions should be specially treated and well preserved from contamination for long term use.

2.4.2.3 Spectral fitting by second derivative method

Another frequency domain spectral fitting method is so-called the second derivative method (SPSDS Inc. Chicago USA). In this method, spectral peaks, including the hidden ones, are detected as local minima of the spectrum's second derivative. Lenvenburg-Marquardt nonlinear lease squares fitting was used for the maximum likelihood fitting procedure. Very recently, the performance and usefulness of the method were reported [Sokó01] based on quantification results of human brain ^{1}H MR spectra obtained at a 2 T spectrometer with TE = 35 ms. As many as 52 lines in the range of 0.7 ~ 4.2 ppm were found and the estimated concentration ratios of main metabolites, such as NAA/Cr, Cho/Cr, Ins/Cr and Glu/Cr, were reportedly in agreement with those in the literature.

2.4.3 Time domain methods

Time domain MRS quantification methods appeared only in the past two decades [Bark85a,b], [Tang85], [Gesm88], [Veen88], [Step88]. Improvements [Vanh97] (supported by an EU project Magnetic Resonance User Interface (MRUI)[1]) and new methods [Bart99] arose in recent years.

Time domain methods can be classified into two categories: the non-iterative or "black-box" methods and the iterative methods. The representative black-box methods are the Singular Value Decomposition (SVD) based Linear Prediction SVD method [Step88] and state-space method [Kung83][Bark87]. The first widely used iterative time domain MRS quantification method is VARPRO [Veen88], which was extended to AMERES [Vanh97] by incorporating more types of prior knowledge into the fitting. A new method using a template of prior knowledge deduced from model spectra in the model function fitting was proposed in [Bart99]. A recent review of time domain methods is found in [Vanh01].

2.4.3.1 Black-box methods

The discrete FID signal superimposed by Gaussian white noise is rewritten as follows,

$$y_n = x_n + w_n = \sum_{k=1}^{K} a_k z_k^n + w_n \text{ , n = 0, 1, 2, …, N-1,} \qquad \text{Eq. 2.4-6}$$

[1] see: http://carbon.uab.es/mrui/mrui_Overview.shtml

where N is the number of data points, a_k is the complex amplitude of the kth spectral components, z_k is the so called signal pole,

$$a_k = |a_k| e^{i\varphi_k} \qquad \text{Eq. 2.4-7}$$

and

$$z_k = e^{-\alpha_k + i\omega_k} \qquad \text{Eq. 2.4-8}$$

where $|a_k|, \varphi_k$, α_k and ω_k are the absolute amplitude, phase, decay rate and angular frequency of the sinusoidal, and i denotes $\sqrt{-1}$.

From the data sets $\{y_n\}$ a data matrix with the Hankel structure is formed,

$$Y = \begin{pmatrix} y_0 & y_1 & \cdots & y_{M-1} \\ y_1 & y_2 & \cdots & y_M \\ \vdots & \vdots & \ddots & \vdots \\ y_{L-1} & y_L & \cdots & y_{N-1} \end{pmatrix} \qquad \text{Eq. 2.4-9}$$

where L, M > K and L + M = N +1.

Matrix Y will in general be of full rank due to noise corruption. The matrix can be decomposed in such a way as follows,

$$Y = U \begin{bmatrix} \Sigma \\ 0 \end{bmatrix} V^+ \qquad \text{Eq. 2.4-10}$$

where U is an $(N-L)\times(N-L)$ matrix, V is an $L \times L$ matrix and $\Sigma = \text{diag}(\sigma_1, \sigma_2, \ldots, \sigma_R)$ is a diagonal matrix of rank $R \leq \min(N\text{-}L, L)$. The elements $\sigma_1 \geq \sigma_2 \geq \ldots \geq \sigma_R \geq 0$ are called singular values and the decomposition are called singular value decomposition (SVD). Thus,

$$Y = \sum_{k=1}^{R} \sigma_k u_k v_k^+ \qquad \text{Eq. 2.4-11}$$

An important feature of SVD is that larger singular values are related to signals and the smaller singular are related to noises. If one can determine the number of signals K, one is able to reconstruct the signal from the first K singular values according to the above equation.

The above scheme could only reconstruct the noise free signal, but the parameters of the signal, i.e. the amplitude, frequency, decay rate of each resonance line, need to be determined. This can be achieved either by the state-space method [Beer92] or the Linear Prediction Singular Value Decomposition LPSVD method [Kölb92].

With state-space method, the above matrix is truncated to rank K:

$$Y_K = U_K \Sigma_K V_K^+ \qquad \text{Eq. 2.4-12}$$

If the signal is noise free, it can be shown that the following equation holds:

$$U_{K,t} = U_{K,b} Z_K \qquad \text{Eq. 2.4-13}$$

where $U_{K,t}$ and $U_{K,b}$ are obtained by removing the top row or bottom row from the original matrices, and Z_K is a diagonal matrix consisting of signal poles, which can be solved exactly. If there is noise in the signal, the above equation approximately holds and can be solved in the least squares sense. Once $\{Z_k\}$ are solved, the complex amplitudes can be calculated from equation (2.4-1).

The other time domain method is LPSVD method [Kölb92]. The principle of the method is based on the assumption that each time domain data can be predicted by a linear combination of preceding or afterwards data points. A forward linear prediction can be written as,

$$y_n = \sum_{k=1}^{K} q_k y_{n-k} \qquad \text{Eq. 2.4-14}$$

It can be shown that a noise free FID signal expressed in Eq.2.4-1 satisfies exactly the above relation and exactly K terms on the right-handed side is enough to uniquely determine the data point y_n.

The non-iterative time domain methods such as LPSVD and HLSVD are most successfully used in quantifying ^{31}P and ^{23}Na *in vivo* MR spectra [Vanh01], mainly because these spectra are less overlapping than *in vivo* ^{1}H, though heavy overlapping of MR spectral lines and a dominant broad baseline exists in ^{31}P spectra and unresolved quadruple line broadening is typical in ^{23}Na spectra. In quantification of ^{1}H MRS, the SVD based methods have been successfully used in removing the residual water signal [Zhu97] [Vanh98].

2.4.3.2 Iterative methods

A widely used iterative time domain method is the VARiable PROjection (VARPRO) method [Veen88]. This method can be regarded as a time domain model function method, in contrary to frequency domain model function fitting method described earlier.

The noise-free part of the signal in Eq.2.4-6 can be rewritten in matrix notation as,

$$Y = ZA \qquad \text{Eq. 2.4-15}$$

where $A = [a_1, a_2, \ldots a_K]^T$, and

$$Z = \begin{pmatrix} z_1^0 & z_2^0 & \cdots & z_K^0 \\ z_1^1 & z_2^1 & \cdots & z_K^1 \\ \vdots & \vdots & \ddots & \vdots \\ z_1^{N-1} & z_2^{N-1} & \cdots & z_K^{N-1} \end{pmatrix} \qquad \text{Eq. 2.4-16}$$

is a N×K matrix of full rank.

The time domain fitting is to minimize the square difference of the measured data and the model function,

$$\left|S - ZA\right|^2 \to 0 \qquad \text{Eq. 2.4-17}$$

If Z is known, A can be determined by A = Z^+S, where Z^+ is the pseudo-inverse of Z. Thus, the formal solution of A is given as,

$$A = (Z^+Z)^{-1}Z^+S \qquad \text{Eq. 2.4-18}$$

Substituting Eq.2.5-18 into Eq.2.5-17, the vector A is eliminated from the least square expression, and the non-linear parameters $\{z_k\}$ can be obtained by solving the least square problem of Eq.2.5-17. The linear terms A are calculated from Eq.2.5-18.

A new method named AMARES (Advanced Method for Accurate Robust and Efficient Spectral fitting) [Vanh97] improved the VARPRO method. Some features of the new method are allowing the imposing prior knowledge and the fitting to echo signals, the possibility of choosing both Lorentzian and Gaussian lineshapes and introducing constraints on the parameters. With this method, as many as 7 metabolites were quantified from short TE (16 ms) and high field (4.7 T) *in vivo* ^{1}H MRS [Mier98].

Recently, a new time domain method is proposed by Bartha et al. [Bart99], which is a time domain version of a frequency domain quantification method [Stan95]. Both methods incorporate prior knowledge from *in vitro* metabolite spectra into the nonlinear spectral fitting routine, but in a way different from that of LCModel [Prov93]. Instead of the full *in vitro* spectra being used as prior knowledge, the parameters of the major spectral lines of the *in vitro* spectra were deduced and the relative frequencies, relative amplitudes and relative phases of the spectral lines of each individual metabolite were calculated to form a template of prior knowledge, which was then used in the fitting routine. The model function in the time domain

is as follows,

$$y(n) = \sum_{k=1}^{K} c_k e^{i(2\pi\omega_k(n\Delta t+t_0)+\varphi_k)} . e^{-\pi\alpha_k|n\Delta t+t_0|} . e^{-(\pi^2/(4.\log 2))\beta_k^2.(n\Delta t+t_0)^2} \quad \text{Eq. 2.4-19}$$

where y is the estimated time domain signal at point n, k is the line index, K is the total number of lines involved, c, ω, φ, α and β are the amplitude, frequency, phase, Lorentzian damping and Gaussian damping, respectively; t_0 is the delay time, and Δt is the dwell time.

The prior knowledge of macromolecule resonances was also incorporated in the template and in the fitting to account for the baseline. While metabolite lines were only fitted in the spectral region 1.9 ppm – 3.5 ppm, the baseline were fitted in the region of 0.5 ppm – 4.0 ppm.

This time domain method, incorporating extensive prior knowledge, can reportedly estimate more than 10 metabolites acquired at short TE (see the table in the next section).

In conclusion, the black-box methods do not need user involvement and can be executed automatically; The iterative methods usually need user involvement and can incorporate prior knowledge in the fitting to improve the performance. At present, the iterative methods outplays the black-box methods in quantifying short TE *in vivo* ^{1}H MRS.

Besides the methods mentioned above, there are numerous other spectral quantification methods employing variety of different approaches and algorithms, such as Maximum Entropy [Hore85], Maximum Likelihood [Zhu98], Principle Component Analysis [Stoy00], Wavelet Transformation [Anto01][Serr97], Pattern Recognition [Preu98] and Artificial Neuro-Network [Hilt02]. Reviewing these methods are beyond the scope of the present work.

2.5 Literature values of metabolite concentrations

Numerous results of metabolite quantification have been reported. In this section, results from three typical studies with three different methods are presented (Table 2.5.1) together with a literature survey by Govindaraju et al. [Govi00].

Because many factors, such as the standard of reference, the relaxation effects, and the units and so on, can affect the results of metabolite quantification, these factors must be taken into account when interpreting and comparing the results.

The data from Study 1 were obtained by LCModel with the following protocols: STEAM sequence, TE = 2 ms, TM = 20 ms, TR = 4 s; No relaxation correction; Water signal was used as an internal reference assuming a water content of 83% of the rat brain. Obtained with 9.4 T field and at TE = 2 ms, the MRS spectra had a high resolution and wealthy information. Thus,

as many as 18 metabolites were estimated by the LCModel. This is by far, to the best of knowledge of the author, the highest number of metabolites ever estimated from an *in vivo* ^{1}H MRS experiment.

Tab.2.5.1 Concentrations of metabolites.

Metabolites	Study 1 by LCModel [Pfeu99]	Study 2 by AMARES [Mier98]	Study 3 in [Bart99]	Literature Survey in [Govi00]
	Mean +/- SD (mM/kg ww)	Mean +/- SD (mM)	Mean (a.u.) +/- CV (in %)	Concentration range (mM/kg ww)
NAA	8.38 +/- 0.50	6.64 +/ 0.78	13.7 +/- 3.5	7.9 – 16.6
NAAG	0.32 +/- 0.12		2.0 +/- 23.0	0.6 – 2.7
Cr/PCr	7.78 +/- 0.58	6.0 (Reference)	9.3 +/- 6.4	5.1 - 10.6, 3.2 - 5.5
Cho/PCh	0.71 +/- 0.10	1.38 +/- 0.15	2.9 +/- 6.5	0.9 – 2.5
Clu	8.67 +/- 0.70	7.04 +/- 0.86	9.5 +/- 11.4	6.0 – 12.5
Gln	1.25 +/- 0.38	1.51 +/- 0.39	4.9 +/- 19.2	3.0 – 5.8
Glc	3.51 +/- 0.46	2.76 +/- 0.57	1.6 +/- 61.9	1.0
GSH	1.46 +/- 0.15			2.0
Ins	4.08 +/- 0.55	2.70 +/- 0.31		3.8 – 8.1
Tau	4.25 +/- 0.59		2.4 +/- 19.9	0.9 – 1.5
PE	1.98 +/- 0.20			1.1 – 1.5
Asp	1.43 +/- 0.44		3.2 +/- 20.7	1.0 – 1.4
Lac	1.89 +/- 0.34			0.4
GABA	1.11 +/- 0.25		1.4 +/ 66.4	1.3 – 1.9

Study 2 was obtained by AMARES on STEAM spectra (rat brain, 4.7 T, TE = 16 ms, TR = 30 ms, TR = 4 s) using tCr as reference (6.0 mM).

Study 3 by Bartha et al. [Bart99] was performed on STEAM spectra (Human, 1.5 T, TE = 20 ms, TR = 30 ms, TR = 1.5 s) with no relaxation correction, and results were given in arbitrary units.

In comparing the results with different units, unit conversion should be made using the specific gravity of brain of 1.04kg/L [Graa01], or using the ratios to a common reference metabolite, such as tCr.

The data from [Govi00] were literature values for normal human brain and biospy tissues obtained using a variety of analytical techniques.

3 Quantification of ^{1}H MRS without water suppression

3.1 Introduction

3.1.1 Dynamic range problems

The *in vivo* ^{1}H MR spectrum without WS features a large signal dynamic range, which is defined as the ratio between the amplitudes of the largest and the smallest signal components,

$$d = \frac{A_{\max}}{A_{\min}}. \qquad \text{Eq.3.1-1}$$

The signal dynamic range of *in vivo* ^{1}H MRS is over 10^4, which puts harsh requirements on the resolution of the analogue-to-digital converter (ADC) of the spectrometer. The dynamic range of a N-bit ADC is,

$$r = 2^{N-1}, \qquad \text{Eq.3.1-2}$$

with one bit reserved for the sign. The large dynamic range of the signal also imposes difficulties on the postprocessing procedure. Therefore, several WS techniques, such as CHESS [Haas85], WATERGATE [Piot92] and MEGA [Mesc96], have been developed and WS has been conventionally used as a routine in the *in vivo* ^{1}H MRS. Fig.3.1-1 shows the *in vivo* ^{1}H MRS acquired without and with WS.

In principle, the signal should be large enough to cover one bit to be detected and be smaller than r to be recorded without overloading. However, in practice, some factors and technique can effectively reduce lower limit of resolution and reduce the signal dynamic range.

If the total signal amplitude is large and/or the noise level is high enough to cover at least 3 or 4 bits of the ADC, it has been shown that the signal components smaller than one bit can still be recorded [Lind80]. The presence of noise effectively reduces the signal dynamic range [Widr96],

$$d = \frac{A_{\max}}{\sigma}, \qquad \text{Eq.3.1-3}$$

where σ is the standard deviations of the noise entering the ADC.

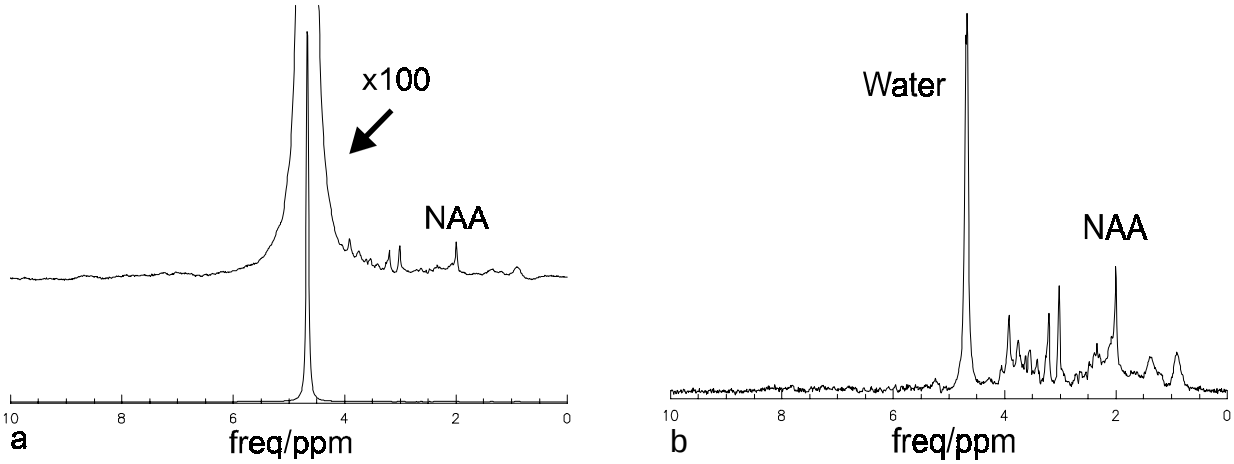

Fig.3.1-1 Water unsuppressed (a) and water suppressed (b) *in vivo* ^{1}H MR spectra.

It is seen from Eq. 3.1-3 that σ must be much larger than the least significant bit of the ADC to effectively reduce the signal dynamic range and to avoid quantization errors. Table 3.1.1 shows the noise levels and the unsuppressed water signals measured from a single voxel of a phantom. As can be seen that for a large range of receiver gains, the SNR remains constant, implying that no quantization error occurred.

Table 3.1.1 Noise level, unsuppressed water signal and SNR measured from a single voxel of a phantom. The parameters were: TR = 1 s, TE =144 ms, voxel = 4*4*4 mm^3.

Receiver Gain	1500	2000	3000	6000	10000
Noise (a.u., mean/SD)	0.026/38.2	-0.028/46.6	-0.016/76.4	-0.043/142.6	-0.100/232.2
Water Signal (a. u.)	19458.9	23981.0	38885.2	72582.2	118632.0
SRN	509.4	510.5	509.0	509.6	510.8

The oversampling technique improves the effective dynamic range of ADC [Dels86]. Oversampling acquires the data at a higher rate than the Nyquist frequency, say n^2 times of Nyquist frequency, and then adds the adjacent n^2 data points to produce a new data point. With n^2-fold oversampled data, the SNR is increased by a factor of n and the dynamic range of the signal as defined in the above equation is decreased by a factor of n.

With a modern spectrometer equipped with 16-bit ADC, it is possible to acquire *in vivo* ^{1}H MR signals without WS, and several measurements have been made [Hurd98] [Veen00].

3.1.2 Motivation

Although WS is widely used in the proton MRS, the *in vivo* ^{1}H MRS acquired with WS has also several disadvantages. (i) Signals with small chemical shift differences to water are partially

suppressed also. The typical linewidth (FWHM) of a water signal *in vivo* is 0.05 ppm or 10 Hz on a 4.7 T spectrometer. Strong signal components of water can extend to a range of about +/-0.5 ppm or +/- 100 Hz. The excitation spectrum of WS pulses should cover that range to ensure sufficient degree of WS. As a result, metabolite signals in high field region up to 4.0 ppm might be suppressed and cannot be observed. (ii) Some WS methods may cause magnetization transfer effects to metabolites and thus may cause systematic quantification errors [Leib01]. de Graaf et al [Graa99] showed that presaturation and water eliminated Fourier transform (WEFT) may cause considerable signal changes, especially to CH_2 and CH_3 groups of tCr, while CHESS did not cause observable signal changes. However, Kreis et al [Krei98] reported that for long delays between WS and excitation of metabolites CHESS might also cause significant signal changes. (iii) RF pulses used for WS increase the total RF power deposition. The specific absorption rate (SAR) of the biological tissue is proportional to the square of the main magnetic field strength and the irradiating RF field [Bott81]. The shaped RF pulses for spectral selective excitation in WS increase the RF power and thereby the SAR. This effect is more pronounced at high fields. (iv) Additional measurements are necessary if water is used as an internal reference for absolute quantification, which will increase the total measurement time. (v) Spoiler gradients increase the acoustic noise level. RF pulses for WS are accompanied by strong spoiler gradients to destroy the unwanted water signals. The spoiler gradient coils will be forced to vibrate [Wu00] [Henn99] and produce strong noise, which will make the patient uncomfortable.

On the other hand, proton MRS acquired without WS not only avoids the disadvantages of the WS, but also offers further advantages. (i) Most of parametric spectral estimation methods assumes certain types of lineshapes.. In localized MRS, the actual lineshapes often deviate from the ideal ones due to, e.g., eddy current effects and field inhomogeneity. A lineshape correction is necessary, otherwise an increase of quantification errors will result [Dong00b]. The experimental lineshape can be corrected to the ideal one by taking the water signal as a reference [Klos90]. Although the water signal can be obtained by separate measurements, it is better to be extracted from the same measurement without WS [Dong00a] to avoid any possible changes of the experimental conditions. (ii) The unsuppressed water signal can benefit the analysis and quantification of MRSI [Spie89]. In MRSI, the field inhomogeneity leads to voxel-to-voxel frequency shifts, which should be known before accurate quantification can be expected. The relative frequency shifts can be determined easily and precisely from the unsuppressed water signal, while it is difficult from the water suppressed spectra.

Although efforts have been made in recent years to quantify *in vivo* ^{1}H MRS acquired without WS, only the spectral quantification on NAA, Cr and Cho were reported based on their prominent

singlets measured at long TE [Dong00b] [Clay01] [Serr01b], because of the special problems associated with proton MRS without WS.

These disadvantages of WS and the advantages of *in vivo* proton MRS without WS, together with the difficulties and the potential applications of *in vivo* proton MRS without WS motivated us to develop a method that can quantify short TE *in vivo* proton MR spectra acquired without WS.

3.1.3 Problems associated with *in vivo* ^{1}H MRS

In this subsection, problems associated with *in vivo* proton MRS will be outlined with emphasis on the special problems of short TE *in vivo* proton MRS, and *in vivo* proton MRS acquired without WS.

Complexity. The most striking characteristic of proton MR spectra are their complexity. Several factors contribute to the complexity. First, most metabolites consist of several groups of protons that are coupled via scalar coupling interactions, often resulting in many resonance lines. Fig.3.1-2 illustrates high resolution short TE (= 20 ms) proton spectra simulated for 18 NMR detectable metabolites in animal brain. At long echo time the J-coupled lines are distorted and possess complicated phase relations. The other factor that contributes to the complexity is that there are more than 20 proton MR visible metabolites in the human body with MR spectra appearing within a frequency range of about 4 ppm. As a result, most of the spectra are overlapping, especially if they are acquired with clinically available low field ($B_0 < 4$ T) spectrometers. Fig.3.1-3 shows the same spectrum as in Fig.3.1-2, but with a Lorentzian line broadening of 8 Hz to approximate the *in vivo* situation. Compared with the high resolution spectrum, the overlapping problem is more serious because of spectral overlapping from both the same metabolite and different metabolites. In fact, what shown in Fig.3.1-3 are only the ideal "*in vivo*" spectra. Field inhomogeneity and susceptibility induced line broadening also lead to structured and overlapping broaden lines that make the spectrum even more difficult to resolve.

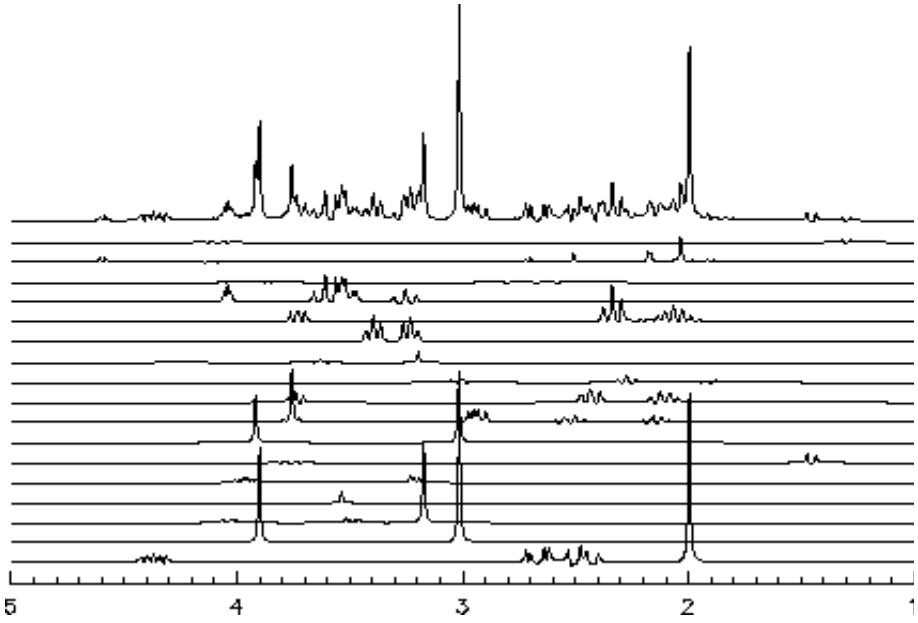

Freq/ppm

Fig. 3.1-2 Simulated high resolution proton spectra of main metabolites in animal brain. The metabolites are (from bottom up, with assumed concentrations in a.u. in brackets): NAA (10.0), Cr (8.0), Cho (1.5), Gly (1.0), PE (1.5), Ala (1.0), PCr (4.0) , GSH (2.0), Gln (8.0), GABA (1.5), PCh (0.6) Tau (6.0), Glu (8.0), Ins (6.0), Asp (1.0), NAAG (1.5), Lac (0.4). Chemical shifts and J-couplings used are given in the Appendix. Simulation parameters are: Pulse sequence: PRESS, SF = 200.3 MHz, SW = 4006 Hz, number of data points = 4096, TE = 20 ms. Lorentzian linebroadening of 2 Hz was applied on the simulated time domain signals.

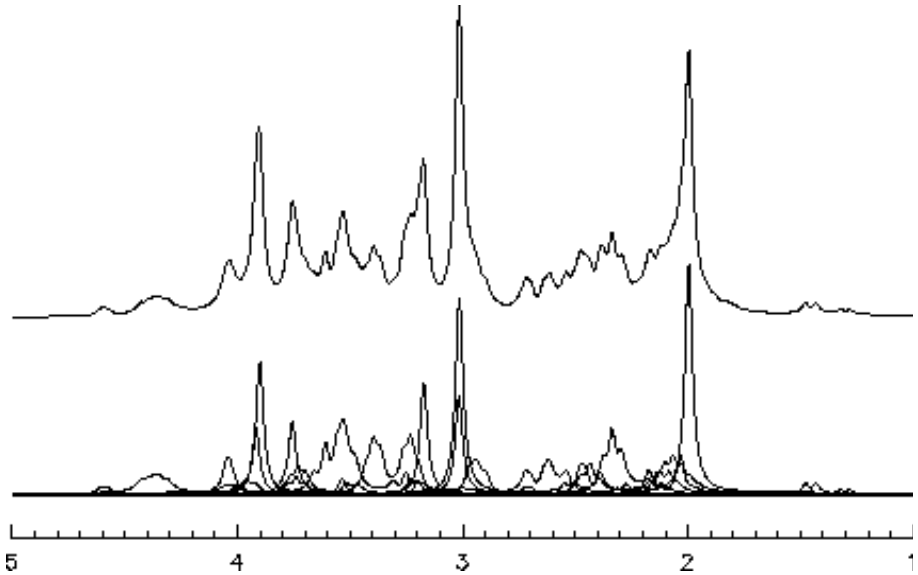

Freq/ppm

Fig. 3.1-3 Simulated proton spectra of main metabolites in animal brain. The metabolites and the simulation parameters are the same as those in Fig.3-1. Lorentzian linebroadening of 8 Hz was applied on the simulated time domain signals to approximate the ideal *in vivo* spectra. The lower trace are the metabolite spectra overlaid. The upper trace is the sum spectrum of the metabolite spectra.

Baseline/lineshape distortion. Signals of macromolecules and lipids possess much shorter T_2 values and have much broader resonance peaks than the low molecular weight metabolites. The contributions of the macromolecules and lipids to the spectra become smaller at long TE (e.g. TE = 144 ms) because of the short T_2. However at short TE, the resonance lines from macromolecules and lipids will form broad and distorted baseline lying under the metabolite peaks. These baselines are difficult to model or to characterize thus causing problems for spectral quantification. Other instrumental effects, such as incomplete WS can induce baseline problem in the vicinity of water signal. Eddy current effects caused by gradient pulses may produce lineshape distortion, making the lineshape asymmetric.

Low SNR. Low concentrations of metabolites in humans and animals, limited measurement time in *in vivo* situation and the inherent insensitivity of NMR signal result in a low signal-to-noise ratio of the MR spectrum. The above mentioned scalar coupling interactions not only add to the spectral complexity but also deteriorate the SNRs of coupled spins. Taking NAA as an example, though it has the prominent singlet from the CH_3 group at 2.01 ppm, the coupled lines of the CH proton at 4.38 ppm may be immersed in the noise. Some experimental approaches such as using long TE to simplify the spectra and the post-processing approach to drop out the first few points of FID to remove the baseline components also reduce the SNR.

Artifacts. A special problem associated with signals without WS is the strong artifacts caused by the gradient pulses, which are larger than the signals of metabolites next to water signal [Hurd98], constituting severe obstacles to the spectral estimation.

These problems must be properly addressed to achieve an accurate metabolite quantification.

3.2 Matrix Pencil Method based spectral fitting

3.2.1 Introduction

The time domain NMR signal, the FID, can be expressed as a summation of exponentially decaying sinusoids. The conventional analysis method of an NMR signal is the Fast Fourier Transform (FFT), which transforms the FID into frequency domain spectrum consisting of a series of spectral peaks. The time domain FID data and frequency domain spectrum are equivalent in the sense that they contain the same amount of information. However, time domain signal and frequency domain signal have their own features, as already mentioned in Chapter 2. In the past decade or so, several time domain methods, such as LPSVD[Kölb92] and VARPRO [Veen88], have been developed to

quantify NMR signals.

The Matrix Pencil Method (MPM) [Hua90], a time domain signal parametric analytical technique, provides another alternative to the FFT. The MPM decomposes the signals to be analyzed into a group of exponentially damped sinusoids each with specific parameters of frequency, amplitude, phase and damping rate. Compared to the FFT method, MPM performs extremely well for highly damped signals, short data series, truncated signals and signals with low SNR. This method is good for signal modeling and signal component extraction/separation, i.e., serving as an artifact-free filter in a sense.

Compared with the popular method of LPSVD, MPM based method has lower breakdown SNR threshold, improves the estimation accuracy by a factor of 2-4 and reduces computing cost by about an order of magnitude [Lin97]. In this section, a scheme is developed based on MPM to quantify *in vivo* proton MRS acquired without WS.

3.2.2 Implementation of MPM

The FID series consisting of a sum of exponentially decaying sinusoids and additive white noise are given in Eq. 2.4-1 – Eq. 2.4.-3.

The detailed theory of MPM analysis is found in [Hua90] and [Lin97]. An implementation of MPM used in the present thesis is described as follows.

Step 1. Construct data matrices Y_1 and Y_2.

$$Y_1 = \begin{pmatrix} y_1 & y_2 & \cdots & y_L \\ y_2 & y_3 & \cdots & y_{L+1} \\ \vdots & \vdots & \ddots & \vdots \\ y_{N-L} & y_{N-L+1} & \cdots & y_{N-1} \end{pmatrix} \text{ and } Y_2 = \begin{pmatrix} y_2 & y_3 & \cdots & y_{L+1} \\ y_3 & y_4 & \cdots & y_{L+2} \\ \vdots & \vdots & \ddots & \vdots \\ y_{N-L+1} & y_{N-L+2} & \cdots & y_N \end{pmatrix} \qquad \text{Eq. 3.2-1,2}$$

Step 2. Perform SVD [Ande95] on Y_1.

Step 3. Determine the number of signal poles K, using the Minimum Description Length (MDL) method [Riss87].

Step 4. Reconstruct the matrix $\hat{Y}_1$ from the first K singular values of Y_1.

Step 5. Solve the eigenvalue problem for signal poles $\{z_k\}$, corresponding to eigenvactors $\{q_k\}$:

$$\hat{Y}_1^{\#} Y_2 q_k = z_k q_k \qquad , \text{k} = 1, 2, ..., \text{K.} \qquad \text{Eq. 3.2-3}$$

where # stands for the Moore-Penrose pseudo-inversion.

Step 6. Solve the least squares problem of Eq. 2.4-1 for the complex amplitudes, a_k.

Step 7. Calculate the parameters of the signal.

$$\tilde{a}_k = |a_k|, \quad \text{Eq. 3.2-4}$$

$$\varphi_k = \arg(a_k), \quad \text{Eq. 3.2-5}$$

$$\omega_k = \arg(z_k), \quad \text{Eq. 3.2-6}$$

$$\alpha_k = -\log|z_k|. \quad \text{Eq. 3.2-7}$$

where arg(·) stands for the phase angle of a complex number (·). In the present work, MPM was implemented by self-developed programs written in C/C++, which employ CLAPACK (available for free at http://www.netlib.org) functions for linear algebra calculations, including SVD, eigenvalue calculation and least squares solution.

3.2.3 Matrix Pencil Method based spectral fitting

The spectral fitting scheme is illustrated schematically in Fig.3.2-1 and is described in details as follows.

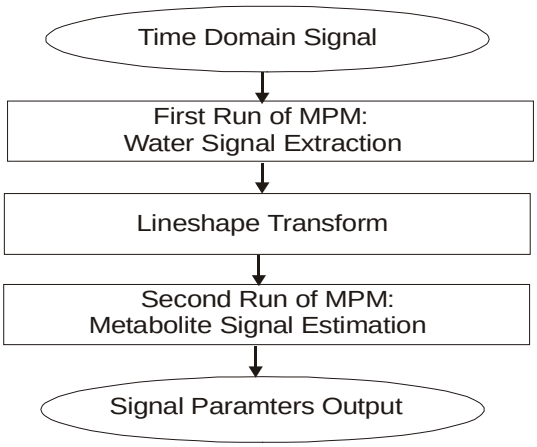

Fig. 3.2-1 Flowchart of the MPM based spectral fitting scheme.

Water signal extraction and reconstruction. The raw time domain data are analyzed by the MPM method first to extract the water component and to reconstruct the water signal. The water signal range depends on the shimming of the field or the linewidth of the unsuppressed water signal. In the

4.7 T system and for about 10 Hz of FWHM of *in vivo* water signal, the water range is set to be +/- 90 Hz. All signals whose frequencies fall into this range are recognized as water components. Usually, less than 10 lines are found in this range. These water components are combined to reconstruct the water resonance,

$$S_w(t) = \sum_{k=1}^{K} a_k e^{i\omega_k t - \alpha_k t} \qquad \text{Eq. 3.2-8}$$

where K is the number of water components, a_k, ω_k, and α_k are the complex amplitude, frequency and decay rate of the k-th component.

The number of the time domain data points involved in the water signal extraction plays an important role in water signal extraction and reconstruction. If the number of points is too small, either the spectral resolution will lose when the same number of points is used in the following procedures or large water residue will remain and even artifacts arise when more data points are used in the reconstruction and the following procedures (Fig.3.2-2). On the other hand, increasing the number of data points will result in a dramatic increase of computation time. A solution to this problem is to undersample the raw data in the water components extraction. This is done by leaving out, for instance, every other raw data point for the water extraction. The undersampled data reduce the spectral width, which is still large enough to cover the range of the water signal, and retain the spectral resolution. With this approach, the virtual sampling time is increased, thereby water components can be determined more reliably without increasing the number of data points and the computing time. A disadvantage of this approach is that the noise from outside of the reduced spectral region is folded into the region and the SNR is reduced by the square root of the undersampling rate. However, this has only minor effects on the water extraction procedure, as the original SNR of water is very high, usually > 50 dB[1]. Fig.3.2-3 shows an *in vivo* spectrum without WS after removal of the water components. The water signal was perfectly extracted and reconstructed with undersampled data points leading to a complete removal of water components. Without the undersampling approach, a total of 600 data points would have to be used for the same results, leading to an increase of computing time by more than 3 times [Lin97].

[1] The SNR is defined as, $SNR = 20\log\frac{a}{\sigma}$ (dB), where a is signal amplitude and σ the standard deviation of the noise.

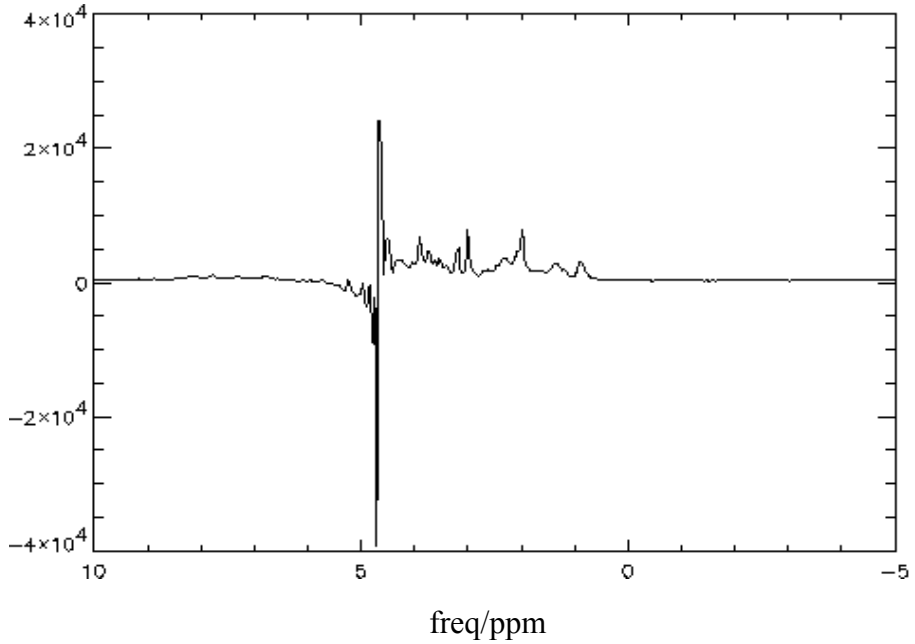

Fig. 3.2-2 Spectrum of *in vivo* signal of rat brain acquired without WS after removal of water components. Water signal was extracted by MPM with 300 complex data points, reconstructed with 600 data points, and subtracted from the original signal. Large residue exists due to imperfect fitting of the last 300 points of water signal.

Lineshape transformation. The MPM assumes exponentially decaying sinusoids of the analyzed signal and therefore works best with this type of signal. However, the *in vivo* signal, due to field inhomogeneities, deviates from the theoretical Lorentzian type. This will cause errors of the spectral quantification [Dong00b]. Several methods have been proposed for lineshape correction [Graa90b] [Klos90] using a reference signal, either the water signal from an additional scan or an isolated singlet in the spectrum. In the present approach, the water signal extracted from the water unsuppressed FID is used to perform the lineshape transformation and then the water resonance is subtracted from the raw data to get the reduced FID.

Defining a normalized non-ideal lineshape function as G(t), which is the same for all signal components, the total signal can be written as follows,

$$S_t(t) = S_w(t) + S_m(t) + w(t), \qquad \text{Eq.3.2-9}$$

where

$$S_w = G(t) A_w e^{i\varphi_w} e^{i\omega_w t - \alpha_w t} \qquad \text{Eq. 3.2-10}$$

$$S_m = G(t) \sum_{k=1}^{K} A_k e^{i\varphi_k} e^{i\omega_k t - \alpha_k t} \qquad \text{Eq. 3.2-11}$$

are the water signal and metabolite signals, respectively, and A, φ, ω and α are the amplitude, phase, angular frequency and decay rate of the signals. The non-ideal lineshape function can be

removed by first dividing the total signal by the water signal. The resultant signal then reads (omitting w(t) for simplicity.),

$$S_d(t) = \frac{S_t(t)}{S_w(t)} = 1 + \sum_{k=1}^{K} \frac{A_k}{A_w} e^{i(\omega_k - \omega_w)t} e^{-(\alpha_k - \alpha_w)t} e^{i(\varphi_k - \varphi_w)} \qquad \text{Eq. 3.2-12}$$

Therefore, the water signal contribution to the time domain signal is a unity after deconvolution. The amplitudes of the metabolites are reduced by a factor of A_w, the frequencies are shifted to lower field by a mount of ω_w and the decay rates are reduced by a mount of α_w.

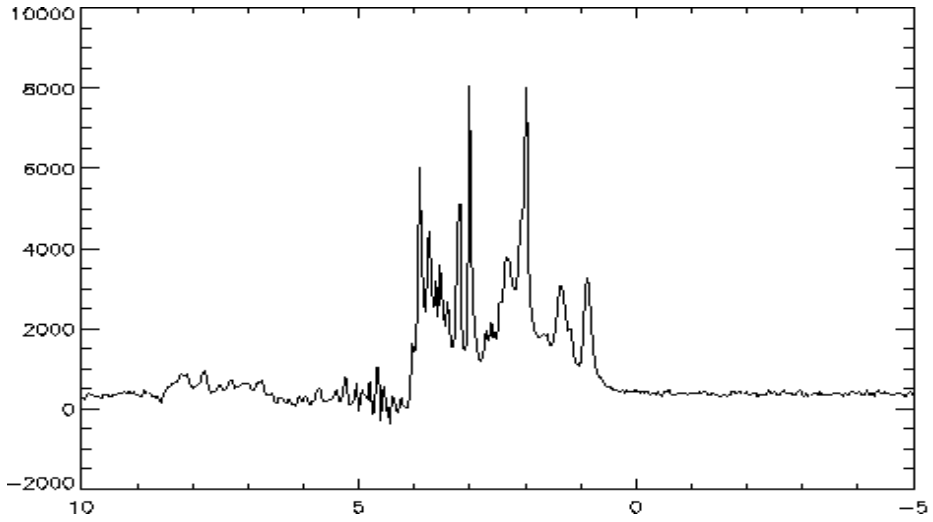

Fig. 3.2-3 Water signal was extracted from 300 data points undersampled from original 600 points and reconstructed with 600 points. Complete water removal was reached due to perfect water signal fitting. The original data were the same as in Fig. 3.2-2

In practice, the water frequency is often set to be on resonance and the phase is corrected to be zero. In this case, multiplying the above signal by $A_w e^{-\beta t}$ recovers the Lorentzian decay characteristic of the signal. If $\beta = \alpha_w$, one obtains,

$$S_d(t) = A_w e^{-\alpha_w t} + \sum_{k=1}^{K} A_w e^{i\varphi_w} e^{i\omega_k t} e^{-\alpha_k t}, \qquad \text{Eq. 3.2-13}$$

and the ideal lineshape determined by Lorentzian decay is recovered.

A difficulty with the final procedure is that the real Lorentzian decay rate of the water signal is usually unknown. The decay rate β can only be determined by experience according to the requirements on the spectral resolution.

The effects of noise should also be taken into consideration. As the water signal decays while the noise does not, the noise will be amplified during lineshape transform even if $\beta = \alpha_w$ as can be seen by,

$$w(t) \rightarrow \frac{w(t)}{G(t)}. \qquad \text{Eq. 3.2-14}$$

Therefore, β should be larger than the Lorentzian component of the decay rate to account for the Gaussian decay and to suppress the noise, and/or the length of the data series taken to the lineshape transform should not be too long, otherwise, large noise will results.

Zoom technique. The time domain signal contains information of the whole spin system. However only a part of the spectrum is of interest. In the time domain spectral analysis, all data points should be included in the calculation in order to maintain the original resolution. This will increase the computing time. A practical solution is the zoom technique [Cava97], [Krei97]. The procedure to perform the zoom technique is as follows.

1. Transform the time domain signal into frequency domain.
2. Select the spectral region of interest, i.e. to define a complex vector that contains the selected spectral region.
3. Fourier transform the selected spectral part back to time domain. The result is the reduced FID corresponding to the spectral region of interest.

The zoom technique greatly reduces the number of data points involved in the time domain analysis and keeps the spectral resolution at the same time. For example, if the spectral width of a 1000 complex points data series is 4000 Hz and the spectral region of interest is about 1000 Hz, 250 points are needed to cover the spectral region of interest. However, zoom technique should be used with caution, because of the ringing effect of the reduced FID due to rectangular filter in the frequency domain. The ringing problem is more serious when the residual water and/or baseline is large.

Second run of MPM. After the processing procedures outlined above, the water-component-free signal is submitted to the second run of MPM for the analysis of metabolite signal parameters. With removal of water signal and especially the lineshape transform, the signal parameters can be estimated accurately.

3.2.4 Quantification strategies

For quantification of metabolites, signal amplitudes estimated by the spectral fitting scheme described in the subsection above must be converted to metabolite concentrations with respect to a reference with known concentration. In this work, the unsuppressed tissue water signal is used as an internal standard of reference.

The MPM method, like other SVD based time domain spectral fitting methods, is non-iterative and has no built-in mechanism of baseline correction. Therefore, the MPM based method does not suit for spectral estimation of MRS acquired at short TE, unless the baseline problem is removed by other method. However, as the macromolecule signals, which contribute to the baseline, decay very rapidly and much faster than metabolite signals do, at TEs longer than 40 ms, the baseline is already very flat (for the MPM method). In this case, the MPM estimated amplitudes of metabolite signals and the water signal must be corrected for T_2 effect according to,

$$S_k(TE) = S_k(0)(1 - e^{-T_R/T_{1k}})e^{-TE/T_{2k}}, \qquad \text{Eq. 3.2-15}$$

where $S_k(TE)$ and $S_k(0)$ are the estimated and corrected amplitudes, respectively, of the resonance k. TE is the echo time and TR is the repetition time and T_1 and T_2 are the spin-lattice and spin-spin relaxation times, respectively.

The metabolite concentrations are calculated by,

$$C_m = C_w \frac{S_m N_w}{S_m N_m}, \qquad \text{Eq. 3.2-16}$$

where C is the concentration, S is the corrected signal amplitude and N is the number of spins contributing to the resonance, m and w stand for metabolite and water, respectively. The typical T_1's are about 1.5 seconds for metabolites and about 1 seconds for water [Graa01] [Mier98]. In the present work, T_R was chosen to be 6 seconds, so as for the signals to be fully relaxed to avoid T_1 correction. To correct for spin-spin relaxation, signals should be measured at different TEs (usually $n > 5$).

3.2.5 Monte Carlo Studies

Monte Carlo (MC) studies were employed to test the performance of the aforementioned spectral quantification method based on MPM, with the emphasis on testing its ability to handle signals with a large dynamic range.

Monte Carlo studies were carried out with the following steps: (i) A noise free signal with

components of a large dynamic range was synthesized with given parameters of amplitude, phase, frequency and damping rate; (ii) A number of complex noise series with Gaussian distributions were generated and each was added to the noise free signal, (iii) Each noisy signal was submitted to the spectral fitting routine; (iv) Statistical analysis was performed on the estimated parameters of all noisy signals giving means and standard deviations by which the performance of the method was evaluated.

The time domain model function used in the MC studies is a sum of exponentially damping sinusoids as described by Eq. 3.2-1. The theoretical values of the parameters of the synthesized signals are given in Tab. 3.2.1. The dynamic range of the signal is 4000:1, similar to that of water unsuppressed *in vivo* proton MRS. 100 noise realizations were added to the synthesized signal for the Monte Carlo studies. A typical spectral estimation result is shown in Fig. 3.2.4. As can be seen, both the dominant signal and the smaller signals were fitted very well. The MC results are given in Tab. 3.2.2.

Tab. 3.2.1 Theoretical values of the parameters of the synthesized signals

Amplitudes(a.u.)	*Frequencies(Hz)*	*Decay rates(1/s)*	*phases*
4000	125	25.13	0
1	250	25.13	0
2	350	25.13	0
3	550	25.13	0

Tab. 3.2.2 Results (mean/SD) of Monte Carlo Studies of the MPM. Number of noise realizations = 100, Standard deviation of noise = 0.5. Number of data points involved in the MPM procedure is 256.

Signals	*Amplitudes*	*Frequencies*	*Decay rates*	*Phases*
1	4000.06/0.41	125.00/0.00	25.13/0.01	0.00/0.00
2	1.02/0.11	250.00/0.73	26.26/4.69	-0.01/0.10
3	2.01/0.11	350.00/0.38	25.47/2.32	-0.00/0.05
4	3.00/0.11	550.00/0.22	25.07/1.70	0.00/0.03

From Tab. 3.2.1 and Tab. 3.2.2 one sees that the biases of estimated values are very small. In fact, they are close to zero for amplitudes, frequencies and phases. This shows that the MPM is a rather unbiased parametric spectral estimation method. MC studies also demonstrated the robustness of the MPM based method as the number of signals was correctly detected in the presence of large noise. In the present case with noise SD = 0.5, all four signal components were correctly detected in all 100 noise realizations. If the noise SD was increased to 0.8, the misdetection rate was 31%,

because the smallest signal was almost immersed into the noise.

For comparison, MC studies were also done on a second data set with the amplitude of the dominant signal in Tab.3.2.1 replaced by a smaller one of 10. The results are shown in Tab.3.2.3.

A comparison of the results of Tab. 3.2.2 and Tab. 3.2.3 shows that the precision of the estimated parameters for the smaller compounds is not reduced by a large dynamic range of the signal.

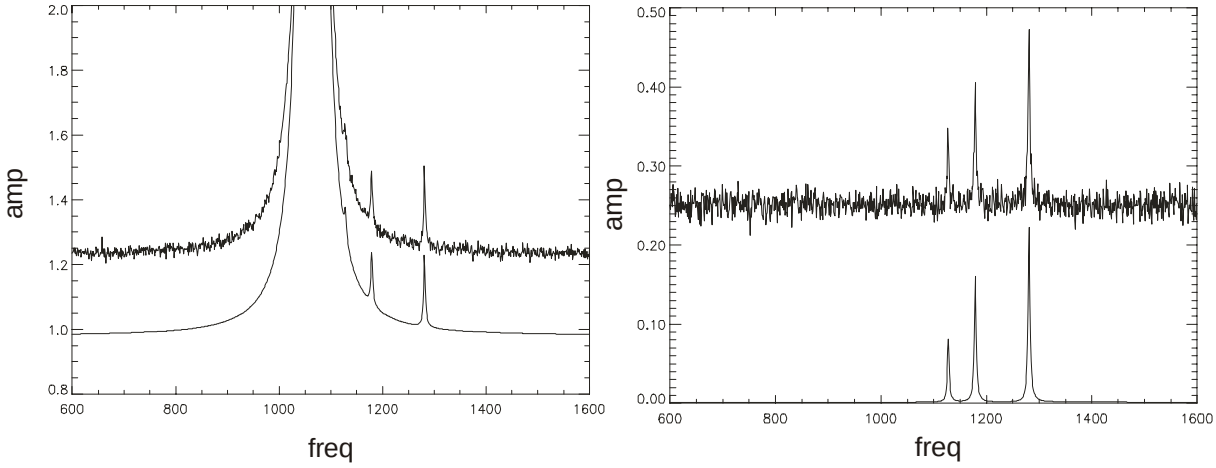

Fig. 3.2-4 Typical spectra of synthesized and fitted signals with dominant signals (left) and after removal of the dominant signals (right). The parameters of the synthesized signals are given in Tab. 3.2.1 and the noise level is 0.5 (a.u.). Please note that the frequency was shifted and the values were not scaled to Hz.

Tab.3.2.3 Results (mean/SD) of Monte Carlo Studies of the MPM. Number of noise realizations = 100, Standard deviation of noise = 0.5. Number of data points involved in the MPM procedure is 256.

Signals	***Amplitudes***	***Frequencies***	***Decay rates***	***Phases***
1	9.998/0.09	125.00/0.07	25.13/0.40	0.00/0.01
2	1.020/0.11	250.00/0.66	26.26/4.81	-0.01/0.09
3	2.012/0.10	350.00/0.33	25.47/2.19	-0.00/0.05
4	3.01/0.10	550/0.23	25.07/1.37	0.00/0.03

Cramer Rao lower bounds (CRLBs, [Rao46], [Cram46], [Cava01]) were used to examine the precision of the parameter estimation of MPM. CRLBs are the lowest possible standard deviations any unbiased parametric spectral estimation method could achieve from the given data. The CRLBs depend on the features of data, such as the noise level, spectral width, the structures of the spectral lines (singlet, doublets, ...), and the number of points involved in the estimation. Therefore, CRLBs can serve as a benchmark to evaluate the potential performance of any model parameter estimation method and as a tool to optimize some spectral estimation parameters. In the present study, the

spectral lines were well separated and were treated as singlets, and the CRLBs were calculated numerically by

$$CRLB = \sqrt{(F^{-1})_{nn}}\,, \qquad \text{Eq. 3.2-17}$$

$$F_{ij} = \frac{1}{\sigma^2}\Re\left[\sum_{n=0}^{N-1}\frac{\partial S_n^h}{\partial p_i}\frac{\partial S_n}{\partial p_j}\right]\,, \qquad \text{Eq. 3.2-18}$$

where F is the Fischer information matrix [Bos82], S is the theoretical model function of the signal, p is the real value parameter vector, N is the number of data points, σ is the standard deviation of the complex noise, h stands for the Hermitian conjugation and $\Re$ denotes the real part.

To calculate the CRLBs, the model function, the noise level and the number of data points are all the same as those used in the MC studies. The results are given in Tab.3.2-4. Comparing Tab.3.2-4 with Tab.3.2-2 and Tab.3.2-3 one sees that most of the standard deviations of the MPM estimated parameters are very close to their theoretical CRLBs. The only exception is the amplitude of dominant signal, whose standard deviation is almost 4 times larger than its CRLB. However the relative standard deviation is still very small. This proved the accuracy of the MPM method.

Tab. 3.2.4 Cramer Rao lower bounds of the noisy signals (Noise SD = 0.5, number of data points = 256)

Signals	*Amplitudes*	*Frequencies*	*Decay rates*	*Phases*
1	0.09	0.00	0.00	0.00
2	0.09	0.62	3.87	0.09
3	0.09	0.31	1.92	0.04
4	0.09	0.21	1.29	0.03

3.2.6 Phantom and *in vivo* experiments

Phantom and *in vivo* experiments were carried out to demonstrate the performance of the MPM based spectral fitting method. The samples for phantom experiments were an NAA solution of nominal concentration of 100 mM and a taurine solution of nominal concentration of 200 mM. The experimental parameters were as follows. For experiments with taurine, TE = 20 ms, TR = 13 s, voxel size = 1 cm^3, SW = 4006 Hz, NA = 32. Signals with WS were also measured using CHESS. The FWHM of the unsuppressed water signal was about 1 Hz. For experiment with NAA, TR = 13 s, TE = 20 ms ~ 1152 ms; voxel size = 64 mm^3. Other parameters were the same as in the taurine experiment. The NAA signals were measured with FWHMs of the water spectra of about 10.5 Hz

and about 0.8 Hz, respectively. Post-processing included 2 Hz linebroadening, water signal extraction (or water residue removal in the case of spectrum with WS) and spectral range selection of the positive frequency part. Originally, 1024 time domain data points were used. Water signals were extracted with an undersampling rate of 8 (128 points) and metabolite signals were analyzed with an undersampling rate of 2 (512 points). Signal components were detected automatically by the program. The fitted spectra were reconstructed with 1024 points in accordance with the original signal. Fig.3.2-5 and Fig.3.2-6 show some examples of spectral fitting.

Tab. 3.2.5 Integrated peak areas (a.u.) of taurine and the standard deviations (n = 6)

Areas from	***Mean +/- SD***
Measured Spectra with WS	7181.5 +/- 48.6
Fitted Spectra with WS	7266.3 +/- 63.8
Fitted Spectra without WS	7201.2 +/- 334.6

Fig.3.2-5a shows that the MPM fitted spectrum agrees well very with the spectrum measured with WS. In Fig.3.2-5b, the residues of FM artifacts are seen. The residues were also fitted by the MPM, but these were removed from the fitted signal for display. Despite this, the taurine spectrum was also very well fitted.

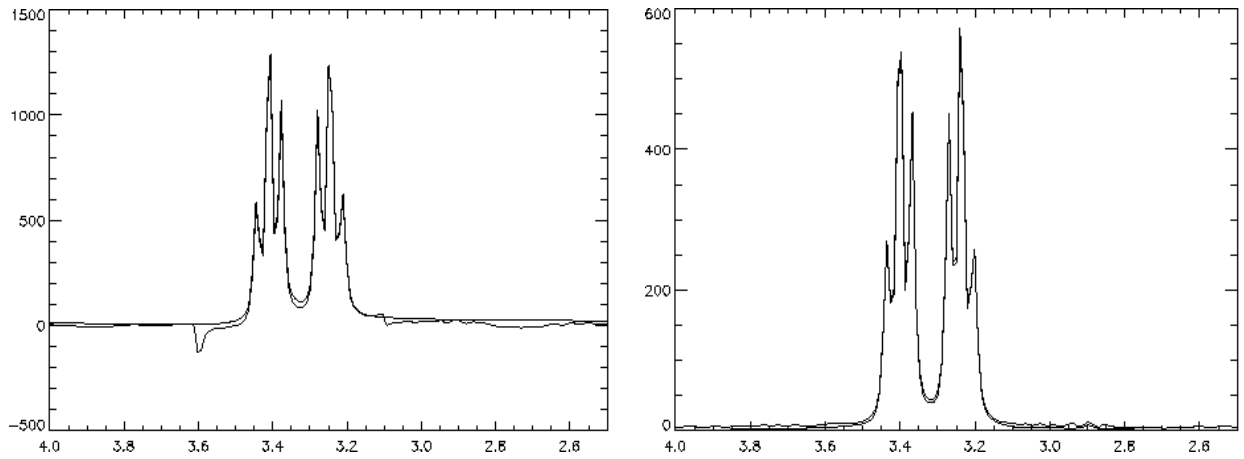

(a) freq/ppm (b) freq/ppm

Fig. 3.2-5 Taurine spectra measured without WS (a) and with WS (b), overlaid with the fitted spectra. The negative peak at 3.6 ppm was a frequency modulation artifact.

Numerical results of the signal estimation of taurine are given in table 3.2.5 as integrated peak areas from measured and fitted spectra with WS and from fitted spectra without WS. These data sets have

very close means, only the fitted spectra without WS have larger variations because of the influence of FM artifacts. No metabolite concentrations were given here because of the lack of T_2 values for signal correction. However, the accuracy of the MPM based spectral estimation method was proven by the NAA data given in the following.

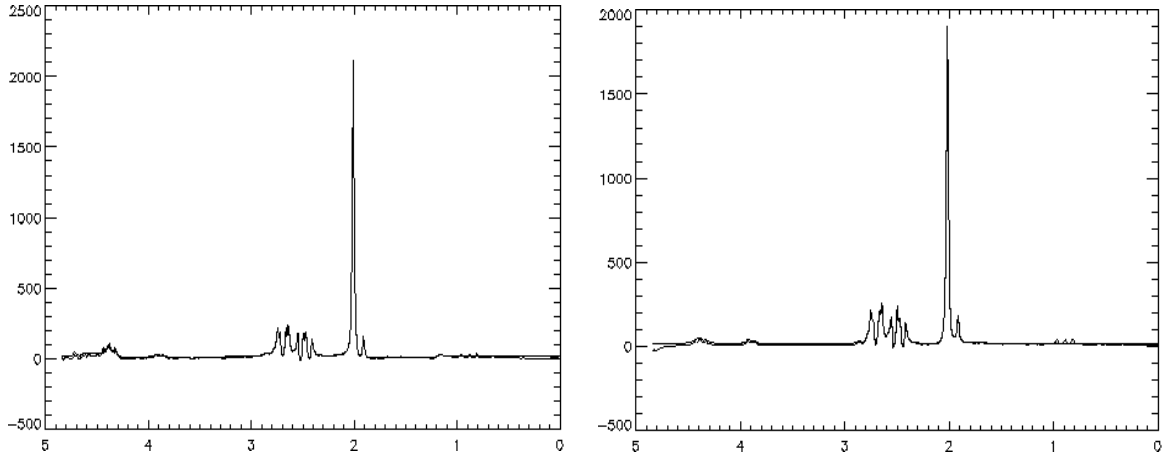

(a) freq/ppm (b) freq/ppm

Fig. 3.2-6 NAA spectra measured without WS (a) and with WS (b), both overlaid with the fitted spectra.

The aims of the NAA experiment were twofold: to test the performance of the method with different lineshapes and to test the accuracy of the method. To this end, the signals were measured with different TE's and the MPM estimated signal amplitudes were T_2 corrected. No T_1 correction was made as the signals were fully relaxed with TR = 13 s. The results are shown in Table 3.2.6.

Tab. 3.2.6 Quantification results (mean +/- s.d. in mM) of NAA spectral with different linewidths, and with or without WS. Nominal concentration of NAA = 100 mM.

Measurements	FWHM = 10.5 Hz		FWHM = 0.8 Hz	
	Without WS	With WS	Without WS	With WS
Conc. (1st run)	116.1 +/- 1.4	117.1 +/- 2.8	100.6 +/- 1.3	100.4 +/- 1.6
Conc. (2nd run)	101.6 +/- 2.8	100.5 +/- 2.6	99.7 +/- 1.4	100.3 +/- 0.4

The results of the first run of MPM show that the concentrations were overestimated by about 17% in the case of broad linewidth, while the concentrations estimated from spectra with narrow linewidth were very close to the nominal value. After transforming the lineshape to the Lorentzian type, the second run of MPM gave better results that are close to the nominal value for the spectra with broad linewidth, while the results for spectra with narrow linewidth remain largely unchanged.

The narrow linewidth of 0.8 Hz at 4.7 T field resulting from perfect shimming of the field implies a near ideal Lorentzian lineshape and the linewidth of 10.5 Hz resulting from bad shimming implies a Gaussian contribution to the lineshape. The results in Tab.3.2.6 indicate that the non-Lorentzian lineshape is the source of errors (overestimation). This is not very surprising, because the MPM method assumes Lorentzian lineshape of the signal and works best with the ideal signals. Thus, a lineshape transformation is necessary for accurate spectral estimation with MPM.

Not only the results of the spectra with broad linewidths were improved by the lineshape transform, but also the spectra with narrow linewidth. The means of concentrations are closer to the nominal value and the variation reduces remarkably for the spectra with WS. This may also be attributed to the lineshape transformation.

In both cases ("good" and "bad" shims) shown in the table, the results for spectra without WS and with WS are identical. This validated the efficiency of the method in estimating proton MRS acquired without water suppression.

In vivo experiments on male Wistar rats were performed using the following parameters: TR = 6 s, TE = 40 ~ 216 ms, NA = 16 ~ 96. The rest of the parameters were the same as in the phantom experiments. The typical linewidth of the unsuppressed water signal was 10 Hz. Signals acquired at different TE's were estimated for singlets of NAA (2.01 ppm), tCr (3.04 ppm) and tCh (3.24 ppm) and the estimated signal amplitudes were used to perform T_2 corrections, but no T_1 correction was made.

1024 complex data points were acquired for each data set. Signal estimations were made using 512 complex data points of the time domain signals. An example of spectral fitting is given in Fig.3.2-7. after the removal of the dominant water signal.

Metabolite quantification results are given in Table 3.2.7 for 4 rats using water as an internal reference. Water fraction was taken as 78.6% [Roon96]. As seen in the table, the concentration values fall within the range of literature values.

Tab.3.2.7 Quantification (mean +/- s.d. in mM) of major metabolites in rat brains.

Rats	NAA	tCr	Cho
1*	10.7+/- 0.2	10.3 +/- 0.2	1.7 +/- 0.2
2*	10.5 +/- 0.3	9.5 +/- 0.3	1.7 +/- 0.3
3**	11.0 +/- 0.3	10.2 +/- 0.8	2.0 +/- 1.1
4***	11.2 +/- 0.6	11.0 +/- 0.9	1.8 +/- 1.3

Note: *: NA = 96, **: NA = 64, ***: NA = 32

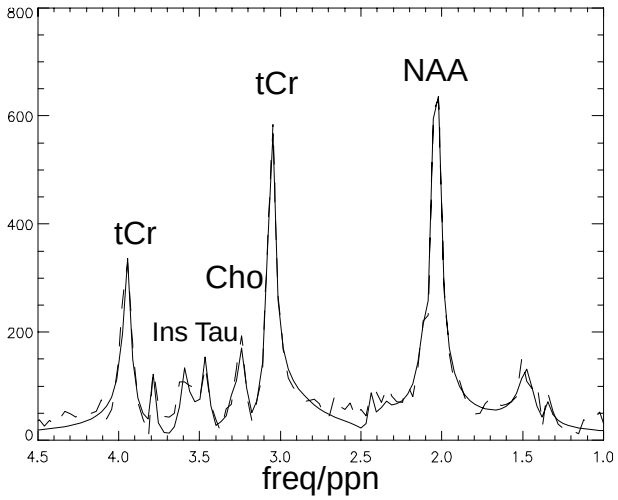

Fig. 3.2-7 An example of *in vivo* ^{1}H MR spectral fitting: measured (dashed) and fitted (solid) spectra overlaid.

3.2.7 Discussion

The Monte Carlo study and phantom experimental results showed that the MPM based signal estimation scheme developed in the present work can accurately estimate small signal components in the presence of dominant signal component. The accuracy of the estimation strongly depends on the lineshape of the signal. Non-ideal lineshape must be transformed to the ideal Lorentzian lineshape to ensure accurate signal estimation, which can be done easily with this method using the accurately extracted water signal. The MPM based method is also very good for fitting signals with strongly overlapping spectral components, but the problem in this respect is that the decomposition here is mathematical but not physical. Extensive prior knowledge is needed for assigning the lines to certain metabolites. The other difficulty of the method with *in vivo* proton MRS is that this method does not have the build-in mechanism for baseline recognition and characterization, simply because the broad baseline was decomposed into the combination of several narrower lines. This limits the application of the method with respect to short TE *in vivo* proton MRS. As a result, only the metabolites with prominent singlets were quantified from signals acquired at TE > 40 ms in the present work.

Taking all the strengths, advantages and shortcomings of the MPM based method into consideration, the author believes that with the necessary prior knowledge and combined with other baseline characterization method, the presented method can also be exploited to quantify efficiently and accurately short TE *in vivo* proton MRS.

However, the present work will not further develop the method in that direction. Instead, the present MPM based method is used to extract water signal components and to remove unwanted signal components or artifacts, preparing the signal for quantification by a method developed in the following sections.

3.3 Experimental method to eliminate first order phase errors

Phase correction is a difficult task for *in vivo* MRS, especially in short TE cases. The spectral overlapping, baseline and lineshape distortions make it difficult to determine the pure absorption line, either manually or automatically. As a result, considerable errors may remain after the phase correction.

However, the first order phase errors can be eliminated experimentally. The first order phase errors arise mainly from the timing error of the pulse sequence or hardware imperfection of the spectrometer. Therefore, a simple principle of eliminating the first order phase errors is to carefully adjust the timing of the pulse sequence so that the starting point of the acquisition is exactly at the top of the echo. The optimized timing of the pulse sequence can be done in an iterative way described as follows.

1. Measure the on-resonance and off-resonance (e.g. 3 – 4 ppm) water signals of a phantom.
2. Adjust the starting time of the acquisition to narrow the differences of the zero phases of on- and off-resonance signals;
3. Repeat the above steps until the phase differences of the on- and off resonance water signals are satisfactorily small.

A test was performed on a phantom of a 100 mM NAA solution. The offset frequency was 3.5 ppm, i.e., 700 Hz on a 4.7 T spectrometer. The PRESS sequence with TE = 20 ms was used. The zero order phase was calculated from the real and imaginary parts of the first point of the FID. Because of the high SNR of the unsuppressed water signal, the phase can be determined with great accuracy. The timing of the pulse sequence was performed according to the steps listed above. The results of zero order phases of water resonances at 0 and 700 Hz are given in Table 3.3.1. Due to perfect timing of the pulse sequence the phase differences of on- and off resonances are as small as the standard deviations of the phase fluctuations of the resonances. A student T-test ($p = 0.27$) shows that there is no significant difference ($p < 0.05$) between the means of the zero order phases of on- and off-resonance signals; And F-test ($p = 0.38$) shows that there is no significant difference ($p < 0.05$) between the variances of zero phases of the two signals. This proved that the first order phase errors were effectively eliminated. Table 3.3.2 shows the same results measured from an experiment a week later. The T-test and F-test results are 0.76 and 0.38, respectively. As expected, the performance of the method is very stable. A phantom spectrum of NAA solution and an *in vivo* spectrum of rat brain measured with optimally timed pulse sequence are displayed in Fig. 3.3.1 and

Fig. 3.3.2, respectively. In both cases only zero order phase corrections were performed in the post-processing. The phantom spectrum shows that the first order phase errors were completely removed. The *in vivo* spectrum suffers severe lineshape and baseline distortions, which make the manual phase correction rather subjective and the software methods inaccurate.

We conclude from the experimental results:

1. The first order phase errors can be eliminated experimentally by carefully timing the pulses sequence.
2. The timing of the pulse sequence needs to be performed only once and the parameters can be kept for future experiments.
3. The performance of the method is superior to the post-processing method and is time saving.

Tab.3.3.1 Zero order phases (degree) of water resonances at 0 and 700 Hz for five measurements

Freq. offset	***1***	***2***	***3***	***4***	***5***	***Mean +/- SD***
0 Hz	171.4	171.5	171.2	171.2	171.5	171.4+/-0.2
700 Hz	171.5	171.3	171.1	171.2	171.1	171.2+/-0.2

Tab.3.3.2 Zero order phases (degree) of water resonances at 0 and 700 Hz, measured a week later than the data in Tab.3.3.1

Freq. offset	***1***	***2***	***3***	***4***	***5***	***Mean +/- SD***
0 Hz	57.9	57.6	58.3	58.3	58.1	58.0+/-0.3
700 Hz	58.1	57.5	57.6	57.9	58.7	57.8+/-0.2

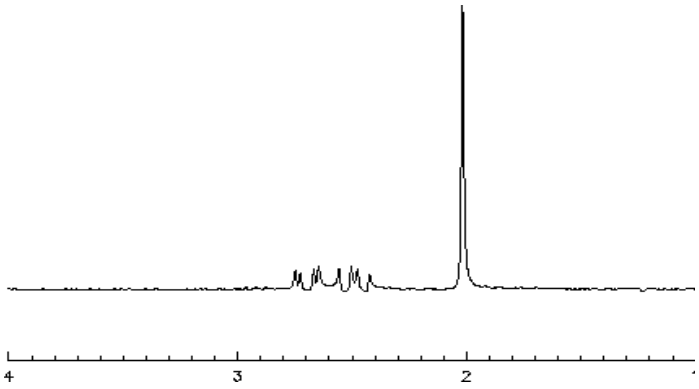

Fig.3.3-1 NAA spectrum measured with optimally timed pulse sequence (PRESS), TE = 20 ms, with water suppression. Zero order phase correction was performed in time domain. No post-acquisition first order phase correction was performed.

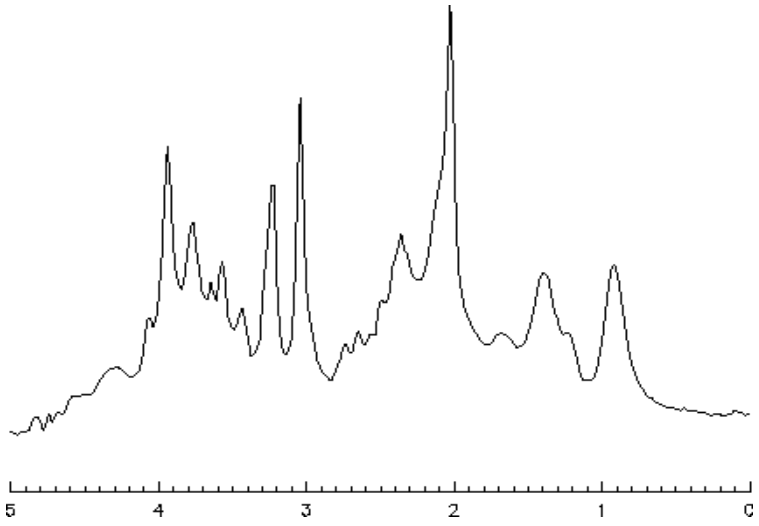

Fig.3.3-2 *In vivo* spectrum of rat brain measured with the same pulse sequence as in Fig.3.3-1. Water residues around 4.7 ppm were removed by the Matrix Pencil based method. Only zero order phase correction was performed in time domain automatically.

3.4 Experimental elimination of frequency modulation sidebands

3.4.1 Introduction

One of the special problems associated with proton MRS acquired without water suppression is that there are strong artifacts on both sides of the unsuppressed water signal. The striking characteristics of the artifacts are that they are located symmetrically but with antiphase around the water signal, thus often termed as sidebands. The sidebands appear in a frequency range from less than 100 Hz up to several hundred Hz, overlapping with the metabolite signals, and their intensities can be larger than metabolite signals *in vivo*. Observed in the frequency domain, the artifacts cause severe baseline and lineshape distortions. Fig. 3.4.1 shows a typical localized water unsuppressed proton spectrum measured on a phantom of NAA of nominal concentration of 100 mM. As can be seen from the figure, the signals of metabolites *in vivo*, with concentrations in the order of mM, would be smaller than the artifacts. Therefore, the artifacts constitute obstacles to spectral analysis and quantification.

In the first measurement of proton MRS without WS, Hurd et. al. [Hurd98] introduced a 2D method to avoid the baseline artifacts in the spectrum. Based on F1 oversampled J-resolved spectroscopy,

this method was able to separate metabolite signals from the artifacts. While the artifacts were removed from the spectrum sampled even at short echo time (TE = 35 ms), spectral analysis being thus possible, the measuring time was too long, making it impractical for its application to MRI [Clay00]. Another approach to circumvent the problem of baseline artifacts is to acquire spectra at very long TE when the artifacts decay to a level that can be ignored, as did by van der Veen et. al. [Veen00], where TE = 288 ms was used. While indeed the spectra thus obtained were free of artifacts associated with unsuppressed water signal and free of general baseline problems of other sources, severe spectroscopic information losses and low SNR were the consequences. As a result, only three prominent singlets of NAA, Cr and Cho could be analyzed, and the measuring time was increased dramatically in order to reach sufficient SNR for reliable spectral analysis.

Recently, the sources of the sideband artifacts were identified [Wu00]. The activation of gradient pulses induces acoustic vibrations of the gradient coils, which in turn induce fluctuations of the main magnetic field or a time dependent magnetic field superimposing the static field. The time varying magnetic field produces a frequency modulation (FM) on the FID signal, and the resulting signal can be mathematically modeled as,

$$S(t) = \left(\sum_{k=1}^{K} a_k e^{i\omega_k t - \alpha_k t}\right) e^{i\sum_{m=1}^{M} c_m \cos(\omega_m t)} = S_0(t) e^{i\sum_{m=1}^{M} c_m \cos(\omega_m t)} \qquad \text{Eq. 3.4-1}$$

where $S_0(t)$ is the original and artifact free time domain signal, ω_m is the modulation frequency and c_m is the modulation index, and K and M are the total number of signals and the total number of modulation frequencies. The modulation indices describe the strengths of the modulation.

Recently, two software approaches have been developed to remove the sideband artifacts [Serr01b] [Elli01]. In [Serr01b], the modulus of the frequency modulated FID was calculated, from which a sideband-free analytic signal was obtained by Hilbert transform. Though this approach is very robust and easy to implement, it has two major shortcomings: (i) By taking the modulus of the complex FID, thus canceling the artifacts, the metabolite signals in the low field region with respect to water [Govi00] were also reflected to the high field region mixing up with the spectra of interest, causing potential problems for spectral quantification; (ii) The SNR was reportedly reduced by 18% [Serr01b], though the simulation results showed more than 40% decrease. An SVD based method was used in [Elli01] to model the sidebands in low field region and to subtract them from the high filed region, by making use of the phase property of the first order sidebands. The problems with this approach are that the sidebands may not be modeled completely while the metabolite signals in low field region may also be modeled. As a result, a considerable amount of residues of the sidebands still remains after applying this method.

An experimental approach is developed in this thesis based on the sources [Wu00] and the characteristics of the FM artifacts. As illustrated in Fig. 3.4.2, a carrier signal, with a zero frequency in this example, is frequency modulated by a signal of 150 Hz. A series of modulation sidebands occur symmetrically around the carrier signal, located at integer multiples of modulation frequency. The pairs of odd order sidebands are antiphase and the pairs of even sidebands are in phase on both sides of the carrier signal. The intensities of the sidebands are proportional to the intensities of the carrier signals and decrease rapidly with the orders of sidebands. In localized proton spectra, the apparent artifacts arise from the dominant first order frequency modulation sidebands, but one should keep in mind that the second order sidebands also contribute to the artifacts.

Understanding the relations between the frequency modulation artifacts and their sources leads to the development of an experimental method to eliminate the artifacts. The phases of FM artifacts are coherent to the phases of the gradient pulses [Clay99] [Dong02]. If the phases of the gradient pulses are inverted, the phases of the artifacts will be also inverted, while the phases of the signals remain the same. By measuring the spectra with positive gradient pulses and negative gradient pulses and adding up the two measurements, the artifacts are cancelled while the metabolite signals are accumulated. However, satisfactory artifact cancellation cannot be reached in general with this simple approach. In the present work, factors affecting the performance of the cancellation were investigated and corresponding approaches leading to perfect cancellation of the artifacts were developed. The following sections describe the detailed approaches and show the efficiency of the developed method for perfect artifact cancellation in both phantom and *in vivo* experiments.

3.4.2 Refocusing gradients

A typical pulse sequence with PRESS localization is shown in Fig. 1.4.4. The gradient pulses in solid lines are slice selection and refocusing gradients. The pulses in dashed lines are spoiler gradients to crush the unwanted signals from outside of the voxel. If this pulse sequence is the positive gradient pulse sequence, the one with negative gradients is obtained by inverting all the gradient pulses. In principle, the gradient induced sidebands can be eliminated if the signals measured with positive gradients and negative gradients are added. However, the results are usually far from satisfactory. Fig. 3.4.3. shows a result of such a simple approach. The spectrum on the top of the figure is the combination of the spectrum with positive gradients (at the bottom) and the spectrum with negative gradients (in the middle). Large residues are seen resulting from the incomplete cancellation of the artifacts. To investigate the source of the problem, the time domain signals of the two measurements are displayed in Fig. 3.4.4. These figures show that:

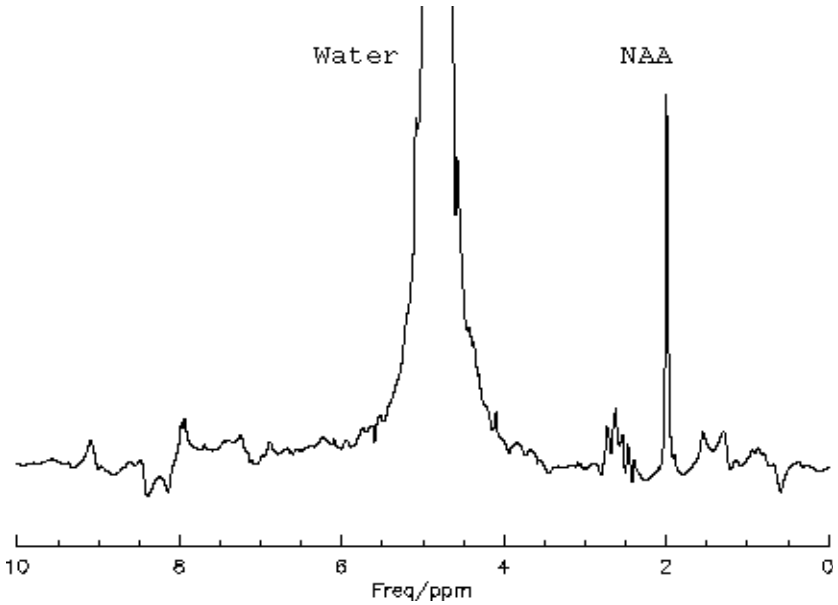

Fig. 3.4-1 A localized water unsuppressed proton spectrum measured on NAA solution with nominal concentration of 100 mM. The artifacts on both sides of the water resonance distorted severely the baseline and the lineshape of the spectrum. The phases of the artifacts on the high field and the low field sides relative to water signal are in antiphase. Note that in *in vivo* spectra, the intensities of artifacts can be larger than signal amplitudes of metabolites whose concentrations are in the order of mM.

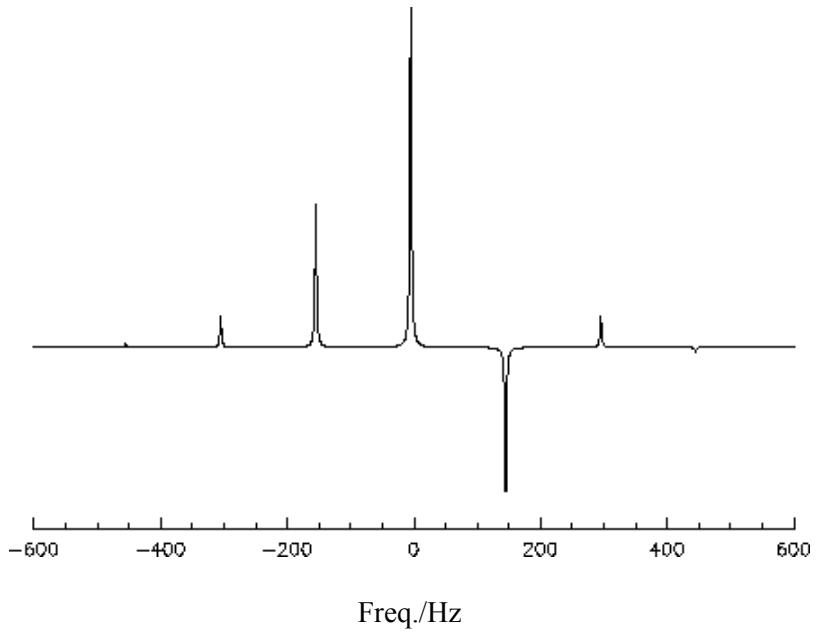

Fig. 3.4-2 Simulated frequency modulation spectrum. A signal, called carrier signal, with zero frequency here, is frequency modulated. The modulation frequency is 150 Hz. Modulation sidebands are located symmetrically at integer multiples of modulation frequency around the carrier frequency. The pairs of odd order sidebands are anti-phase and the pair of even order sidebands are in phase.

1. The amplitudes of the two signals are different.

2. The decay rates and therefore the linewidths are different.

3. There are small frequency shifts between the two signals.

These differences between the dominant water signals measured with positive and negative gradients lead to differences in their artifacts and in turn result in the incomplete artifact cancellations.

The mean reason for the differences of signals measured with opposite gradients is that the spins, which are well refocused with, e.g., positive gradients, may not be well refocused with negative gradients obtained by simply inverting the sign of the positive gradients, because the gradient amplifiers may be not symmetrical for the two cases. Eddy currents [Graa98][Klos90] may also induce different phase and frequency shifts to the FID signals for the positive and the negative gradient pulses, resulting in subtle differences in frequencies and in the opposite phases of the sidebands between the corresponding spectra. For a system equipped with active shielding, the contribution to those differences by eddy currents should be much smaller.

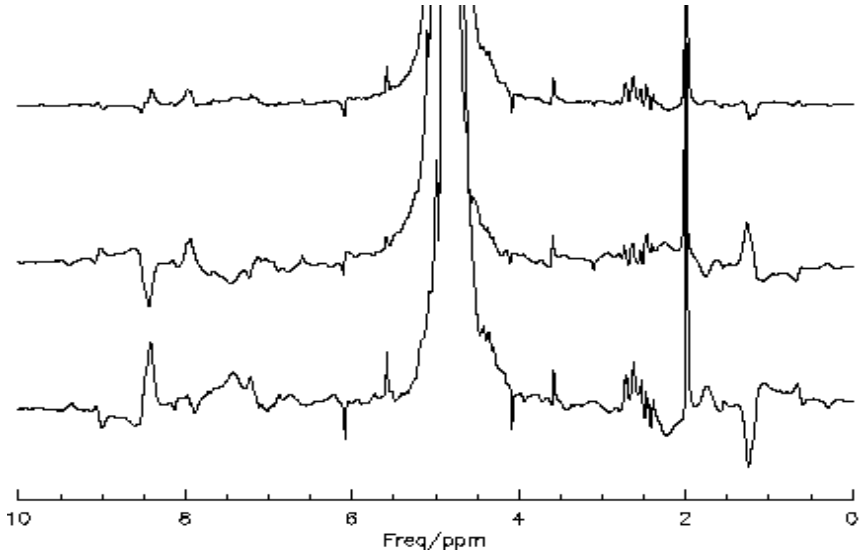

Fig. 3.4-3 NAA spectra measured without water suppression and with positive gradient pulses (bottom), negative gradient pulses (middle). The upper spectrum is the combination of the two, scaled by a factor of 0.5.The experimental parameters are: PRESS, TE = 20 ms, Voxel size = 1 cm^3, NA = 16. NAA concentration = 100 mM, spoiler gradient intensity = 67 mT/m.

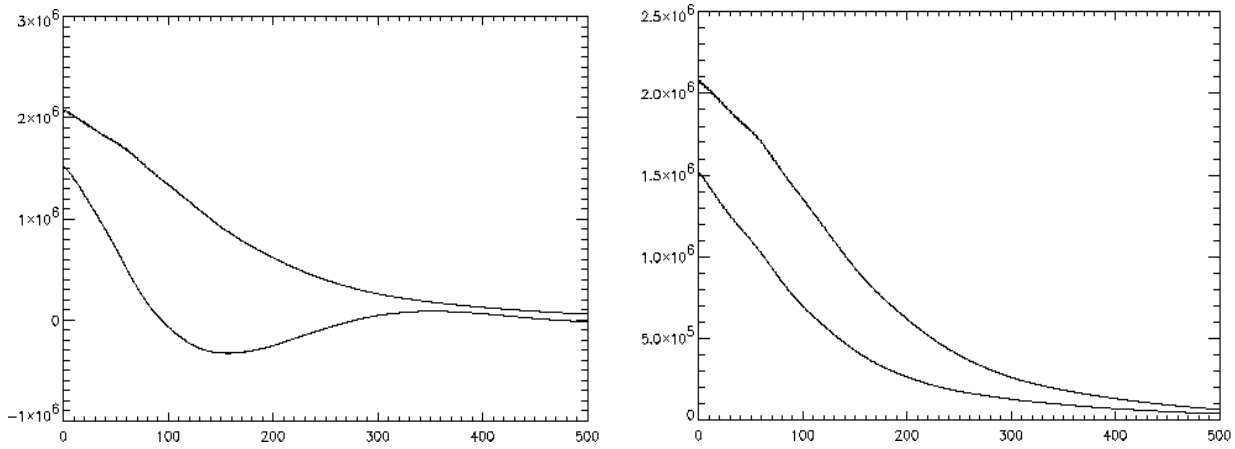

(a) Time/ms (b) Time/ms

Fig. 3.4-4 Real parts (a) of and magnitudes of FID's (b) corresponding to spectra in Fig.3.4-3. In both cases, the upper trace lines are signals measured with positive gradient pulses and the lower trace are with negative gradient pulses. Lines were broadened by 1 Hz.

To address the problem of non-ideal refocusing, the refocusing gradient values for both sequences must be trimmed separately. When both sequences were optimized, the signals would have identical amplitudes and the identical linewidths, as can be expected for a well refocused magnetization, thereby resulting in great improvement in the sideband cancellation. The phase and frequency differences of signals with opposite gradient pulses can be removed by zero phase correction and frequency shift in the post-processing procedures. Fig. 3.4.5 shows the results of trimming of the refocusing gradients. Due to perfect trimming of the refocusing gradients, the magnetization were well refocused in the presence of either positive or negative gradient pulses, leading to identical amplitudes and decay profiles of the FID's (Fig. 3.4.5a). With these identical parameters of the water signals, the corresponding amplitudes, frequencies and decay rates of the FM sidebands would be the same, and the phases would be opposite with the opposite gradient pulses, thus ensuring perfect cancellation of the sidebands (Fig 3.4.5c). As can be easily seen from the flat baseline in the combined spectrum, the residual artifacts are immersed in the noise.

Some remarks should be noted here: (i) Trimming should be made individually for each gradient pulses sequence (timing and spoiler gradients) and for each voxel size. (ii) First order phase errors can be experimentally eliminated by the method described in a previous section otherwise they must be corrected with software before combining the two spectra. The experimental method is recommended. Zero order phase error must be corrected before the spectra are combined. (iii) The trimmings might be rather time consuming, but they need to be performed only once for each pulse sequence and each voxel size and the parameters can be use in subsequent experiments.

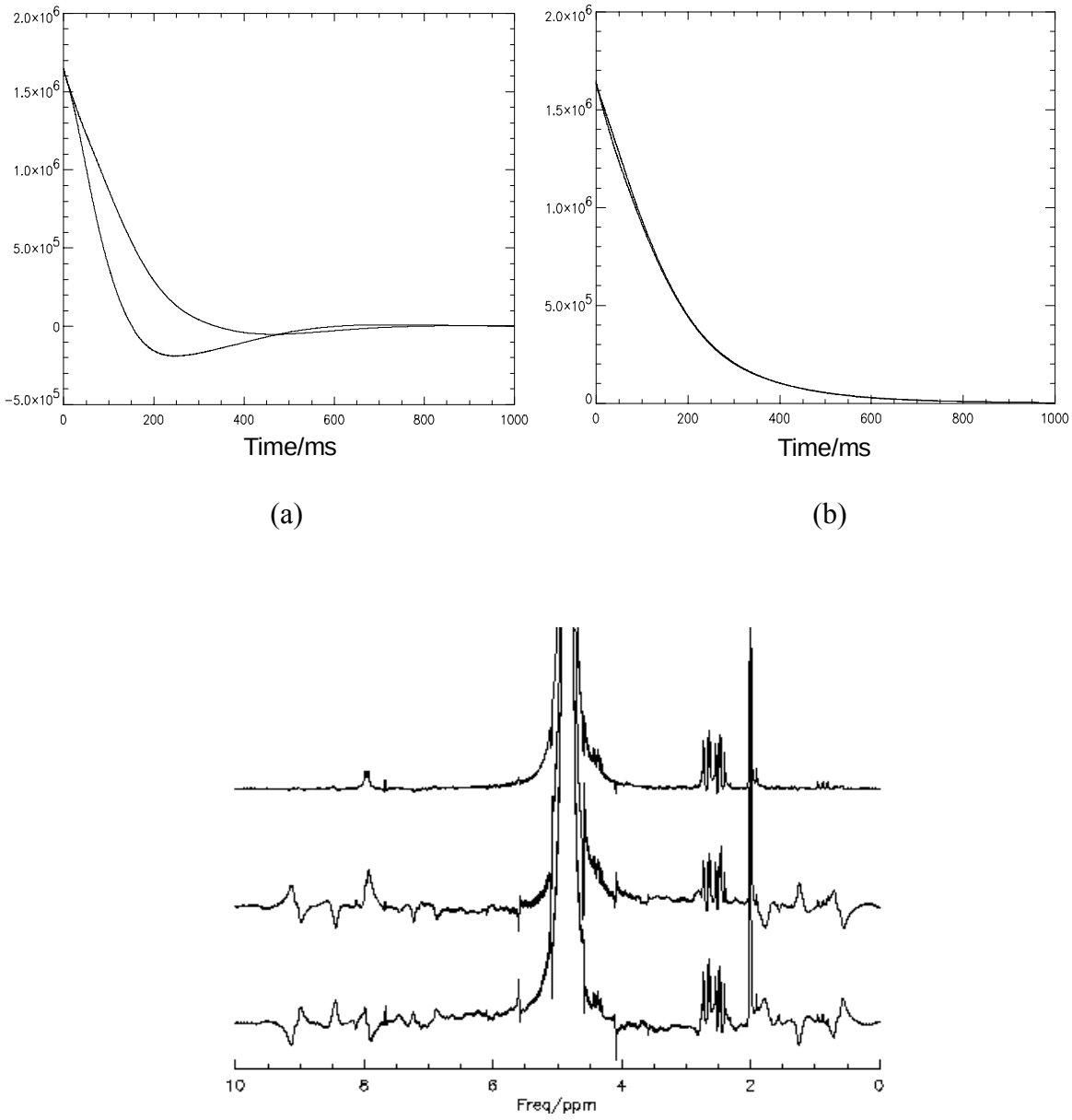

Fig. 3.4-5 Real parts (a) magnitudes (b) of FID's of unsuppressed water signals measured with trimmed refocusing gradients in opposite gradient pulse sequences. Curves in (a) show the identical amplitudes and the identical decay profiles of the FID's. The small frequency shifts in (b) can be corrected in the post-processing procedures. (c) shows the spectra measured with positive gradients (lower trace), with negative gradients (middle trace) and the combination of the two (upper trace) scaled by a factor of 0.5.

3.4.3 Gradient strength/orientation dependencies of FM sidebands

In this section, the gradient strength/orientation dependencies of the FM sidebands are investigated, aiming at the objective to further reduce the residues of the sideband artifacts. The idea is that, if the

sidebands themselves are reduced, their residues would be eliminate even further.

The investigation of gradient strength dependency is straightforward: varying the strengths of the spoiler gradient pulses and observing the intensities of the FM sidebands. Fig.3.4-6 shows spectra obtained with spoiler strengths of 67 mT/m and 34 mT/m, respectively. The intensities of sidebands with smaller spoiler gradient strengths are reduced by half of the intensities with stronger spoiler gradients. If other conditions were the same for both strengths, the residues of artifacts of the smaller spoilers would be reduced accordingly after cancellation.

However, the strength of spoiler gradients cannot be reduced at will, otherwise the unwanted signals could not be destroyed completely. The strength of 67 mT/m was necessary to eliminate the unwanted signals. The spectrum with 34 mT/m spoiler gradients in Fig. 3.4.6 was obtained with the help of a 16-step phase cycling to eliminate the remaining unwanted signals.

In order to test the possibilities of reducing the artifact intensity without leaving unwanted signals, the gradient orientation dependencies of FM artifacts were investigated. To this end, the spectra were measured with spoiler gradients in one direction each time, and the artifacts were compared. The results are shown in Fig.3.4-7. As can be seen from the figure, the intensities of artifacts induced by spoiler gradients in x and y directions (lower and middle traces) are larger than the artifacts by spoiler gradients in z direction (upper trace). The intensities of artifacts induced by x and y spoilers are similar, as the x and y directions are symmetric with respect to z direction in which the main magnetic field lies. The spectra of the artifacts are different for gradients pulses in different directions.

These findings provide some guidelines to improve the pulse sequence. In order to reduce the intensities of the artifacts, the strengths of spoiler gradients in x and y directions could be reduced while the strength of z direction spoiler gradients should be increased to compensate the x, y spoilers to destroy the unwanted signals.

3.4.4 Optimization

Spoiler gradients are used to crush the unwanted signals from outside of the voxel in the localized MRS. However, they are the main sources of FM artifacts proton MRS without water suppression. Another approach to eliminate unwanted signals is using phase cycling [Henn92], [Roel01]. In this section, all spoiler gradient pulses are removed from the pulse sequence, and instead a 16-step phase cycling is used to eliminate the unwanted coherences.

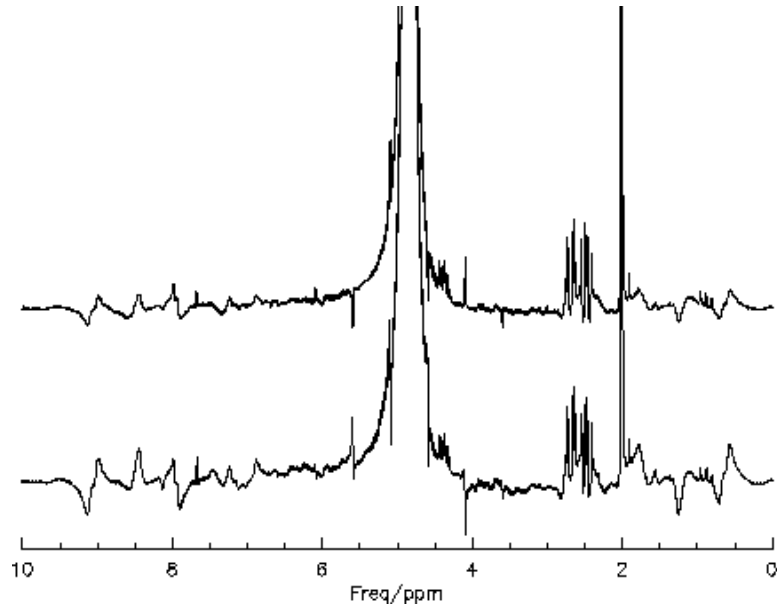

Fig.3.4-6 Water unsuppressed spectra with spoiler gradient strengths of 67 mT/m (lower trace) and 34 mT/m (upper trace). The refocusing gradient pulses were trimmed separately for each spoiler strength. A 16-step phase cycling was used to eliminate the remaining unwanted signals in the case of smaller gradient pulse strength. Other parameters were the same.

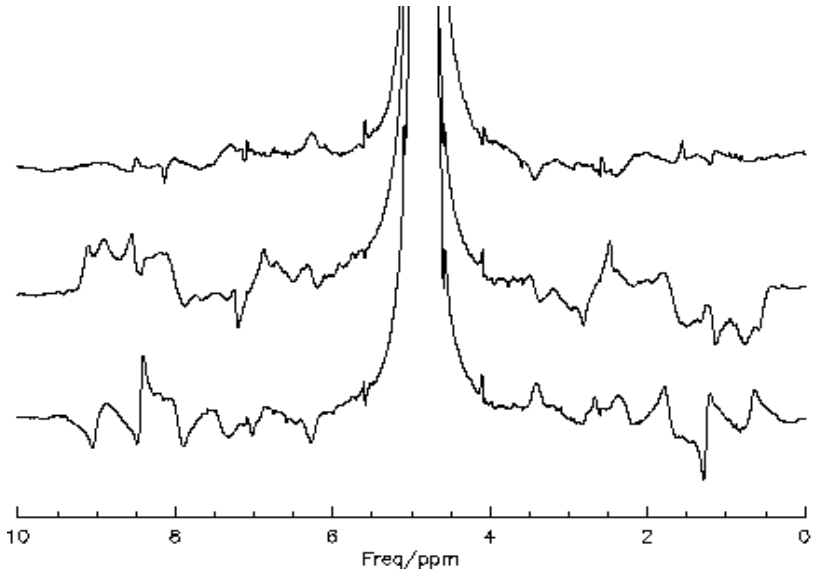

Fig. 3.4-7 Artifacts in spectra of pure water measured with spoilers in direction x (lower trace), y direction (middle trace) and z direction (upper trace). The strength of spoiler gradients is 67 mT/m. The main magnetic field is in z direction. The interval between the spoiler gradient pulses and the acquisition time are the same in all cases.

The procedures of implementing the phase cycling scheme is as follows: (i) Remove all spoiler gradient pulses, including WS spoilers, from the sequences; (ii) Trim the refocusing gradients for the positive and the negative gradient pulse sequences; (iii) Acquire signal with the 16-step phase cycling and with the number of acquisitions which equals an integer multiple of 16.

Phantom and *in vivo* experiments were conducted to test the method. Phantom experiments were made on the NAA solution of nominal concentration of 100 mM. Fig.3.4-8 displays the spectra measured without spoiler gradients and with/without phase cycling. Artifacts of unwanted signals in the spectrum measured without phase cycling are seen in Fig.3.4-8a, while they were removed by the 16-step phase cycling as can be seen from Fig.3.4-8b. Most of the sideband artifacts induced by gradient pulses are removed from the spectrum, leaving very flat baseline. The equidistant narrow spurious peaks around the water resonance are the residues of frequency modulation sidebands caused by the odd order harmonics of 50 Hz industrial frequency. As the changes of the phases and the frequencies of the modulation signals are not purely random, it is difficult to average out the sidebands by a limited number of signal accumulations. However, in principle, the sidebands can be eliminated experimentally by using the modulation signals to trigger the delay cycling acquisitions, if the sources of the these signals are found and the signals are picked up by a sensor.

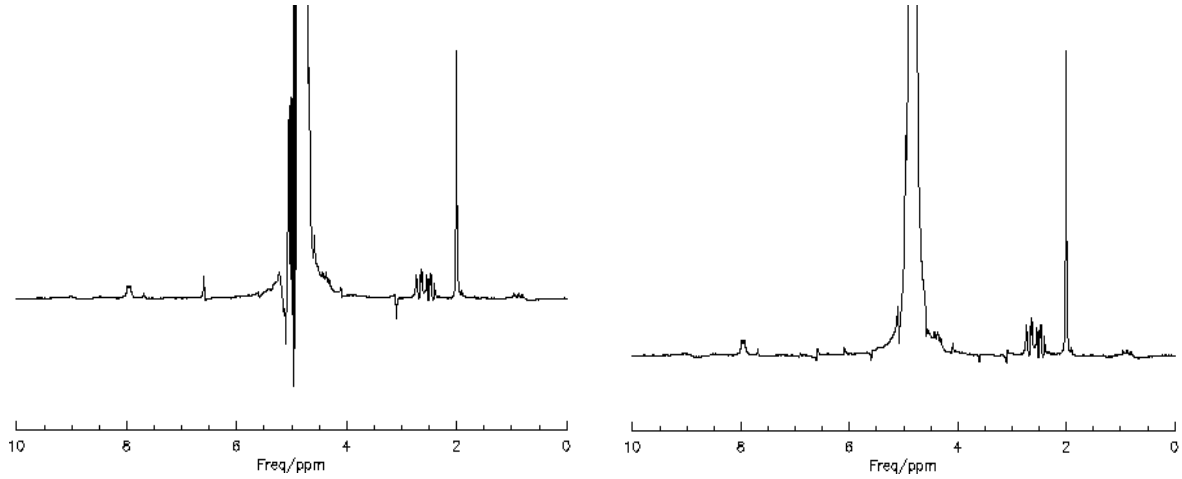

(a) (b)

Fig.3.4-8 Water unsuppressed proton MRS of a NAA phantom measured without spoiler gradient pulses and without phase cycling (a), and with a 16-step phase cycling (b).

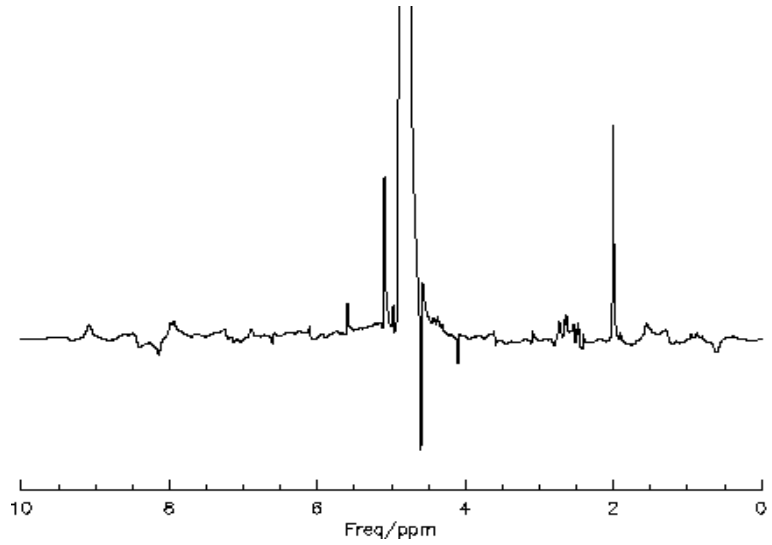

Fig. 3.4-9 Water unsuppressed spectrum of NAA measured with spoiler gradients (PRESS, spoiler gradient strength = 67 mT/m).

The suppression of unwanted signals by phase cycling can be evaluated by comparing the spectra obtained with phase cycling (Fig.3.4-8b) and with spoiler gradients (Fig3.4.9). Fig.3.4-9 shows a spectrum measured with spoiler gradients but without phase cycling. Though the unwanted signals were suppressed by the spoilers, severe artifacts caused by the gradient pulses are still present[2]. The dominant water resonances in Fig.3.4-8b and Fig.3.4-9 show the same profiles and identical amplitudes, manifesting the efficiency of the phase cycling approach in eliminating the unwanted signals. The advantages of the phase cycling approach is evident in comparison with the spoiler approach as the spectrum in Fig.3.4-8b is virtually artifacts free (only refer to the sidebands caused by gradient pulses), especially in the spectral region of interest. This is because only slice selection gradient pulses, whose intensities are much smaller than the spoiler gradients, contribute to the sidebands in the phase cycling scheme.

The artifacts induced by the slice selection gradients can be eliminated further by combining the spectra measured with opposite pulse sequences. This is demonstrated by spectra in Fig.3.4-10.

The performance of this optimization is better demonstrated by comparing the spectrum obtained without spoiler gradients and spectrum obtained with WS. To this end, the water signals in the non-water suppressed spectra and the water residue in the water suppressed spectrum were removed in the post-acquisition procedure by MPM. Fig.3.4-11 displays the results. First, a very flat baseline is

[2] *The 50 Hz problem happened to be more pronounced in this spectrum.*

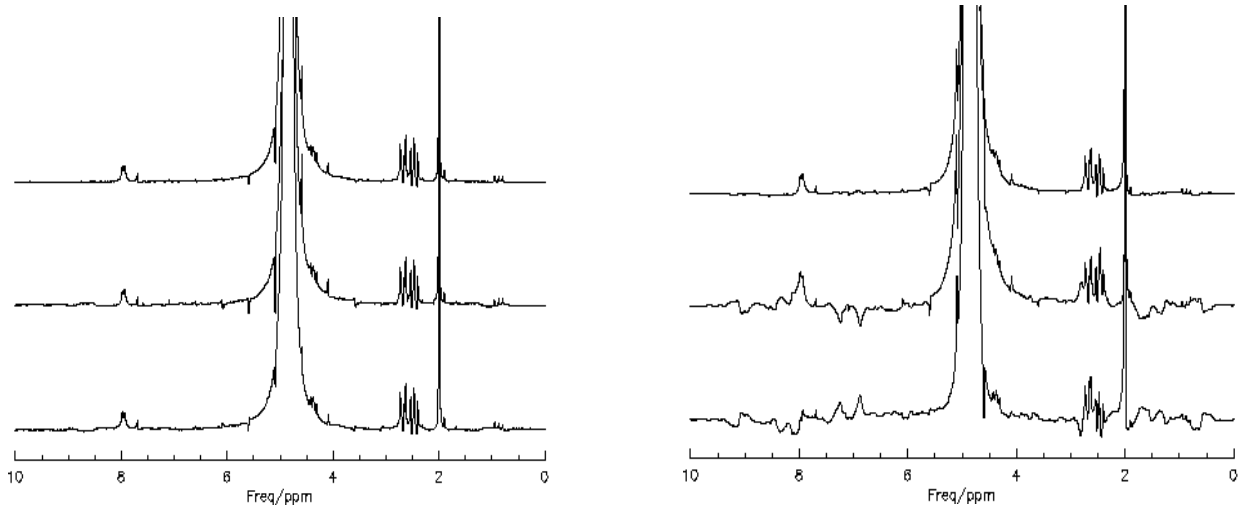

(a) (b)

Fig. 3.4-10 Water unsuppressed spectra of the NAA solution (100 mM) measured without spoilers (a) and with spoilers (67 mT/m). In both a and b, spectra from bottom to top are: with positive gradient pulses, with negative gradient pulses and the combination of the two.

seen in the spectrum with spoiler gradients (b). By close examination, very small residual artifacts can be seen around 1 ppm and 9 ppm. These small residues were eliminated completely by the phase cycling approach as seen in Fig.3.4-11a. In both spectra there exist some equidistant spurious peaks induced by higher order 50 Hz harmonics, which can be removed either by MPM based method described in section 3.2 or by some hardware approaches. Apart from this, the baseline of the spectrum in Fig.3.4-11a is perfectly as flat as the baseline of the spectrum acquired with WS in Fig.3.4-11c. Fig.3.4-11c shows that the J-coupled lines from the lactate CH proton at 4.4 ppm were partially saturated by the water suppression pulses, while in the water unsuppressed spectra these lines remain intact.

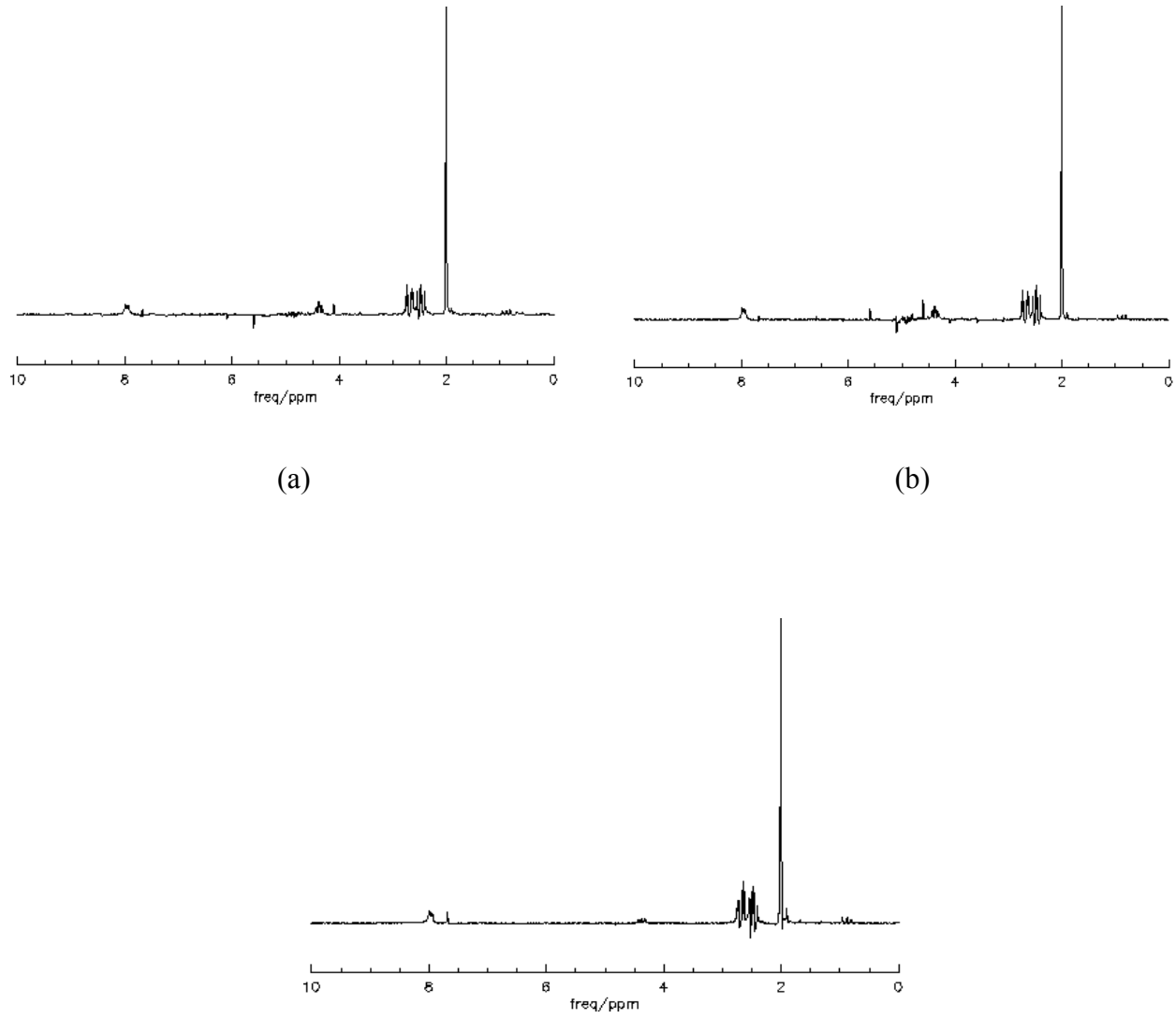

Fig. 3.4-11 Water unsuppressed proton spectra acquired without spoiler gradients (a) and with spoiler gradients (b, spoiler = 67 mT/m), and spectrum with water suppression (c). The water signals in a and b and water residues in c were removed by Matrix Pencil Method. Water signal occurs at about 4.85 ppm. The same receiver gain was used for measurements with or without WS.

The application of the optimized method to *in vivo* measurements was conducted on rat brain. Fig.3.4-12 displays spectra measured without WS and without spoiler gradients. The efficiency of the method is better demonstrated by comparing the water unsuppressed spectrum with water suppressed spectrum as shown in Fig.3.4-13. For a better comparison, the water resonance in the water unsuppressed spectrum (Fig.3.4-13a) and the water residues in water suppressed spectrum (Fig.3.4-13b) were removed. The baseline in Fig.3.4-13a is as flat as that in Fig.3.4-13b, which is intrinsically sideband free, and the lineshapes in both spectra are identical. We thus conclude that the spectrum in Fig.3.4-13a is virtually artifacts free.

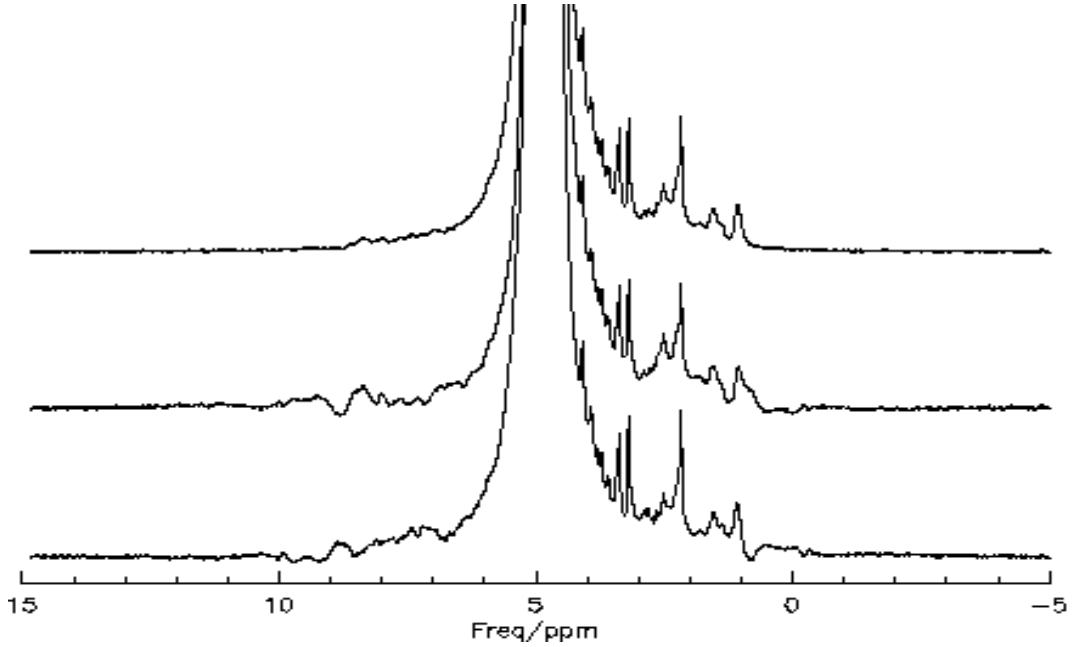

Fig. 3.4-12 *in vivo* proton spectra measured without water suppression and without spoiler gradients. From bottom up are the spectra measured with positive pulse sequence, with negative pulse sequence and the combination of the two. A 16-step phase cycling was used to suppress the unwanted signals. Other experimental parameters include: PRESS localization, voxel size = 4*4*4 mm^3, SW = 4006 Hz, TE = 20 ms, TR = 1.5 s, NA = 256, FWHM = 9.5 Hz for water resonance, 2 Hz line broadening was applied on the displayed spectra.

Note from Fig.3.4-13a, there exist metabolite signals in the lower field close to water. These signals might be modeled by the software method [Clay01] and added to the high field region causing quantification errors. With the presented method, this error is avoided.

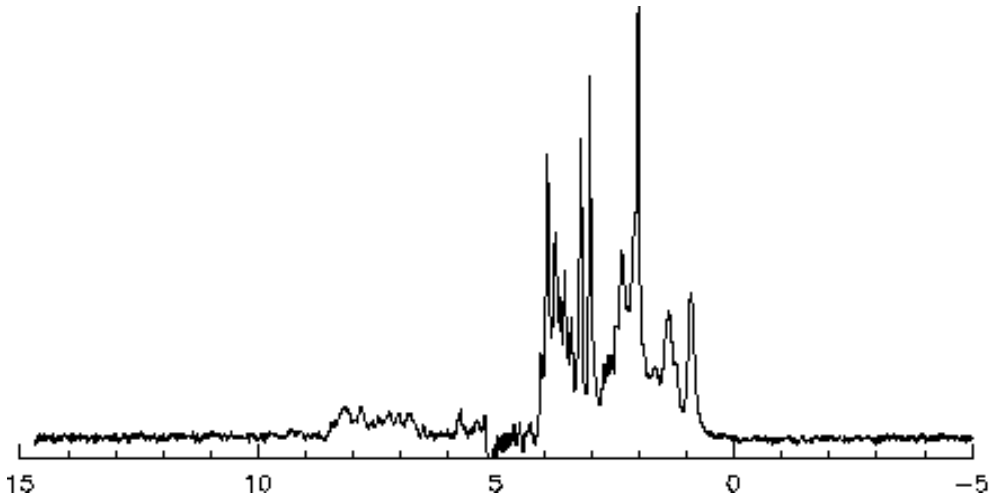

freq./ppm

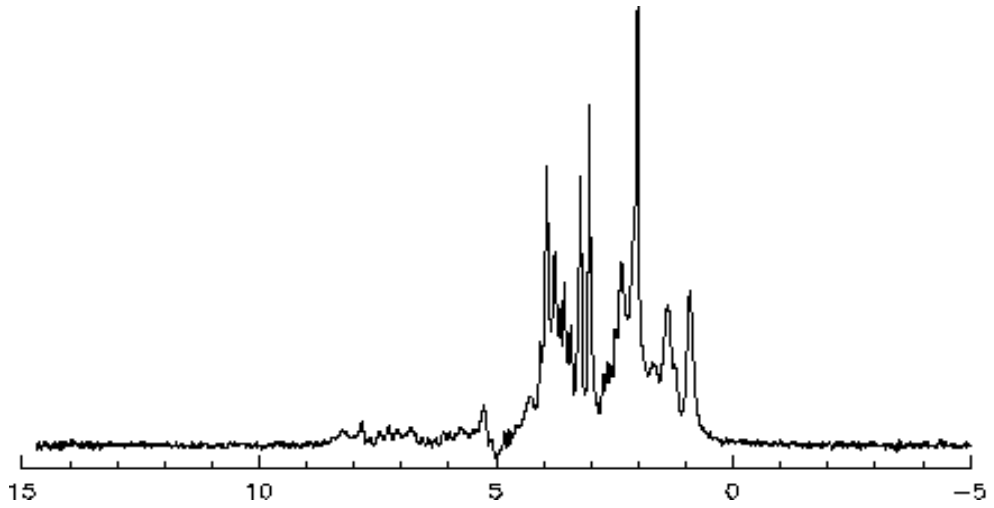

(b) freq./ppm

Fig. 3.4-13 *in vivo* proton MS measured on rat brain without WS (a) and with WS (b), the water signal in a and water residues in b were removed by MPM. A 16-step phase cycling was used in both measurements. No spoiler gradient was used for water unsuppressed measurements. CHESS was used for water suppression. Other experimental parameters include: PRESS localization, voxel size = 4*4*4 mm^3, TE = 20 ms, TR = 1.5 s, NA = 512. Receiver gain was kept the same for both measurements.

3.5 Spectral simulation

Spectral simulation is becoming an important tool in NMR methodological developments and NMR

applications. There are numerous computer softwares, both programs and libraries, for simulating NMR spectra or NMR experiments[3]. In the present work, a C++ library, GAMMA. [Smit94], was used to simulate PRESS spectra.

3.5.1 GAMMA library

GAMMA is a library of C++ functions written by Smith et al [Smit94] for the simulation of NMR experiments. These functions describe NMR systems, simulate operations of NMR experiments and perform various complex signal calculations and processing, allowing to simulate a variety of NMR experiments.

The basic steps to program with GAMMA for spectral simulation are as follows.

1. Define the NMR system. This includes specifying the number and types of spins, chemical shifts and J-coupling constants and the spectrometer frequency.
2. Define the pulse sequence. This includes specifying the pulse shapes, phases, durations, flip angles or strengths, offsets, channels and delays.
3. Write simulation programs. This includes tree parts. (i) Initializations: reading in system file, setting up parameters and variables, and defining pulses; (ii) Implementations of operations: application of pulses, system evolution under Hamiltonian; (iii) Data acquisition: acquisition channel, dwell time, number of points, apodization, output format,....
4. Compile and execute the simulation program.

This GAMMA software is free and the source codes, examples and user manuals can be obtained from the WWW at http://gamma.magnet.fsu.edu.

3.5.2 Prior knowledge and spectral simulation

Prior knowledge of proton NMR chemical shifts and J-coupling constants of metabolites in the brain are needed for the spectral simulation. The prior knowledge used was mainly from the literature [Govi00] based on high resolution phantom spectra measured at high field with the same conditions of normal physiological temperature and pH value. The chemical shifts and J-coupling constants were obtained by direct measurements of the spectra and by optimizing the obtained values with a spectral simulation and optimization program. The chemical shift values for D-

3: such as WWW.biochem.ucl.ac.uk/~salek/NMR_software.htm, bmrl.med.uiuc.edu:8080/edusoft.html and WWW.organil.uni-erlangen.de/research/NMR/software.html.

Glucose and NAAG in H_2O were not available from the literature, but the values in D_2O were used instead.

The PRESS sequence used in the model simulations is illustrated in Fig.3.5-1, where the slice selective pulse is an hb_Lurie pulse [Luri85] with τ_1 = 1.5 ms duration. The two refocusing π pulses are Mao_6 pulses [Mao88] with τ_2 = 2.5 ms duration. t_1 = 2 ms.

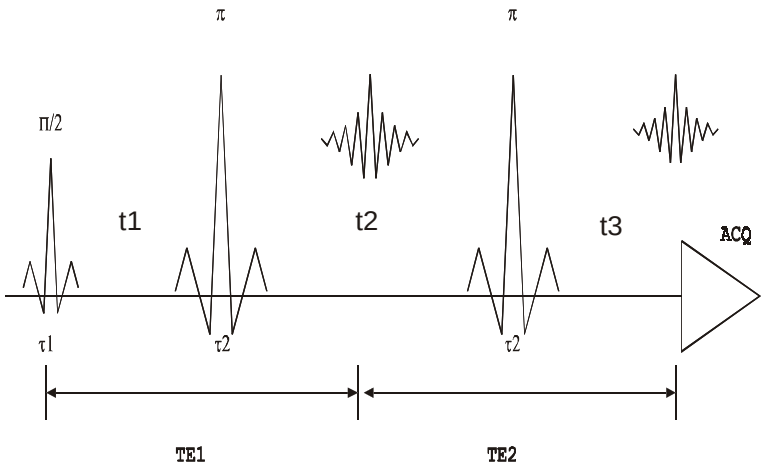

Fig. 3.5-1 PRESS sequence used for the spectral simulation.

No gradient pulses, phase cycling and data accumulation were used in the simulation. The dwell time and system frequency were the same as the *in vivo* experiments. Acquisitions started exactly at the top of the echo.

No relaxation mechanism was involved in the simulation because no complete prior knowledge of relaxation rates was available for all spins. However, the FIDs were apodized by an exponential function corresponding to 1 Hz Lorentzian linewidth. Not incorporating relaxation in the spectral simulation has the advantage that the signal amplitudes of the model signal do not change with the TE's, which simplifies the scaling of the estimated amplitudes in the signal fitting.

The digitized FIDs were the outputs of the spectral simulation and were saved in files specified for each metabolite.

The computing time of the simulation increases dramatically with the number of spins in the compound. For compounds with more than 10 spins, the computing time would be prohibitively long. To speed up the simulation, the spins were divided into coupling groups and their spectra were simulated separately. The total spectrum was then obtained by adding spectra from all groups together.

The signal amplitudes of the simulated spectra are not proportional to the number of spins involved

in the simulation. It was found that if the spins are all protons, then the signal amplitude is related to the number of spins by,

$$a = n \cdot 2^{n-2}, \; n \geq 2. \qquad \text{Eq. 3.5-1}$$

If other spins, such as ^{14}N and ^{31}P, are coupled to protons and are involved in the spectral simulation, the above relation no longer holds. For example, the amplitude of the simulated signal of four ^{1}H and one ^{14}N is 48 (a.u.) instead of 40. The signal amplitudes of these mixed systems were determined from the signals simulated with the ideal one-pulse-FID, where no amplitude modulation due to J-coupling effects occurred.

The simulated signals were normalized to their number of spins involved in the simulations for the purpose of spectral quantification.

3.5.3 Examples

Model signals were simulated for nearly 20 metabolites with significant spectral contributions to the *in vivo* MRS. Some of the simulated spectra are given as examples in Fig.3.5-2. The simulation parameters are: Spectral width = 4006 Hz, number of complex data points = 4096, system frequency = 200 MHz (4.7 Tesla), pulse sequence: PRESS, TE = 20 ms. 2.5 Hz linebroadening was applied to the simulated signals for display in the frequency domain.

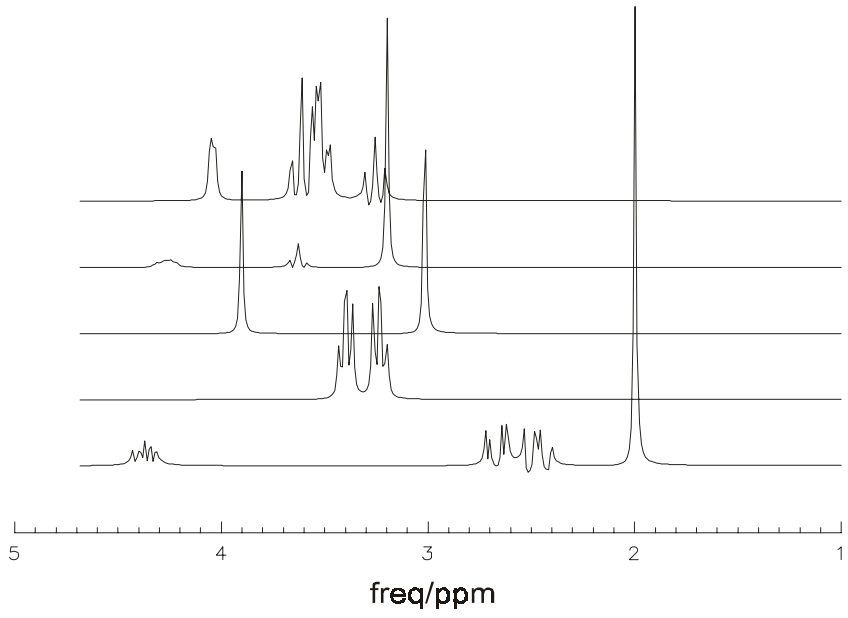

Fig. 3.5-2a Simulated spectra (from top to bottom): Ins, PCh, Cr, Tau and NAA.

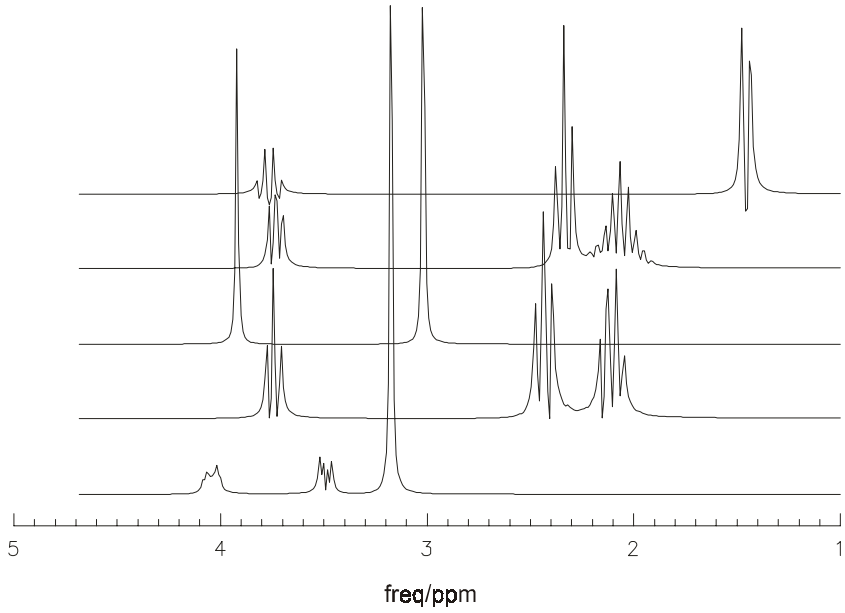

Fig. 3.5-2b Simulated spectra (from top to bottom): Ala, Glu, PCr, Gln, Cho.

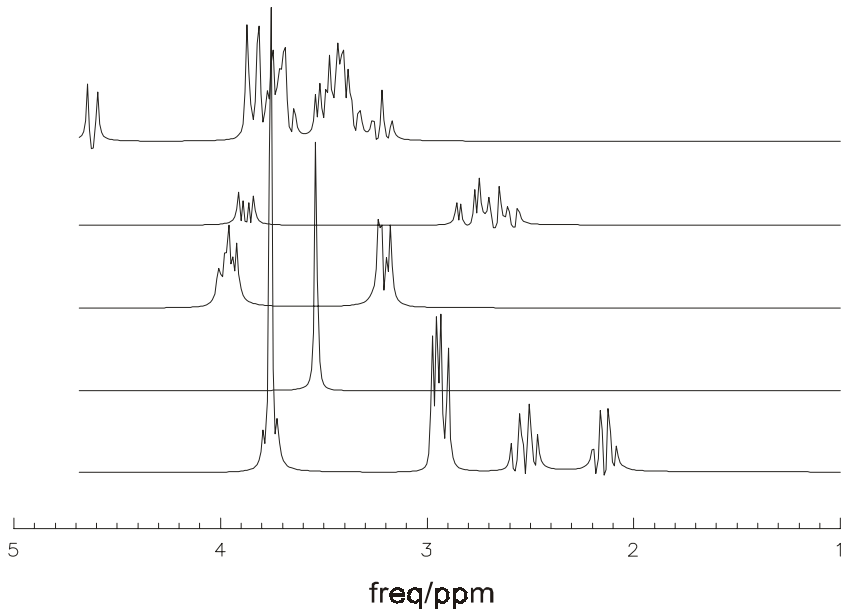

Fig. 3.5-2c Simulated spectra (from top to bottom): Glc, Asp, PE, Gly, GSH.

To demonstrate how well the spectra were simulated, some of the simulated spectra are compared with the measured phantom spectra. Fig.3.5-3 shows the overlaid simulated and measured spectra of Tau, NAA and Ins. As can be seen, the Tau spectrum was very well fitted with the simulated spectrum. The CH_3 and CH_2 peaks of NAA were very well fitted, but the CH proton was not fitted well, because the measured peaks were partially saturated by the WS pulses and because the

simulated spectrum, instead of each individual peak, was used as a whole in the spectral fitting.

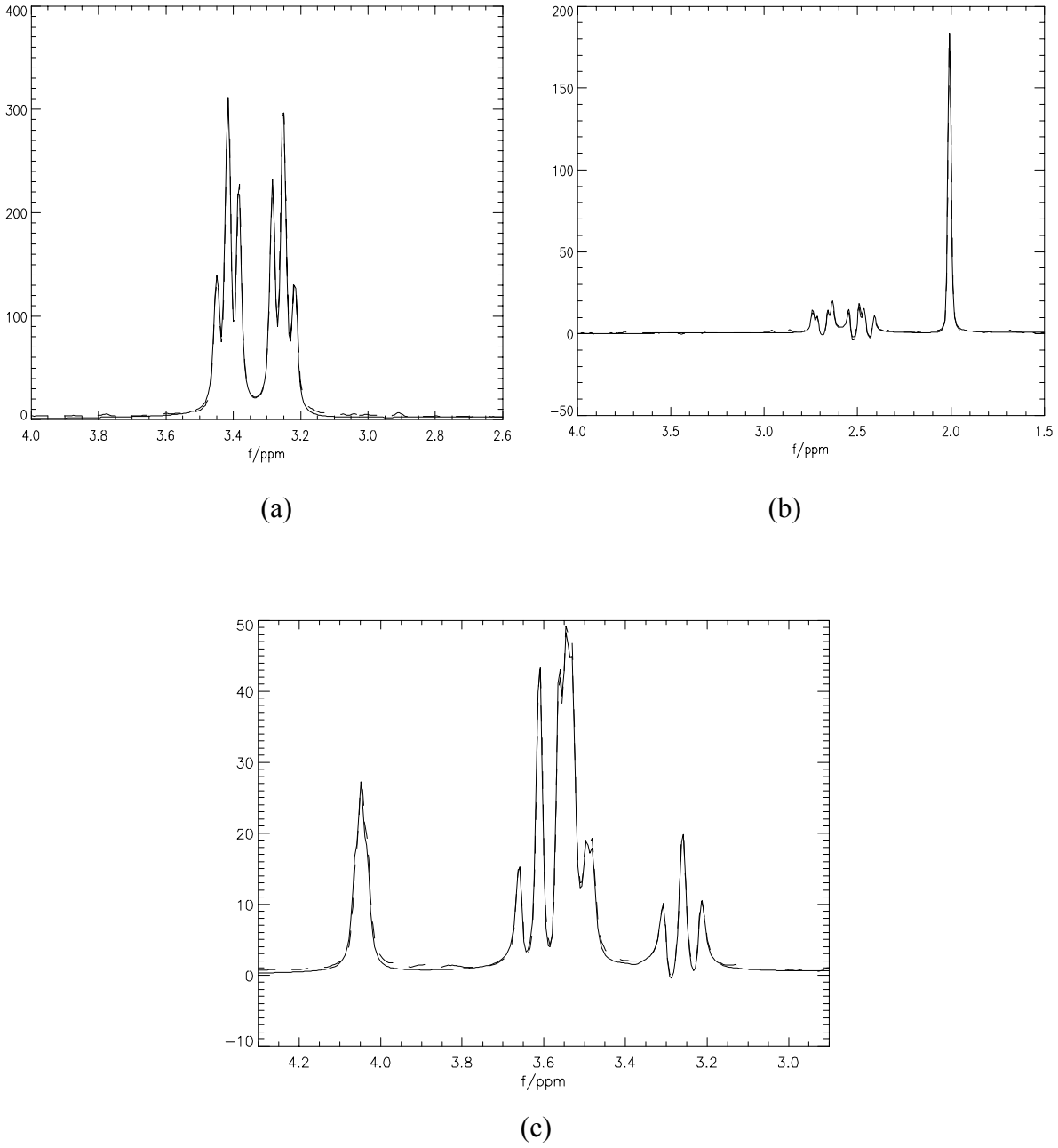

Fig. 3.5-3 The measured phantom spectra overlaid with the simulated spectra of Tau (a), NAA (b) and Ins (c).

The Ins spectrum was fitted well in general, but with a few subtle discrepancies, which may be due to the relaxation differences among the resonances of the measured spectrum.

3.5.4 Discussion

Compared with the traditional method of obtaining model spectra by measuring model solutions of metabolites in phantom experiments, the simulation method is faster and, time and cost saving. For a compound with less than 6 spins, the simulation of a spectrum took only several minutes on an AMD K7 1200 MHz computer. While it would take hours for a similar phantom experiment, preparing the sample, adjusting experimental conditions and acquiring data. The spectral simulation approach is more reproducible and less user dependent as the simulation results depend only on the limited simulation parameters and will be exactly the same in the repeated simulations if the parameters are identical. On the other hand, the phantom experimental results, such as signal amplitudes, frequencies and linewidths, would vary in the repeated experiments even with the same experimental parameters simply due to factors such as system instability and temperature differences. These variations would further cause extra work in signal calibration and amplitude conversion in the spectral quantification procedure. Another advantage of spectral simulation is that the simulation provides ideal spectra free of noise and free of all kinds of distortions, which will benefit the accuracy of metabolite quantification.

The accuracy of the simulated spectra depends on the accuracy of the prior knowledge of chemical shifts and J-coupling constants deduced from phantom measurements of the metabolite solutions. Possible sources of errors of the prior knowledge are related to different experimental conditions between the phantom and the *in vivo* measurements, and to the postprocessing procedures of extracting spectral parameters from the measured signals [Govi00]. For example, the differences in pH values, temperatures between the phantom experiments and *in vivo* experiments will inevitably introduce spectral differences, mainly in the chemical shifts. These differences will cause quantification errors if the whole model spectra, instead of individual lines, are used in the spectral fitting. However, the errors thus introduced should be very small because the linewidths of the *in vivo* spectra are much larger than the chemical shift differences of corresponding metabolite spectra in phantom and in *in vivo*. Furthermore, the experimental conditions of measurements for deducing chemical shifts and J-coupling constants can be controlled as good as, if not better than, the experimental conditions for the measurements of model spectra directly used for the spectral quantification. Therefore, no extra errors are added to this approach in this respect in comparison with the other approaches of quantification methods mentioned. The errors introduced from the post-processing procedure in extracting chemical shifts and J-coupling constants depends mainly on the resolutions of the phantom spectra and also sometimes on the J-coupling patterns assumed. The values reported in [Govi00] are believed to be accurate to the order of 4 decimal places as they were determined from high resolution spectra at 500 - 600 MHz. The effects of these errors on the spectral estimation would be very small on the spectra acquired with lower field strengths as used in

the present work of 4.7 T, corresponding to proton resonance of 200 MHz.

No T_2 relaxation mechanism was taken into account in the spectral simulation, implying that all resonances in a spectrum of a metabolite have the same relaxation rate. The example of spectral simulation and spectral fitting shown in Fig.3.3-3c indicate that if there exist different relaxation rates among resonances of a spectrum in either phantom or *in vivo,* ignoring these differences may cause discrepancy in the spectral fitting if the entire simulated spectrum of each metabolite is used as a whole, and thus may introduce errors in spectral quantification. Even if the relaxation were involved in the spectral simulation, it would still have very limited improvement in the spectral fitting of *in vivo* signal. Compared with the case of using *measured model* signals in the spectral fitting, such as the LCModel, [Prov93], the only difference is that in that case the relaxation of the model spectra is carried into the spectral fitting. But the relaxation rate differences of resonances in the model spectra are much smaller than the relaxation rates of the *in vivo* spectra. The gain of including relaxation of the model signal in the spectral fitting is small. Therefore, ignoring T_2 relaxation in the spectral simulations does not cause much disadvantage as compared to using the measured model spectra. The errors caused by the relaxation differences are significant only if the differences are large and the TE's are long. At short TE, the errors should be very small. In the methods proposed by Bartha et al [Bart99] and by Young et al [Youn98], the prior knowledge extracted from the model spectra was used to fit each *individual* resonance independently, but not used to fit the *whole spectrum* of a metabolite. In these cases, the relaxation differences between resonance lines in a compound were taken into account, thereby the possible errors can be avoided.

In conclusion, the simulated spectra showed a high degree of agreement with the measured phantom spectra and thus validated the usefulness and advantages of this approach. The simulated spectra will be used as model spectra for the purpose of spectral quantification of the *in vivo* proton MRS, in place of model signals measured by phantom experiments.

3.6 Baseline characterization by wavelet transformation

In recent years wavelet transform (WT) has arisen as a new signal processing technique finding increasing applications in a variety of fields, such as physics [Berg99], chemistry [Leun98], medicine and biology [Aldr96], electrical engineering [Sark02], and geology and meteorology [Torr97]. Compared with the conventional FT, WT possesses the unique strength in data compression, feature extraction, non-stationary signal characterization, multi-resolution analysis and noise suppression. In the field of NMR, WT technique was used to quantify MRS [Serr97], to

characterize baseline [Youn98] and to denoise NMR signal [Lu97] and MRI [Nowa99].

It is instructive to understand WT by comparing WT with FT. In FT, the data in the original domain are transformed to a new domain with orthogonal basis functions of sines and cosines, and the data are represented by the FT coefficients, which correspond to projections of the original data onto the basis in the new domain. In WT, the original data are transformed into the wavelet domain with basis functions of wavelets, and are represented by the WT coefficients. Any functions satisfying certain mathematical requirements can be used in principle as WT basis functions, different only in their efficiencies in representing the special features of the original signals. Like FT, WT is invertible, which means that original signals can be recovered from the WT coefficients. Unlike FT basis, WT basis are localized in space/time, as well as in scale. This feature offers WT the aforementioned unique properties of representing and analysing signals. Many signals may be very closely represented by only a small number of WT coefficients, making data compression possible. WT may also be used to represent localized features of interest in a signal, making it very efficient in extracting features of signals. The structures and magnitude distributions of WT coefficients, together with the inverse WT (IWT), allow to suppress noise from the signal. In the present work, WT technique was used to characterize the baseline of MRS spectra with a scheme initiated by Young et. al. [Youn98] and to denoise the MR signals.

3.6.1 Wavelet transform

A function $\psi(x)$ can be used as a mother wavelet, if FT$\{\psi(x)\}$ satisfies the following admissibility condition needed for the IWT[Daub92],

$$\int_{-\infty}^{\infty} \frac{|\psi(\omega)|^2}{|\omega|} d\omega < \infty \qquad \text{Eq. 3.6-1}$$

Given the mother wavelet, the set of wavelets are obtained by translation and dilation of the mother wavelet according to the equation,

$$\psi_{a,b}(x) = \frac{1}{\sqrt{a}} \psi\left(\frac{x-b}{a}\right) \qquad \text{Eq. 3.6-2}$$

where $a > 0$ is the dilation and $b \in \Re$ is the translation.

Let $s(x)$ denote the signal, its WT with the mother wavelet ψ is given by,

$$S(a,b) = \frac{1}{\sqrt{a}} \int_{-\infty}^{\infty} \psi^{+}\left(\frac{x-b}{a}\right) s(x) dx \qquad \text{Eq. 3.6-3}$$

where ψ^+ is the complex conjugation of ψ.

WT can be performed either in continuous form (CWT) or in discrete form (DWT). The basis function set of CWT is overcomplete or the basis functions are non-orthogonal. The CWT allows good discretization and efficient detection capabilities [Anto01], but is very redundant and computationally costly. The DWT, on the other hand, uses an orthogonal basis function set and is computationally efficient. In the present work, DWT was used.

In the DWT, the basis functions are obtained from the mother wavelet by taking special values for dilations and translations: $a = 2^{-j}$ and $b = 2^j k$, where j and k are integers. Thus, the wavelet bases for DWT read,

$$\psi_{j,k}(x) = 2^{\frac{j}{2}}\psi(2^j x - k); \text{ j, k = 1, 2, 3} \qquad \text{Eq. 3.6-4}$$

The scale index j indicates the width of a wavelet and k denotes the position of a wavelet. The $2^{j/2}$ is a normalization factor for a constant norm of each wavelet independent of scale j. The DWT of a signal, s(x), at scale j is given as,

$$S(j,k) = \sum_{i=1}^{n} \psi^{+}_{j,k}(i)s(i) \qquad \text{Eq. 3.6-5}$$

where S(j, k) is the wavelet transform coefficient (WTC) at scale j and position k. Larger values of j correspond to higher resolution.

The DWT has the following properties:

1. The DWT, like The FFT, is a fast, linear and invertible transformation. DWT transforms an N element array in the original domain into an array of N elements in the wavelet domain, called an array of WTC. The inverse WT (IWT) reconstructs the signal from the array of WTC.
2. The individual wavelets are localized in time/space and in frequency, which makes it possible to represent images and large data set by a small number of WTC thus leading to data compression.
3. The scales of wavelet basis function vary. WTCs corresponding to large scales represent gross features and small scale WTCs reveal detailed features. As Graps [Grap95] expressed: “The result in wavelet analysis is to see both the forest and the trees”. This property makes wavelet a useful tool for feature extraction and data denoising [Tasw99].

Unlike the FFT, whose basis functions consist only of sine and cosine functions, there are in principle infinite number of functions that can be used as mother wavelets in the WT. In some cases

it is important to chose wavelets that are suitable to the specific problems of interest, as they will effect, for example, how well or how compact the data under investigation can be represented in the wavelet domain. However, in the present work, no attempts were made to compare the performances of different wavelets in characterizing the baseline of MRS. Instead, the popular and widely used Daubechies wavelet [Daub88] was used as the mother wavelet.

3.6.2 Wavelet denoising

The WT represents the noisy signal in the wavelet domain by the WTCs. While the prominent features of the signal can be represented by only a small number of larger WTCs, the WTCs representing noise are distributed on each scale. By setting the small coefficients below certain threshold to be zero and reconstructing the signal, the prominent features of the signal can be recovered, with the noise largely being removed and without losing detailed features of the true signal. This is the main idea behind the technique of wavelet denoising. In general, the wavelet denoising is realized with the following steps [Tasw99], [Dono95].

- Perform WT on the signal so as to represent the signal in the wavelet domain with its wavelet coefficients.
- Set or calculate the threshold to distinguish the significant coefficients associated with the prominent features of the signal from the non-significant coefficients related to noise.
- Replace the noise related coefficients by zeros.
- Perform inverse wavelet transform of the thresholded coefficients to reconstruct the denoised signal.

The wavelet denoising differs from the spectral smoothing in that the smoothing averages out high frequency noise (also high frequency signal components), while the wavelet denoising retains the signal without losing its high frequency components. The wavelet denoising also differs from the time domain exponential multiplication. The latter suppresses the noise at the expenses of linebroadening, while the former removes noise without losing the detailed information of the spectrum.

The thresholding technique falls into two categories: hard thresholding and soft thresholding. In hard thresholding, coefficients smaller than a critical value are set to zero. Donoho and Johnson [Dono94] derived the optimal hard thresholding as,

$$w = \frac{\sqrt{2\log(n)}}{\sqrt{n}}\sigma, \qquad \text{Eq. 3.6-6}$$

where w is the threshold, n is the number of data points and σ is the standard deviation of Gaussian noise. Fig. 3.6.1 shows an example of wavelet denoising with hard threshold on a simulated NAA spectrum and Gaussian white noise.

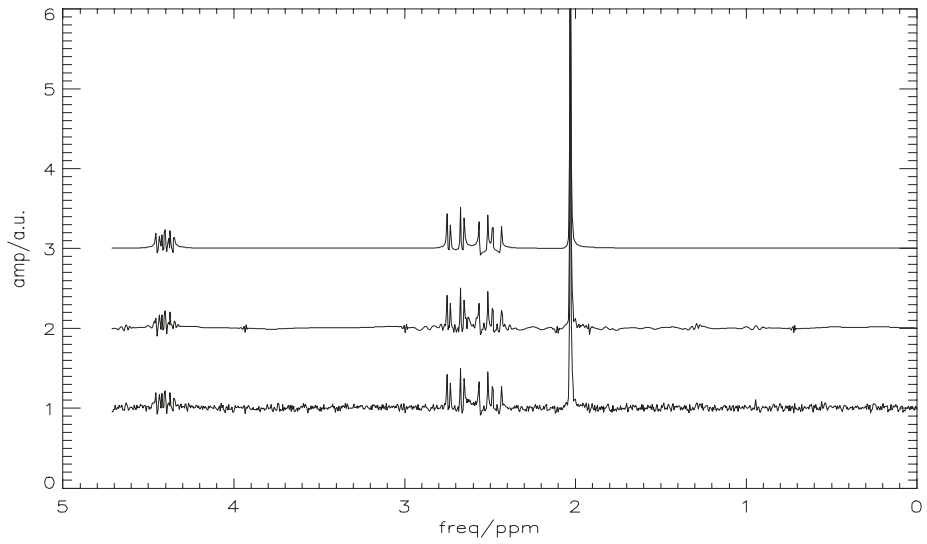

Fig. 3.6-1 An example of wavelet denoising on simulated NAA signal. From bottom up are the noisy, the denoised and the noise-free spectra.

3.6.3 Wavelet baseline characterization

It has been mentioned that the DWT is a multiresolution analysis, meaning that it represents signals with wavelet coefficients with different scales. The algorithm of DWT is illustrated by Fig. 3.6.2. and an implementation is given by Press et al [Pres92]. As seen from Fig. 3.6.2 the original signal is first submitted to the high pass filter, $f_{max}/2 \sim f_{max,}$ and the low pass filter, $0 \sim f_{max}/2$. The high frequency part is subsampled by 2 and constitutes the first level of WT coefficients, which correspond to the highest scale index of j. The low frequency part is also subsampled by 2 and repeats the filtering and subsampling procedure as the original signal. This process is repeated till only two data points are left. The WT coefficients correspond to the lowest scale index of j = 1. The scales, scale indices and their corresponding frequency bands are illustrated by Fig. 3.6.3 The figure expresses the following characteristics of WT coefficients.

1. Lower scale index corresponds to larger scale (width) of wavelet and higher scale index corresponds to smaller scale of wavelet;
2. Larger scale WT coefficients represent lower frequency (slowly varying) features of the signal and smaller scale WT coefficients represent higher frequency (rapidly varying) features of the

signal;

3. The number of WT coefficients increases with the index of the scale as 2^j;

4. The frequency band is doubled and scale is halved as the index j increases by 1.

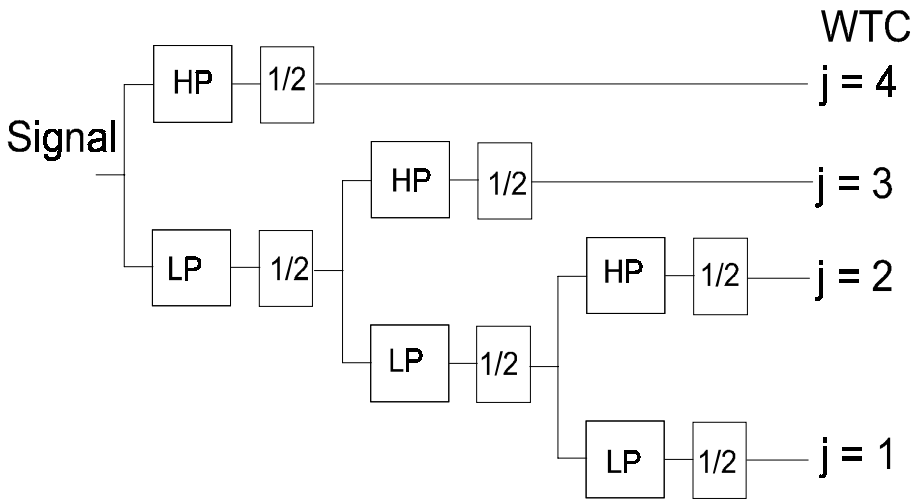

Fig. 3.6-2 Schematic illustration of DWT algorithm. HP and LP stand for high pass and low pass filters, respectively; WTC stands for wavelet coefficients.

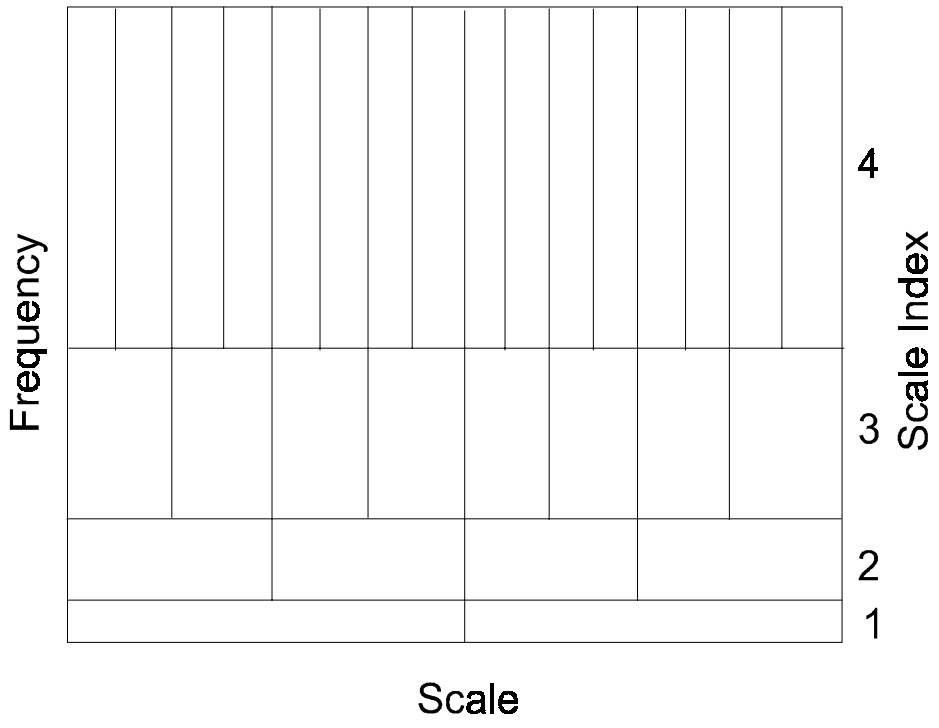

Fig.3.6-3 Relation of scale, scale index and frequency band of DWT.

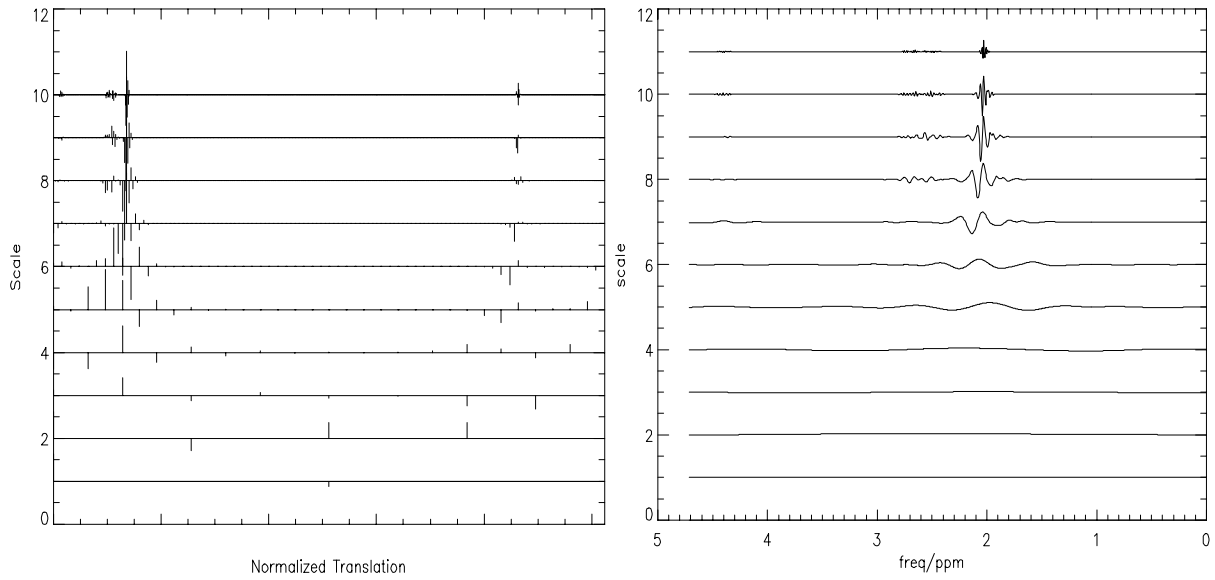

Fig. 3.6-4 Wavelet representation (a, left), wavelet coefficients distribution on each scale of a simulated frequency domain NAA signal with linewidth of 3 Hz; Reconstructed NAA spectral components (b, right) from wavelet coefficients of each scale. Note that the WTCs are shown for the whole spectrum (20 ppm) while the spectral components are shown only for the range of 0 ~ 5 ppm, corresponding to about the first quarter of the normalized translation in (a).

It is noteworthy to point out that the above statements are valid both for time domain signal and frequency domain signal. For the frequency domain signal, the "frequency" is understood as the frequency of variation. As far as frequency domain NMR signal is concerned, the narrow NMR peaks are regarded in this sense as high frequency (rapidly varying) components and the broad baseline is regarded as low frequency (slowly varying) component. Therefore, if frequency domain NMR signal with narrow peaks and broad baseline is transformed to the wavelet domain, the NMR peaks are mainly represented by the smaller scale WT coefficients and the baseline is mainly represented by the larger scale WT coefficients. A simulated spectrum of NAA with linewidth of 3 Hz and a simulated baseline composed of broad lines of over 50 Hz, both with a spectral width of 4000 Hz, were used. Both the NAA spectrum and the baseline were DWT transformed and reconstructed from the WT coefficients. Fig.3.6-4 shows the WTCs of different scales (a) and the spectral components of NAA reconstructed from WTCs of each individual scale (b). Most of NAA signal components are represented by WTCs of large scale indices or small scales, while only a small portion of spectral components is represented by WTCs of large scales. As a result, the NAA signal can be approximated by components reconstructed from WTCs of larger scale indices (Fig.3.6-4b). In contrary, baseline signal is mainly represented by WTCs of large scale wavelets (Fig.3.6-5a) and virtually no signal components are reconstructed by WTCs of large j (Fig.3.6-5b).

Therefore, baseline can be very well approximated by WTCs of the first several scales as shown in Fig.3.6-6. Due to the linear feature of DWT, the WTCs of real world NMR signal with narrow spectral peaks of interest and underlying baseline are exactly the summation of WTCs of the spectral peaks and the baseline. Therefore, the WTCs with small j, or with large scales, represent mainly the baseline, while the WTCs with large j, or with small scales, correspond almost purely to the spectral peaks. If one reconstructs the signal with WTCs of large scale, for instance with scales $j < 8$, the reconstructed signal will consists of the baseline and a small portion of the spectral peaks. With reduced peak magnitudes, the portion of the spectral peaks in the reconstructed signal also reduces. This constitutes the basis of the baseline characterization by means of DWT.

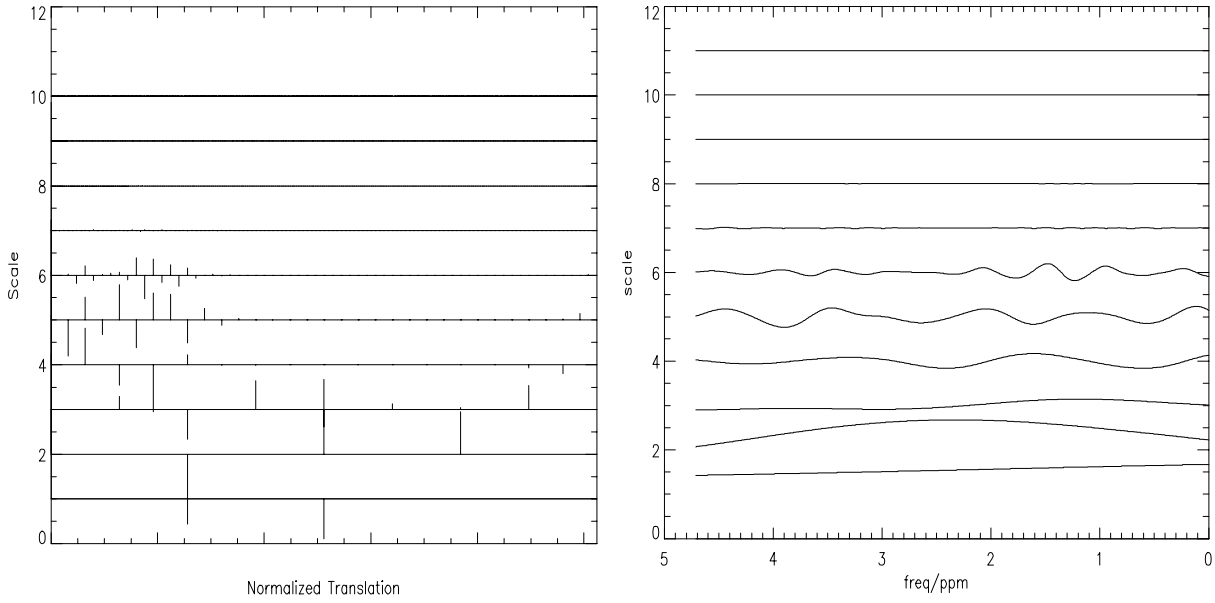

Fig.3.6-5 Wavelet representation (a, left),of simulated baseline, and reconstructed baseline components (b, right) from wavelet coefficients of each scale. Note that the WTCs are shown for the whole spectrum of 20 ppm but the spectral components are shown only for the range of 0 ~ 5 ppm, corresponding to the first quarter of normalized translation in (a).

The principle of wavelet transform baseline characterization is to combine wavelet baseline reconstruction and parametric spectral estimation and, to separate the baseline and spectral signals by making use of the competitions between non-parametric wavelet baseline reconstruction and parametric spectral estimation [Youn98]. The algorithm is described as follows.

1. Give an initial estimation of parameters of all metabolites to be quantified and calculate the metabolite signal, S(m, p), where m stands for the model signals and p for the parameters;
2. Subtract the signal S(m, p) from the raw signal S_0 to obtain the first estimation of baseline signal $b_0 = S_0 – S(m, p)$;

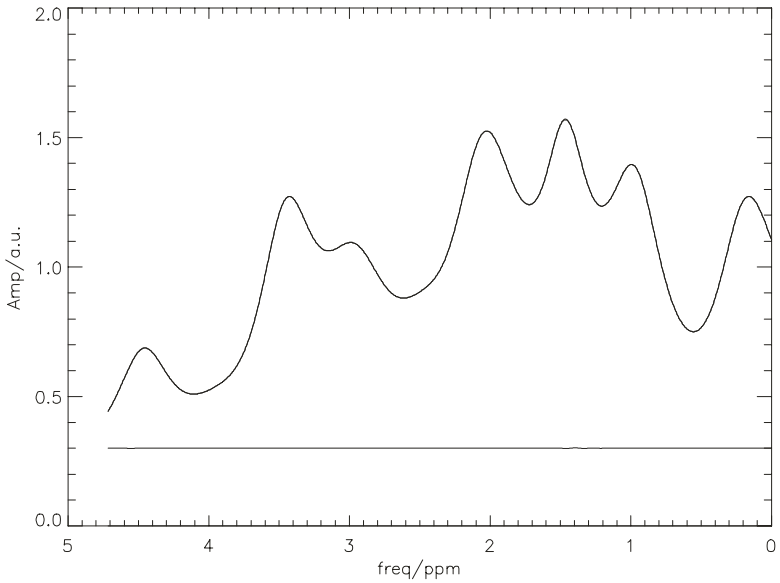

Fig. 3.6-6 Simulated baseline overlaid with the reconstructed baseline from the wavelet coefficients of the largest 7 of total 11 scales (upper trace) and their difference (lower trace).

3. Smooth b_0 by a LOWESS local filter [Clev79] and moving average filter;
4. Pass b_0 through WT to obtain the WT coefficients and reconstruct baseline from WT coefficients corresponding to scales larger than certain criteria j_c:

$$C_{j,k} = w(b_0) \qquad \text{Eq. 3.6-7}$$

$$b = w^{-1}(C_{j,k}), \mathrm{j} < \mathrm{j_c} \qquad \text{Eq. 3.6-8}$$

   where w and w^{-1} stand for DWT and inverse DWT, respectively;
5. Subtract b from the raw signal S_0: $S' = S_0 - b$;
6. Pass S' through the parametric spectral estimation routine for the parameters of the signal and reconstruct the metabolite signal S(m, p);
7. Repeat steps 2 – 6 for N iterations or till convergence is reached.

The WT is performed on frequency domain baseline signal and the parametric spectral estimation can be carried out in time domain or frequency domain. In the present work, a time domain spectral fitting algorithm described in Section 3.7 was used.

3.7 Time domain non-linear least squares spectral fitting

3.7.1 Time domain model function

The spectral fitting scheme of the present method is to fit the *in vivo* time domain signal with the combination of simulated model signals. The time domain model function reads,

$$S_{met}(t) = \sum_{m=1}^{M} a_m B_m(t) e^{i\Delta\omega_m t + \Delta\alpha_m t} e^{i\Delta\varphi + \Delta\beta t^2} \qquad \text{Eq. 3.7-1}$$

where $S_{met}(t)$ is the time domain metabolite signal, M is the number of model signal to be involved in the fitting, $B_m(t)$ is the simulated model signal of the mth metabolite. a_m, $\Delta\omega_m$ and $\Delta\alpha_m$ are the relative amplitude relative frequency and relative Lorentzian damping factor, respectively, of the mth model signal, with respect to the corresponding metabolite signal component in the measured signal. $\Delta\varphi$ and $\Delta\beta$ are the overall relative phase and overall relative Gaussian damping factor.

The first two factors in Eq. 3.7-1 express the linear relationships between the amplitudes of the measured metabolite signal and the signals of metabolites involved in the fitting.

The nonlinear factors in the model function account for the differences of frequency, phase and damping factors between the model signals and the measured signals of the metabolites. Among which the frequency differences and the Lorentzian decay differences are different from metabolite to metabolite. The zero order phase error and Gaussian damping rate, on the other hand, are the same for all metabolite signals. Therefore, the Gaussian damping factor is used as an overall variable to fit the Gaussian lineshape. It is preferable that the zero order phase is corrected before spectral fitting. In this case the phase term can be used to correct the remaining zero order phase errors, or it can be removed from the model function.

The number of parameters is an important factor in parametric spectral fitting methods, which will effect all aspects of the performance of the method, such as efficiency, speed, accuracy, robustness and so on. Too less parameters cannot account for the features of the spectrum leading to mismatching and quantification errors. Too many parameters will increase the complexity of the algorithm and computing time, and the redundant parameters can interfere sometimes with the necessary parameters causing also quantification errors. The selection of the parameters of the model function should accord with the scheme of the quantification method. In the present method, the main scheme includes, that (i) the whole spectrum of a metabolite instead of each individual resonance in the spectrum is used in the spectral fitting, (ii) some experimental errors such as first order phase, eddy current effect distortion, and the FM artifacts induced by gradient pulses are eliminated experimentally, and (iii) the undesired features of the spectrum such as baseline or lipid

signals are characterized by other software procedures. As a result, the model function only but completely describes the intrinsic features of the spectrum, i.e., the amplitudes, frequencies, phases and decay rates of metabolic component spectra. The number of parameters of the model function is minimized. For M metabolites, only 3M+1 (if the phase term is removed from the model function) or 3M+2 parameters in the model function are necessary to fit the spectrum. Otherwise, if individual lines are fitted, the number of parameters will increase dramatically and so will the computing time.

The number of model signals of metabolites involved in the spectral fitting, M, is determined by the user prior to the spectral fitting. In principle, M should be chosen to include as many model signals as those metabolites that contribute significantly to the measured MR spectrum. Other factors such as spectral resolution and SNR should also be taken into account. More metabolites can be involved and accurately estimated for signals with higher resolution and higher SNR.

In case the measured signal is free of baseline distortion, FM artifacts and first order phase errors, this model function can be used independently in the spectral fitting. If these problems exist, this model function must be combined with other experimental and software approaches to perform spectral estimation. The initial motivation was to avoid some difficulties of the time domain spectral analysis method, for instance, to avoid the difficulties of first order phase correction in time domain using the model spectral fitting algorithm. However, as was shown in the previous section, the experimental elimination of the first order phase errors is superior to the software approaches, no matter the software methods are performed independently or are integrated into the model function. It is generally true that experimental methods to eliminate errors are better and more preferable than to correct the errors in the post-procession.

Some unique features of the model function can be better revealed, if the variable t in Eq. 3.7-1 is substituted by t_n in the model function, where t_n is the discrete sampling time.

This model function only requires that t_n be the same on both sides of the equation. No assumption is made that t_n must be equidistant. Therefore, the model function can be used for non-equidistant sampling. This model function does not require the starting point be $t_0 = 0$. Arbitrary but the same number of points can be omitted from the model signals and the measured signal. If no relaxation is involved in the model spectra, the estimated amplitudes A are still in the absolute unit of number of spins. In case a relaxation is introduced in the model signals by multiplying an exponentially damping factor in the post-processing of the model spectral simulations, the amplitude should be corrected according to the dwell time, the number of points omitted and the damping rate.

The primary requirement of the method is that the parameters of the simulations for $B_m(t)$ must be exactly the same as those of real world experiments for $S_m(t)$. See §3.5.

3.7.2 Non-linear least squares fitting

Suppose, the measured data set is given as $\{S_n, \sigma_n, t_n\}$, n = 0, 1, ..., N-1, where N is the number of data points, $\{\sigma_n\}$ are estimated errors of the measured data $\{S_n\}$. The model function to fit the measured data set is $S(t_n) = S(p, t_n)$, where $p = [p_1, p_2, ..., p_L]$ is the vector of adjustable parameters. In general, model function fitting is to adjust the parameters of the model function so as to minimize the differences between the model function and the measured data set. The maximum likelihood estimation of the model parameters is obtained by minimizing the so called "chi-square"[Pres92],

$$\chi^2 = \sum_{n=1}^{N} \left[\frac{S_n - S(p, t_n)}{\sigma_n} \right]^2 \to 0 \qquad \text{Eq. 3.7-2}$$

Because the model depends nonlinearly on the parameters as shown in Eq. 3.7-1, the minimization of chi-square is the nonlinear least squares problem.

3.7.3 Implementation

The implementation procedure of the developed method consists of four parts: (1) The pulse sequence optimization; (2) Data preprocessing and quantification parameter initialization; (3) Spectral fitting; (4) Post-processing and metabolite quantification. A flowchart for data preprocessing and the spectral fitting is shown in Fig.3.7-1. Some of the general approaches of these steps are explained in some more details as follows.

- Pulse sequence optimization includes experimental elimination of first order phase errors by RF pulse sequence timing and experimental elimination of FM artifacts caused by gradient pulses using gradient cycling and phase cycling techniques. Detailed procedures were described in earlier sections.

- Data preprocessing and quantification parameter initializations include combining spectra obtained with positive gradients and with negative gradients, setting the number of data points, choosing the model signals of metabolites that are involved in the spectral fitting, modifying the table of initial values and table of constrain values. Upon loading in the FID data acquired with opposite gradient pulses, the signals were first zero order phase error corrected in time domain and frequency shifted in frequency domain to align the water signals at zero frequency. Then the spectra were transformed back to time domain and combined to cancel out the FM sidebands caused by gradient pulses.

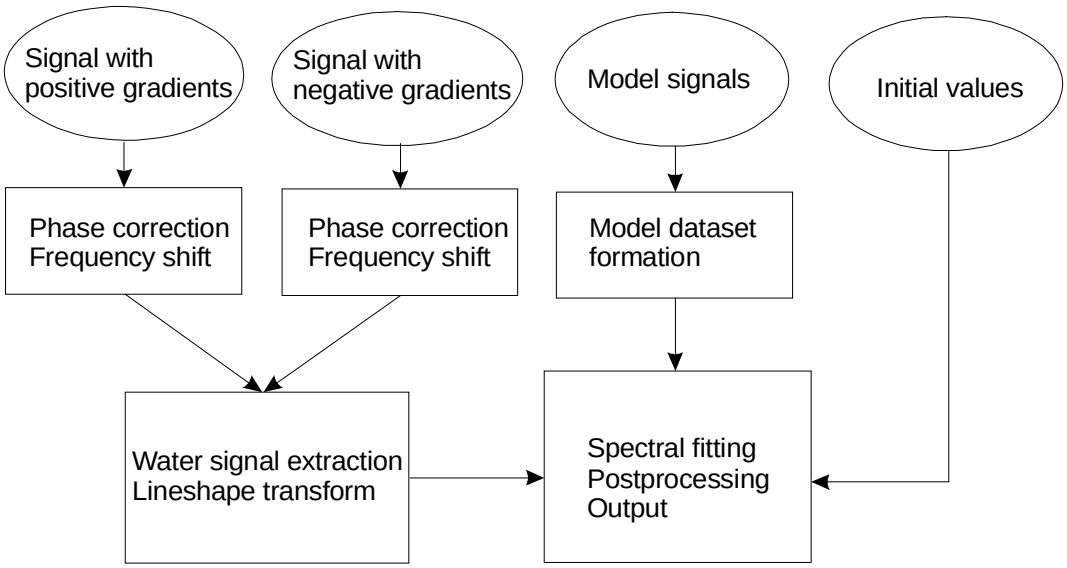

Fig.3.7-1 Flowchart of data preprocessing and spectral fitting.

In general, all metabolites that contribute significantly to the spectrum or whose concentrations are in the order of mM in normal conditions or in common pathological conditions should be included in the spectral fitting, but the spectral resolution should also be taken into consideration. For example, for a spectrum at the field strength of 4.7 T and with a linewidth of unsuppressed water of 9 Hz, about 14 metabolites can be included. Due to the nature of the algorithm of baseline characterization and parametric estimation of the method, the spectral contribution of the non-involved metabolites will be assigned to baseline and/or residue or cause errors to other metabolite quantification.

The table of initial values contains the starting values of the parameters of metabolites provided by the user for the spectral fitting. Some of the starting values such as the frequencies and the damping rates can be obtained from the prior knowledge of the model spectra and the measured spectra. The unsuppressed water signal can provide a good reference for the initial values of amplitudes of the metabolites.

The table of constraint values sets the lower and higher bounds for the possible values of the parameters, for instance, the amplitudes cannot be negative. Other values can be obtained from user's experiences.

- Preparing model signal includes loading in original model spectra and forming the model data

set. In forming the model data set, the starting points and the number of data points should be set in accordance to those of the signal to be estimated to ensure the point-to-point correspondence between model and measured signals. The model signal may be Lorentzian or Gaussian linebroadened at this stage, but this should be taken into account in setting the initial values.

- Spectral fitting includes loading initial values and constraint values, extracting water components, performing iterative baseline characterization and parametric spectral fitting.

  Extracting water components can be performed with undersampled data to reduce the number of data points and drastically reduce the computing time. At the same time some prominent spectral lines, such as the singlet of NAA, can also be estimated in order to obtain some initial values for the spectral fitting, in case the initial values are to be determined automatically. However, this should be applied with caution with short TE spectrum, as NAA might be overestimated because of baseline and spectral overlapping.

- Post-processing and metabolite quantification include the conversion of the estimated relative amplitudes to the "absolute" amplitudes, T_1 and T_2 correction of the estimated amplitudes and the conversion of signal amplitudes to the metabolites concentrations.

  The absolute amplitudes of the metabolites are obtained by,

$$a_m = N_m A_m \qquad \text{Eq. 3.7-3}$$

  where N_m is the number of spins of the mth metabolites involved in the spectral estimation.

  The relaxation correction and metabolite concentration can be calculated according to Eq. 3.2.-15 and Eq. 3.2.-16.

The main program of spectral analysis procedure was implemented using IDL (Interactive Data Language, Research Systems Inc., Boulder, CO). Wavelet analysis programs were written in C, among which the wavelet transform and inverse wavelet transform codes were obtained from NRC [Pres94]. MPM was implemented in C utilizing CLAPACK functions (available for free at http://www.netlib.org). The program package for parametric spectral fitting procedure was also implemented with C language which calls the NRC [Pres94] codes of the Marquardt-Levenberg algorithm to perform nonlinear least squares optimization.

3.7.4 Monte Carlo studies

In this section, Monte Carlo studies were carried out for the following purposes,

- To test the performance of Marquardt-Levenberg algorithm in pure spectral fitting with simulated signals, with emphasis on its performances to estimate signals with different lineshapes.
- To test the performance of the spectral estimation method in resolving the overlapped spectra with signals synthesized from the deformed and amplified model signals of the metabolites.
- To test the performance of wavelet transform baseline characterization and parametric model spectral fitting scheme with synthesized signals combined with artificial baselines.

3.7.4.1 Monte Carlo study I: with synthesized singlets with different lineshapes

Three singlet signals were synthesized with parameters given in Table 3.7.1a as model signals. The noise free test signal was obtained by deforming the model signals with the relative parameters of frequency, amplitude and phase and decay rates. The synthesized signal was added with 100 noise realizations with Gaussian distribution to generate 100 noisy signals to be estimated for the MC study. All these noisy signals were fitted with the model function given in Eq. 3.7-1 for the parameters *relative* to those of original model signal components. The SD of the noise is 2 (a.u.) and therefore the SNRs of the three signal components are 14, 18, 24 dB, respectively. MC studies were made on three different lineshapes, namely, pure Lorentzian, pure Gaussian and Voigt. The results were only given for the estimated relative frequencies and relative amplitudes.

Tab.3.7.1a Parameters of the model signals

Signal components	***1***	***2***	***3***
Freq/Hz	250	300	550
Amp./a.u.	0.5	0.75	1.5
Linewidth/Hz	1	1.5	2
Phase/rad	0	0	0

Tab.3.7.1b Relative frequencies, amplitudes and phases of the test signal with respective to the model signals given in Tab.3.7.1a.

Signal components	***1***	***2***	***3***
Relative Freq./Hz	1	2	3
Relative Amp./a.u.	20	20	20
Relative Phase/rad	0	0	0

In the following, the noise free test signal was obtained by deforming the model signals given in

Tab.3.7.1a by the parameters given in Tab.3.7.1b and *one* of the different decay rates in Table3.7.2a,or Table3.7.3a or Table3.7.4a, respectively, for different lineshapes.

(i) Case 1: Pure Lorentzian Lineshape

The relative decay rates of the test signals with respect to the model signal are given in Tab.3.7.2a and the estimated parameters of frequencies and amplitudes are given in Tab.3.7.2b.

Tab. 3.7.2a Relative Lorentzian and Gaussian decay rates of the test signal: Pure Lorentzian lineshape

Signal components	***1***	***2***	***3***
Relative L-linewidth/Hz	5	5	5
Relative G-linewidth/Hz	0	0	0

Tab. 3.7.2b Estimated relative frequencies and amplitudes (mean +/- SD) of the test signal and the CRLBs of amplitudes: Pure Lorentzian lineshape.

Signal components	***1***	***2***	***3***
Estimated Rel. Freq./Hz	0.976 +/- 0.095	1.983 +/- 0.075	2.986+/- 0.063
Estimated Rel. Amp./a.u.	19.927 +/- 0.520	20.011 +/- 0.425	20.005 +/- 0.286
CRLBs of amplitudes	0.36	0.24	0.12

(ii) Case 2: Pure Gaussian Lineshape

The relative decay rates of the test signals with respect to the model signal are given in Tab.3.7.3a and the estimated parameters of frequencies and amplitudes are given in Tab.3.7.3b

Tab. 3.7.3a Relative Lorentzian and Gaussian decay rates of the test signal: Pure Gaussian lineshape

Signal components	***1***	***2***	***3***
Relative L-linewidth/Hz	0	0	0
Relative G-linewidth/Hz	5	5	5

(iii) Case 3: Voigt Lineshape

The relative decay rates of the test signals with respect to the model signals are given in Tab.3.7.4a. and the estimates parameters of frequencies and amplitudes are given in Tab.3.7.4b.

Tab. 3.7.3b Estimated relative parameters (mean +/- SD) of the test signal and the CRLBs of amplitudes: Pure Gaussian lineshape

Signal components	***1***	***2***	***3***
Estimated Rel. Freq./Hz	1.032+/- 0.059	2.031 +/- 0.046	3.032 +/- 0.044
Estimated Rel. Amp./a.u.	20.016 +/- 0.481	20.001 +/- 0.276	20.010 +/- 0.181
CRLBs of amplitudes	0.25	0.16	0.08

Tab. 3.7.4a Relative Lorentzian and Gaussian decay rates of the test signal: Voigt lineshape

Signal components	***1***	***2***	***3***
Relative L-linewidth/Hz	2.5	2.5	2.5
Relative G-linewidth/Hz	2.5	2.5	2.5

Tab. 3.7.4b Estimated relative parameters (mean +/- SD) of the test signal and the CRLBs of amplitudes: Voigt lineshape

Signals	***1***	***2***	***3***
Estimated Rel. Freq./Hz	1.025+/- 0.099	2.0166 +/- 0.078	3.025 +/- 0.067
Estimated Rel. Amp./a.u.	20.005+/- 0.497	20.018 +/- 0.346	20.016 +/- 0.193
CRLBs of amplitudes	0.29	0.19	0.10

Comparing the estimated relative frequencies and relative amplitudes in Tab.3.7.2b ~Tab.3.7.4b with those in Tab.3.7.1b one sees that the mean values of the estimated results are very close to the true values. The absolute deviations of the frequencies are less than 0.032 Hz. For the test signal with pure Lorentzian lineshape the largest relative bias of the amplitudes is 0.36% (SNR = 14 dB); While the largest biases for pure Gaussian signal and Voigt signal are 0.08% and 0.09%, respectively. In the tables the CRLBs for the amplitudes are also given as references for the evaluation of the results. The lowest CRLBs are those for the pure Gaussian signals and the highest the pure Lorentzian signals. The CRLBs for Voigt signals go in between. The relative values of standard deviations of the estimated amplitudes of the three signal components are in good agreement with the relative values of the CRLBs. Alternatively, the results can be expressed by the coefficient of variation (CV), which is defined as follows,

$$CV = SD/mean \qquad \text{Eq. 3.7-4}$$

The CVs are 2.6% for the most noisy signal (SNR = 14 dB) with pure Lorentzian lineshape and 0.9% for the signal with highest SNR (24 dB) and pure Gaussian lineshape.

It is interesting to note that the MPM based method works well with signals with Lorentzian lineshape, while the model signal fitting based method here produce better results with signals of Gaussian lineshape. This is not surprising, because the MPM method assumes the signal to be a combination of exponential decaying sinusoids. The model signal fitting method used here is in principle model independent. The differences of the estimation results are mainly due to the intrinsic properties of the signals as revealed by the CRLBs. This method fits the signal with model signals in the time domain. As the time domain Gaussian signal decays slower than Lorentzian signal at the beginning when the signal is strong, Gaussian signal can be more accurately estimated then.

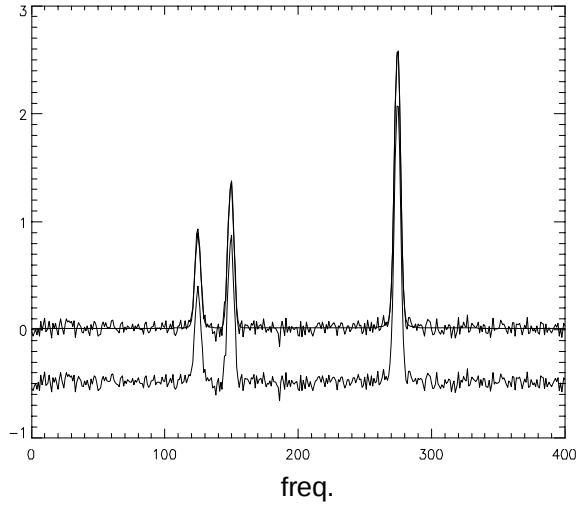

Fig.3.7-2 An example of spectral fitting in the MC study. The lower trace is the test spectrum and the upper trace are the test spectrum and the fitted spectrum overlaid. Note that the frequency axis was scaled by a factor of 0.5.

3.7.4.2 Monte Carlo Study II: with simulated metabolite signals

This Monte Carlo study aims at testing the performance of the method to resolve overlapping spectra as encountered in the *in vivo* situation. For this purpose, the GAMMA simulated model signals of the metabolites, namely, NAA, Ins, Tau, Cr, Glu and Cho, were used. The noise free test signal was obtained by first deforming the model signals with the following relative parameters and then adding them up.

Tab.3.7.5a Relative parameters to obtain the noise free test signal from the model signals for the MC study

Metabolites	NAA	Ins	Tau	Cr	Glu	Cho
Relative freq/Hz	3	2	-2	-3	1	4
Relative amp./a.u.	100	50	60	80	60	20
Relative LW/Hz	7	7	7	7	7	7
Relative Phase/rad	0.01	0.01	0.01	0.01	0.01	0.01

(Note: LW = linewidth).

The test signal was added with 100 noise realizations of standard deviation of 15. The SNRs for the metabolites are NAA: 32.0, Ins: 26.0, Tau: 24.0, Cr: 34.5, Glu: 26.0 and Cho: 24.8 dB. The results of Monte Carlo study for the frequencies and amplitudes are given in Tab. 3.7.5b. One of the spectral fitting results is displayed in Fig. 3.7.3.

Tab.3.7.5b Results (the relative frequencies and amplitudes, mean/SD) of Monte Carlo study on simulated metabolite signals. The CRLBs for the amplitudes are also given.

Metabolites	***NAA***	***Ins***	***Tau***	***Cr***	***Glu***	***Cho***
Freq./Hz	2.99/0.030	1.99/0.108	-2.02/0.16	-3.00/0.03	0.99/0.10	3.99/0.03
Amp./a.u.	100.1/0.85	50.00/0.69	60.11/0.66	80.1/0.62	59.93/1.39	19.99/0.20
CRLBs	0.55	0.60	0.69	0.45	0.88	0.18

The means of the estimated frequencies and amplitudes agree with the theoretical values very well. For instance, the largest relative bias of the amplitude, defined as the ratio of bias to theoretical value of the amplitude is only 0.18% for Tau. The standard deviations of the estimated amplitudes are very close to their CRLBs. The CVs of the estimated amplitudes of the metabolites (in the same order as in the table) are: 0.7%, 1.4%, 1.1%, 0.78%, 2.3% and 1.0%, respectively. The spectra of the 6 metabolites are overlapping to some extent as seen from Fig. 3.7.3. However, the Monte Carlo study results show that these overlapping lines are well resolved. Similar Monte Carlo study with narrow linewidth of 4.0 Hz was also performed, and the CVs are found decreased by about 10%. This confirmed the ability of the method in resolving overlapping lines.

Another Monte Carlo study was made in which choline signal was removed from the test signal but the signal was still fitted with 6 metabolite model signals including choline. The results are given in Tab. 3.7.6, and an example spectral fitting is shown in Fig. 3.7.4. As seen from Tab. 3.7.6 the mean of estimated amplitudes of choline is close to zero and the standard deviation is very small. The mean of choline is only 0.1% or less of the amplitudes of Ins, Tau and Cr, indicating that the overlapping spectra are very well resolved. As a result, the parameters of other metabolites were also reliably estimated, in consistency with the results in Tab. 3.7.5b.

The results of the two Monte Carlo studies are of significance in quantifying *in vivo* proton MRS in that vanishing metabolites due to pathological reasons can be correctly recognized without effecting the results of the estimations of other existing metabolites.

Tab. 3.7.6 Results (relative frequencies and amplitudes, mean/SD) of Monte Carlo study. In this study the choline signal was removed from the test signal.

Metabolites	***NAA***	***Ins***	***Tau***	***Cr***	***Glu***	***Cho***
Freq. (Hz)	2.99/0.03	2.00/0.10	-2.01/0.16	-3.01/0.03	0.99/0.11	0.18/6.8
Amp. (a.u.)	100.3/1.11	50.23/0.67	60.09/1.08	80.42/0.91	60.01/1.26	0.05/0.11

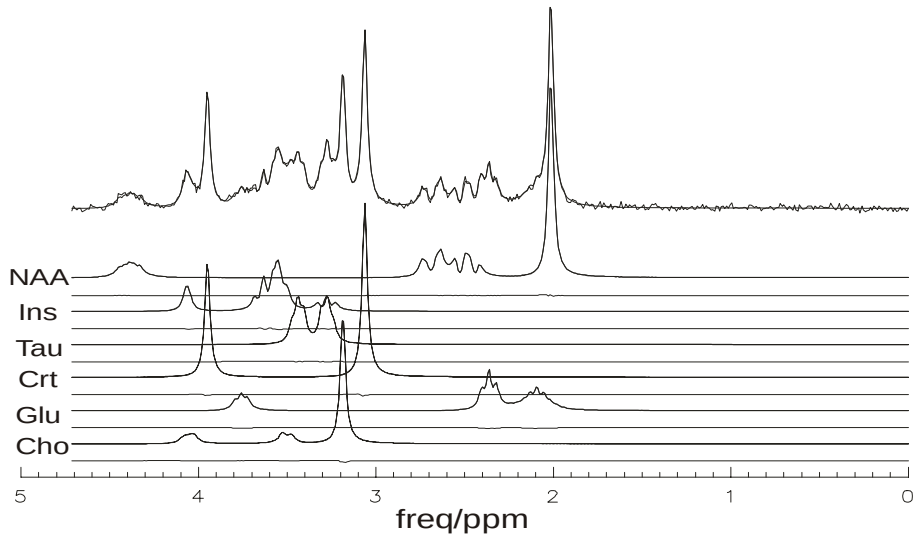

Fig. 3.7-3 An example of spectral fitting of the MC study using a signal comprising of 6 simulated metabolite signals. From top to bottom are: the total test spectrum and the fitted spectrum overlaid, each of the metabolite component spectrum and the fitted one overlaid followed by the residue.

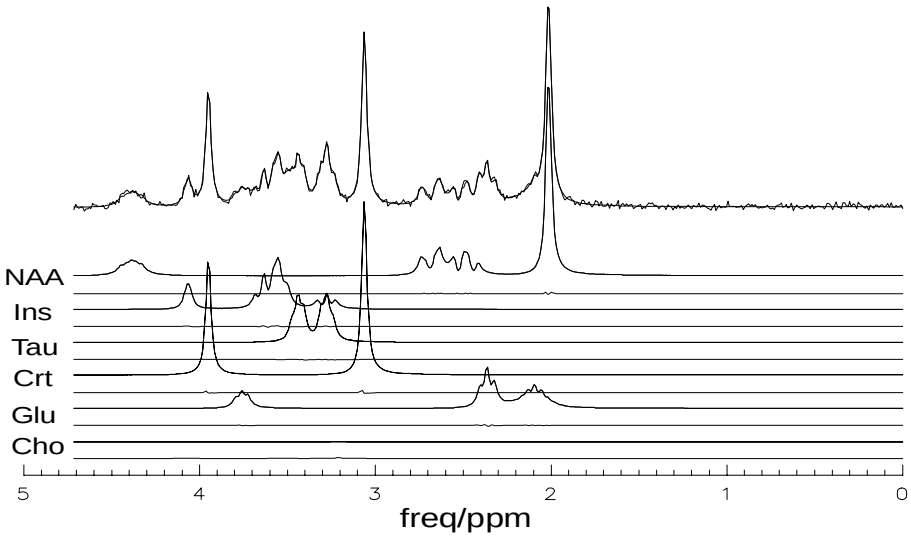

Fig. 3.7-4 The same as Fig.3.7-3 but the choline signal is removed from the testing signal.

3.7.4.3 Monte Carlo study III: with artificial baseline

This subsection is devoted to Monte Carlo studies to test the performances of the wavelet baseline characterization and parametric spectral estimation scheme with simulated and phantom spectra. To this end an artificial baseline was synthesized and added to the simulated spectrum or the phantom spectrum to form the noise free test signals. As before, noise was added to the noise free test signals for the Monte Carlo studies.

(i) Case 1: with simulated spectra

A signal with 3 spectral components and an artificial baseline were synthesized. The parameters of the spectral signal and the baseline are as follows.

Spectral:

Frequency/Hz	300	340	550
Amplitude/a.u.	30	40	60
Linewidth/Hz	8	10	12
Phase/rad	0	0	0

Baseline:

Frequency/Hz	80	150	250	350	450	530	650	750
Amplitude/a.u.	10	30	20	25	20	30	30	10
Linewidth/Hz	100	150	100	70	90	80	80	90
Phase/rad	0	0	0.2	-0.2	-0.3	0.1	0	-0.5

Because the performances of the method in estimating multiple and overlapping lines have been demonstrated and the purposes of the present Monte Carlo studies are to test the performances of the method in baseline characterization and spectral fitting, the model signal was taken as the same as the test signal. Therefore the theoretical relative amplitude of the signal is 1.

As the wavelet transformation based baseline characterization is a non-parametric method, the performances of the method cannot be expressed by the parameters of the estimated baseline. Rather, it can be indirectly indicated by the estimated parameters of the spectrum. For this reason, results of Monte Carlo studies are given by the means and the standard deviations of the parameters of the spectrum instead of the baseline itself. In addition, the estimated baseline will be displayed

together with the simulated baseline for comparison.

Six Monte Carlo studies were carried out, each being performed with 100 noise realizations. Baselines were generated with the parameters listed above and multiplied by a factor from 0 to 15 (see the table below). The results of Monte Carlo studies on the amplitudes of the signals are given in Table 3.7.7. The noise levels of 5 and 10 correspond to SNRs of 28.3 dB and 22.3 dB, respectively. For visualization, the spectra of the tested signal and the estimated signal are displayed for the case with baseline factor 15 and noise level 5 in Fig. 3.7.5.

Tab. 3.7.7 Monte Carlo studies of method with simulated signal and baselines.

Simulated signals				***Estimated amp. mean/SD***
Data set	***Added baseline***	***Added noise***	***True amplitude***	
1	0	0	1	1.000 /0.000
2	0	10	1	0.999/0.02
3	0	10	1	1.004/0.05
4	10	5	1	1.005/0.03
5	10	10	1	1.010/0.07
6	15	5	1	1.005/0.03

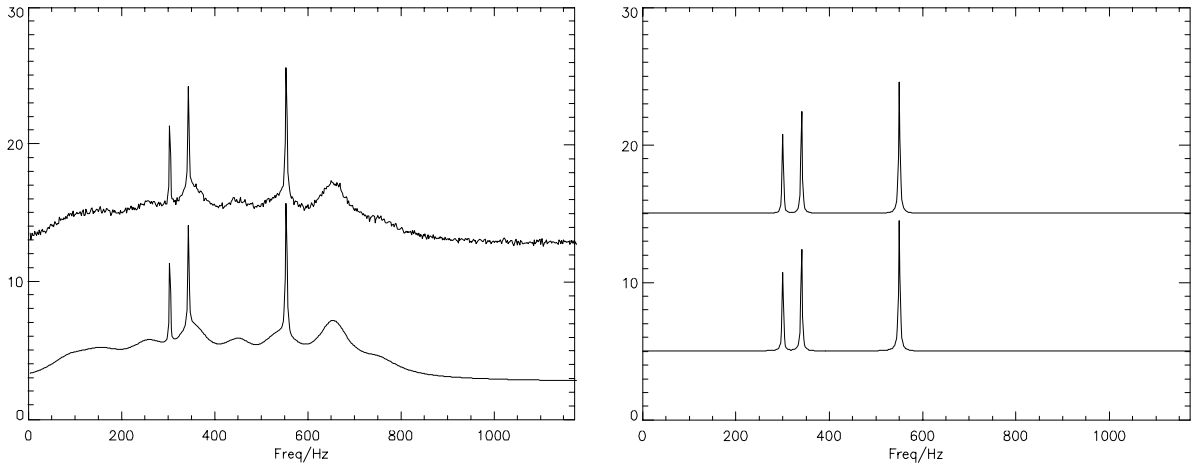

Fig.3.7-5 A spectral fitting from the MC study: the total test (with pure spectrum, baseline and noise; left, upper) and the fitted (left, lower) spectra, and the pure spectral part of the test (right, upper) and the fitted (right, lower) spectra.

The first data set is a noise-free and baseline free signal. Because no artificial baseline was added in the data set, no wavelet baseline estimation procedure was applied in the Monte Carlo studies. As can be expected, the signal was accurately estimated. The second data set is a noisy signal with no artificial baseline. Like in the first case, no wavelet baseline characterization was performed. The

bias of the estimated mean is 0.1%, with a CV of 2%, both stemming from the noises of the signal. The third data set is the same as the second one but wavelet baseline modeling procedure was involved in the spectral fitting algorithm although no artificial baseline was added to the signal. The aim of this Monte Carlo study is to test to what extent the wavelet baseline modeling procedure can effect the performance of the whole scheme, if no baseline exists at all in the signal, and how well the algorithm can recognize and model the baseline, or in other words, how well it can distinguish baseline and signal. The biases of the estimated signals are 0.4% and the CV's are 5%. Compared with the results obtained without wavelet baseline modeling algorithm, the bias increased by 0.5 percent points and the standard deviation increased by 3 percent points, both can be attributed to the baseline modeling procedure. The 0.5 percent points increase in bias is a small amount, but the 3 percent points increase in deviation seems to be large. The results discussed in the following paragraph suggest that these errors are also related to the noise levels.

In the following Monte Carlo studies, artificial baselines were added to the test signals. It is interesting to see that the biases and the standard deviations of the fourth and the sixth test signals are the same (0.5% and 3%, respectively), which have the same noise level but different baseline factors. The biases are only 0.1 percent points larger than the third data set that has no baseline, while the standard deviations are smaller than the third one, which has larger noise. The results of the fifth test signal, with large noise level, show increased bias and standard deviation, though the baseline is the same as the fourth and smaller than the sixth test signals. These results, together with the final point in the last paragraph, indicate that the estimation errors associated with the wavelet baseline characterization are mainly attributed to the noise. The errors induced by the true baseline are only a minor part in the total errors. This validated the performance of the spectral quantification scheme.

That the noise contributes most to the errors in the baseline characterization can be explained as follows. The Gaussian noise, though having zero mean, may have a wide spectrum in the frequency domain, i.e. with slow varying components as well as fast varying components. The former may be attributed to the large scale components in the wavelet analysis, which is regarded as baseline. Due to the zero mean feature of the Gaussian noise the estimated spectral mean may remain small, but the deviation may increases due to the fluctuation feature of the noise.

Some noise suppressing methods can be applied to the measured data before they are submitted to the spectral fitting procedure in order to suppress the errors. The available methods are, for instance, the conventional line broadening and the wavelet denoising.

(ii) Case 2: with model spectra

In this case, Monte Carlo studies are performed on test signals used in Monte Carlo Study II in

Section 3.7.4.2 added with an artificial baseline. The baseline factor is 15 and the standard deviation of noise with Gaussian distribution is 10. The SNR is 35.6dB for NAA, 29.5 dB for Ins, 27.6 dB for Tau, 33.6 dB for Cr, 29.6 dB for Glu and 28.3 dB for Cho, respectively. Monte Carlo studies were made on each data set with 100 noise realizations. The same model signals as in Section 3.7.4.2 were used in the model function for the spectral fitting. Monte Carlo study results are summarized in Tab.3.7.8 .

Tab. 3.7.8 Results (relative frequencies and amplitudes in mean/SD) of MC studies on simulated metabolite signals. CRLBs are for the amplitudes.

Metabolites	***NAA***	***Ins***	***Tau***	***Cr***	***Glu***	***Cho***
Freq./Hz	1.48/0.054	1.015/0.09	-1.02/0.10	-1.52/0.05	0.46/0.09	1.98/0.055
Amp./a.u.	100.65/1.7	49.53/1.13	59.73/1.40	79.73/1.53	60.00/1.81	19.70/0.48
CRLBs	0.37	0.40	0.46	0.30	0.59	0.12

The data in Tab. 3.7.8 indicate that the relative biases of the amplitudes of the metabolites (from NAA to Cho in the table) are 0.35, 0.94, 0.45, 0.34, 0.00 and 1.50%. The CVs of the estimated amplitudes are (in %): 1.70, 2.26, 2.33, 1.91, 3.01 and 2.40. The CVs are very similar for different metabolites, except for NAA and Glu, which are overlapping. Usually, if two metabolite spectra overlap, the one with smaller signal amplitude will suffer from larger CV. Compared with the results in Monte Carlo Study II in Section 3.7.4.2, the CVs increased here. This is mainly because the estimation errors of the spectra and baseline affect each other, leading to increased errors for the spectral fitting. However, the errors and the variations are in general small, if all the sources of errors, such as noise, spectral overlapping and baseline distortions are taking into account.

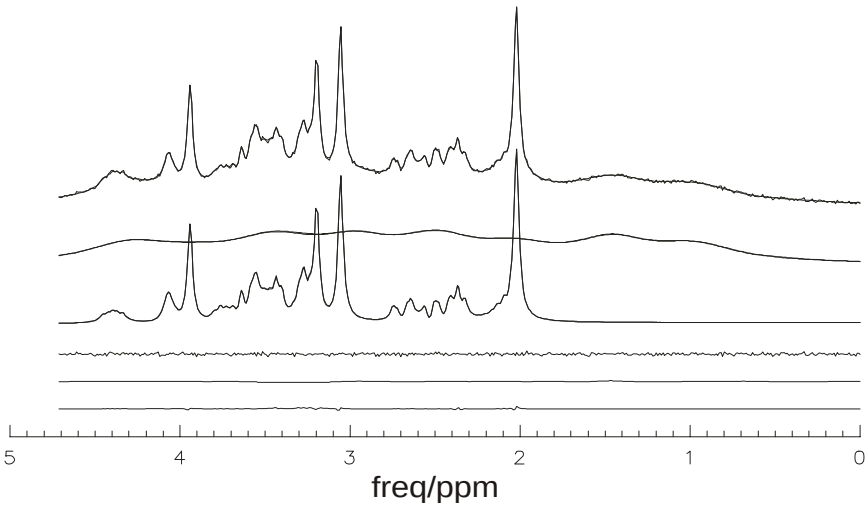

Fig. 3.7-6 An example of spectral fitting with simulated signals from 6 metabolites and artificial baseline. Displayed from top to bottom are the test and the fitted spectra overlaid, the artificial baseline and fitted baseline overlaid, the simulated spectrum and the fitted overlaid, and the residues of total spectrum, baseline and metabolite spectrum.

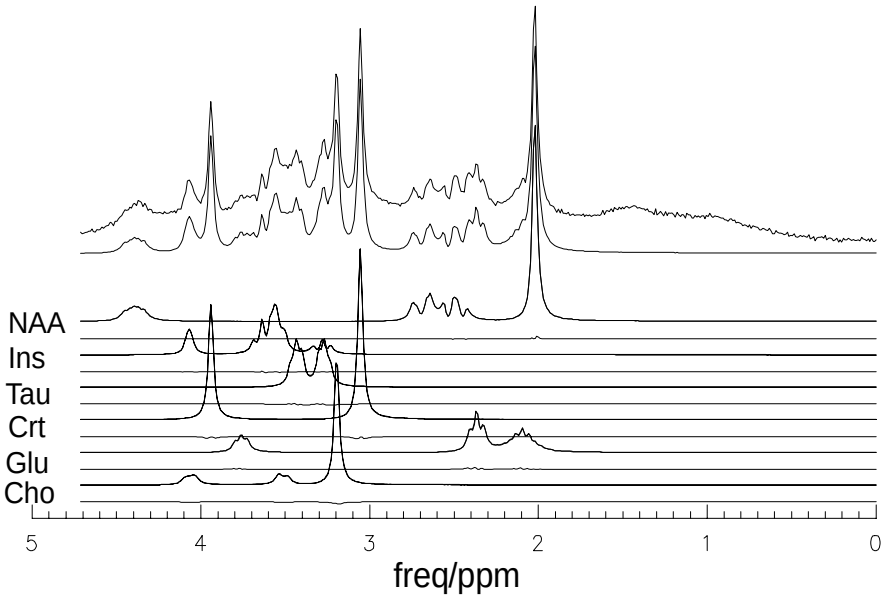

Fig. 3.7-7 The same spectral fitting as Fig.3.7-6. From top to bottom are the total spectrum, the fitted metabolite spectrum, and the decomposition spectra of metabolites and their residues.

In conclusion, various tests were performed under tough conditions and the results were presented numerically as well as visually. The results demonstrated that this method can accurately estimate the spectra with small CV, resolve complicated and overlapping spectra, and effectively separate baseline from metabolite spectra, thus validating the method as a tool to quantify *in vivo* proton MRS. The performances of the method will be tested further with phantom and *in vivo* data in the following sections.

3.7.5 Phantom experiments

In this subsection, test results of the method will be presented which were obtained on phantom data measured on (i) 100mM NAA solution, (ii) 200mM Tau solution, and (iii) from a mixture of several solutions.

The experimental parameters are as follows: Localization sequence PRESS, water suppression with CHESS, TE = 20 ms, TR = 15 s, NA = 16 or 32, SW = 4006 Hz, voxel size = 1 cm^3 or 64 mm^3. Signals without WS were obtained with positive and negative gradients, respectively, and combined, making NA = 32. Data with WS were acquired with positive gradients. The FWHM of unsuppressed water was about 1 Hz. 800 complex data points were used in spectra fitting.

The results of spectral fitting and concentration estimation of Tau are given in Tab.3.7.9, for signals obtained both without and with WS (n=6). The CVs of the estimated amplitudes are 0.56% for

signals without WS and 0.06% for signals with WS. The larger CVs for the former may be due to the residues of the FM artifacts. Despite this, the estimated means from the two data sets are very close with only a relative difference of 0.7%. Please note that no T_2 correction was made on the amplitudes and on the concentrations. A spectral fitting for a signal measured without WS is shown in Fig.3.7-8.

Tab. 3.7.9a Estimation results, amp. (a.u.) and concentration (mM), of Tau spectra measured without WS.

No.	***1***	***2***	***3***	***4***	***5***	***6***	***Mean/SD***
Amp.	1832.80	1858.56	1842.07	1834.59	1849.32	1852.74	1845.01/10.28
Conc.	199.67	202.47	200.68	199.86	201.47	201.84	200.99/1.12

Tab. 3.7.9b Estimation results, amp. (a.u.) and concentration (mM), of Tau spectra measured with WS.

No.	***1***	***2***	***3***	***4***	***5***	***6***	***Mean/SD***
Amp.	1832.56	1831.37	1830.59	1829.98	1829.56	1832.09	1831.03/1.19
Conc.	199.64	199.51	199.43	199.36	199.31	199.59	199.47/0.12

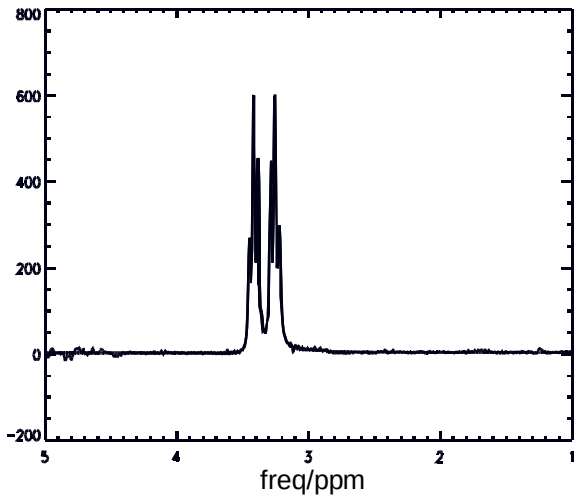

Fig. 3.7-8 An example of spectral fitting: phantom spectrum of Tau and the fitted spectrum overlaid.

Monte Carlo study was performed on measured NAA data. In order to suppress the experimental noise, the time domain data were multiplied with an exponentially decaying function corresponding to a 5 Hz linebroadening. 100 noise realizations with Gaussian distribution were generated for each noise level and added to the "low noise" signal for the Monte Carlo studies. The noise levels of the noisy signals were proven to be dominated by the added noises. In these studies, 6 sets of FID were tested each with 3 different noise levels. The standard deviations of the added noises are 25, 100 and 500 a.u., making the nominal SNRs of the test signals be 52.4, 40.4 and 26.4 dB, respectively.

And the CRLBs are 0.09, 0.35 and 1.73, respectively. 500 complex data points were used in Marquardt-Levenberg fitting. Results of Monte Carlo studies are given as mean/standard deviation in Tab.3.7.10a - Tab.3.7.10c. A typical spectrum with added noise level of 500 a.u. is displayed in Fig.3.7-9.

Tab. 3.7.10a Results of MC studies: SNR = 52.4 dB, CRLB = 0.09.

Datasets	***1***	***2***	***3***	***4***	***5***	***6***
Amp.	109.17/.11	109.31/.11	108.66/.12	109.11/.10	109.20/.10	109.03/.12
Conc.	100.05/.10	100.18/.10	99.58/.11	99.99/.10	100.07/.10	99.99/.11

Tab. 3.7.10b Results of MC studies: SNR = 40.4 dB, CRLB = 0.35.

Datasets	***1***	***2***	***3***	***4***	***5***	***6***
Amp.	109.15/.44	109.34/.54	108.62/.46	109.14/.44	109.09/.56	109.21/.49
Conc.	100.03/.40	100.20/.49	99.55/.42	100.02/.40	99.97/.52	100.09/.44

Tab. 3.7.10c Results of MC studies: SNR = 26.4 dB, CRLB = 1.73.

Datasets	***1***	***2***	***3***	***4***	***5***	***6***
Amp.	108.99/2.5	109.87/2.2	108.92/2.6	108.81/2.2	109.03/2.3	109.09/2.4
Conc.	99.89/2.3	100.69/2.0	99.82/2.4	99.72/2.1	99.92/2.1	100.98/2.2

The concentrations of NAA were calculated with the Eq. 3.7.-4 and with the following parameters: C_w = 55.56 mM, N_{naa} = 6, N_w = 2, S_w = 1.94x10 ^{7} (measured water signal amplitude in a.u.). No T_2 correction was made for the amplitudes. If T_2 effect was taken into account, the estimated concentrations will be increased by about 0.2%, roughly estimated using the assumption of T_2 values of 1100 ms and 900 ms for water and NAA, respectively.

The mean values of the estimated concentrations of NAA are very close to the nominal values of the sample, indicating a non-bias estimation at different noise levels. The standard deviations of the estimations are very close to the CRLBs, which were calculated with the assumption of a total linewidth of 6 Hz and the noise level given in the MC studies.

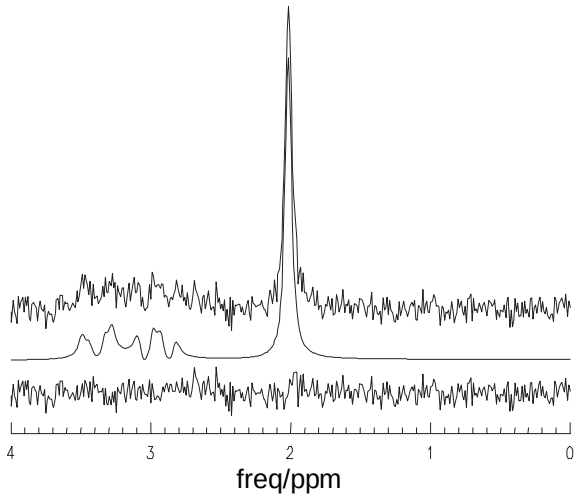

Fig. 3.7-9 A representative spectral fitting of the MC study. From top to bottom are: the measured spectrum with added noise, the fitted spectrum and the residue.

The same phantom data sets were also used in Monte Carlo study with added artificial baseline. Linebroadening of 6 Hz was performed on the phantom time domain signals. The standard deviation of noise with Gaussian distribution was 150. The SNR was 35 dB for total signal, 31 dB for the singlet of the CH_3 group and 21 dB for the multiplets from the CH_2 group of NAA, respectively, ignoring the measured noise in the phantom experiments. Monte Carlo studies were made on each data set with 100 noise realizations. Monte Carlo study results are summarized in Tab. 3.7.11.

Tab. 3.7.11 Results (amplitudes and concentration in mean/SD) of MC studies on phantom data of NAA solution of nominal concentration of 100 mM and artificial baseline.

Datasets	***1***	***2***	***3***	***4***	***5***	***6***
Amp.	109.38/3.3	109.52/3.2	110.11/3.9	109.03/3.3	109.92/3.9	109.96/3.7
Conc.	100.24/3.0	100.37/2.9	100.91/3.6	99.92/3.0	100.74/3.6	100.77/3.4

The concentrations were calculated with the same protocol as used in the last example. The means of the estimated concentrations are very close to the nominal concentrations 100 mM of the NAA phantom and the standard deviations are about 3.3% of the mean values. It is interesting to note that these results are in agreement with the results in §3.7.4, where the biases are 0.5% and the standard deviations are about 3% for the simulated signals with comparable noise levels (see Tab.3.7.7). An example of the spectral fitting is shown in Fig.3.7-10.

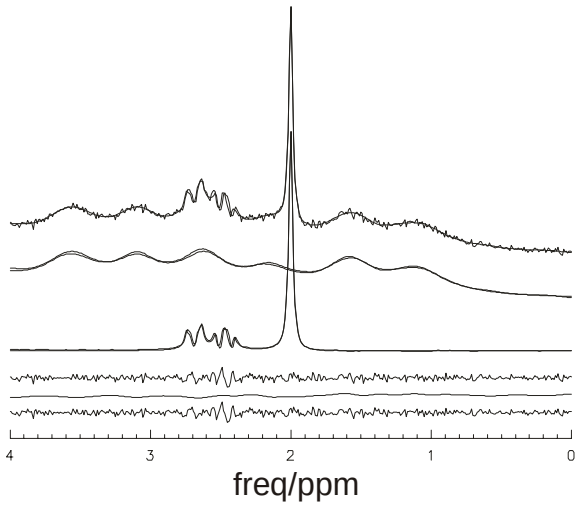

Fig. 3.7-10 Fitting of a phantom spectrum with added artificial baseline. From top to bottom are the total test spectrum and the fitted spectrum, artificial baseline and fitted baseline, measured spectrum and fitted spectrum, all overlaid, and the residues of total spectrum, baseline and NAA spectrum.

3.7.6 *In vivo* experiment

The ultimate goal of this study is to develop a method that can quantify *in vivo* ^{1}H MR spectra acquired without or with WS, therefore it is desirable that the developed method be optimized and modified for *in vivo* spectra and tested on *in vivo* data. In this section, the application of the method to *in vivo* data is described and the performance of the method is evaluated.

3.7.6.1 Initial values

The developed method requires initial values of the parameters be provided by the users for the spectral fitting algorithm. Initial values can affect the performance of the spectral fitting method in many ways. Good initial values, which are close to the real values of the parameters to be estimated, can speed up the convergence of the algorithm and increase the accuracy of the results. On the other hand, bad initial values, which are far away from the real values, may cause a failure of convergence or lead to large estimation errors. While the user's experience can help in choosing initial values, some analyses can provide guidelines for determining initial values. In the following, the characteristics of the parameters and rules to determine the initial values are analyzed.

Frequencies. Initial values of frequencies, $\{\Delta\omega_{m0}\}$, as used in this method, are the initial estimations of the frequency offsets between the simulated model spectra of the metabolites and their counterparts in the measured spectrum, corresponding to the relative frequency $\Delta\omega_{m0}$ in Eq. 3.7.-1,

$$\Delta\omega_m = \omega_m - \omega_m^{'} \qquad \text{Eq. 3.7-5}$$

The frequency ω_m of the model spectrum is determined by the prior knowledge [Govi00] deduced from phantom spectra and are fixed. The frequency of the *in vivo* spectrum $\omega_m^{'}$ may shift from measurement to measurement. However, the relative frequency shifts among the metabolite spectra remain largely unchanged. For instance, the chemical shift difference between the singlets of NAA and Cr may change very little in different measurements, even though their individual frequency may change remarkably. Therefore, the differences of $\Delta\omega_m$ among metabolites, for example, $d_{naa,\,cr} = \Delta\omega_{naa} - \Delta\omega_{cr}$ are largely constant from scan to scan. Though $\omega_m^{'}$ are unknown, the $d_{m,m'}$ among the metabolites can be obtained from statistics of results of a number of spectral estimations. First, choose a data set from a series of measurements of a typical *in vivo* experiment and submit it to the spectral fitting routine with a trial initial value table. In doing so, one may need to adjust the initial value table to obtain stable results. Repeat the procedure for several other data sets of the series of the same experiment. For each data set, the estimated frequency offsets $\{\Delta\omega_m\}$ for all metabolites are obtained. A mean value of the frequency offsets for each metabolite can then be calculated. Then choose a metabolite, e.g., NAA, as the reference and calculate the relative frequency offsets of all other metabolites against the mean frequency offset the reference,

$$d_{m,r} = \overline{\Delta\omega_m} - \overline{\Delta\omega_r} \qquad \text{Eq. 3.7-6}$$

These relative offsets can be regarded as constants and used to determine the initial values in the spectral fitting of other measurements,

$$\Delta\omega_{m0} = d_{m,r} + \Delta\omega_r \qquad \text{Eq. 3.7-7}$$

where $\Delta\omega_r$ can be determined from a metabolite with prominent peak, such as NAA, by estimating the frequency difference between singlets of CH_3 group of measured and simulated model spectra.

In the present work, the estimated frequency offsets (in the unit of rad/s) of some metabolites with respect to NAA are given as follows,

Tab. 3.7.12 Frequency offsets (rad/s) of some metabolites with respect to NAA.

Ins	Tau	Cr	PCr	Cho	PCh	Glu
5	14	-5	-6	23	26	-2.

Amplitudes. The initial values of amplitudes of metabolites can be easily estimated according to water signal amplitude and the prior knowledge of concentrations of water and metabolites of normal tissues. Use the same notations as in Eq. 3.2-16 and Eq. 3.7-3 and note that C_m can be taken

as the average values published in the literature, the initial values of amplitudes of metabolites can then be estimated as,

$$A_{m0} = \frac{C_m}{2C_w} a_w \qquad \text{Eq. 3.7-5}$$

where the factor of 2 is due to the number of spins in water molecule.

In proton MRS measured without WS, a_w is readily obtained. While in the case of MRS with WS, an additional scan without WS is needed to measure the water signal, or other methods of signal calibration can be employed to estimate the initial values of the amplitudes of metabolites.

Phases. Initial value of zero phase can be set to be zero, if zero phase error correction is automatically performed. Otherwise it can be determined from the time domain on-resonance water signal.

Lorentzian and Gaussian decay rates. The initial values of Lorentzian and Gaussian decay rates are most difficult to estimate, because they are effected by several factors. These factors include (i) the field homogeneity achieved in the experiment of the measured signal; (ii) the intrinsic relaxation rates (linewidths) of individual metabolites (iii) the exponential multiplication (line broadening) in the preprocessing steps for the purpose of resolution enhancement or noise suppression; (iv) the exponential multiplication in the lineshape transformation. In estimating the initial values of decay rates, all these factors should be taken into account and, if anyone of the factors changes, the initial values should be changed accordingly. Difficulties also arise from the fact that spectral and baseline overlapping make the contributions of the two types of decay entangle. For these reasons, the initial values of decay rates can only be loosely esitmated. The following can provide guidelines for a better esimation of the initial values. (i) The linewidth of the unsuppressed water signal can be used as a reference. (ii) The FID of unsuppressed water can be fitted to the Voigt function and provide an estimation of Gaussian portion of the decay rates. (iii) Lineshape transform from measured either to Gausssian or to Lorentzian is recommended because, beside other advantages, it can largely reduce the range of uncertainty of the lineshape, and can therefore narrow the range of choices of initial decay rate values.

3.7.6.2 Constraints

In a sense, the developed spectral fitting algorithm decomposes the spectrum into baseline and the metabolite components. The spectral overlapping, the baseline problem and noise make the spectral estimation not a pure orthogonal decomposition. As a result, unreasonable estimations for some parameters can happen under some extreme conditions. Therefore, constraints on the estimated

parameters are necessary to avoid such cases.

Constraints are the lower and upper boundaries that the parameters should not surpass during the iteration procedure of parameter estimation. The constraints on the amplitudes and decay rates are absolute. The lower boundary of amplitude is zero and the upper boundary is a sufficent large number for all metabolites. The lower boundary of Gaussian decay rate is also zero. The upper boundary depends on whether lineshape transform is performed. If lineshape is transformed to Lorentzian, the Gaussian decay rate boundary can be set very small. Otherwise, it is set to a value corresponding to a linewidth of about 0.16 ppm. Lorentzian rate constraints are set to a range corresponding to a linewidth of 0.03 – 0.05 ppm. The constraints on zero phase can be set as absolute, if phase correction is performed, otherwise they are set relative to the estimated zero phase. In both cases, as the zero phase error can be measured and corrected with high accuracy, the constraints on phase can be set within a narrow range. The constraints on frequency offsets are set relative to their most likely real values or relative to their initial values as being determined by the procedures described in the last subsection. The constraints are usually set to be +/- 0.08 ppm.

Unlike the case of initial values, there is no clear rule to follow in deciding constraint values. Experiences show that the algorithm would not converge well or the results are not reliable, if one or more parameters of major metabolites reach their constrain boundaries in the finale results. As long as the initial values are reasonably set, the algorithm will be robust. Therefore, the constraints should be loosely set as suggested above.

3.7.6.3 *in vivo* applications

The method was applied to *in vivo* data measured on rat brains. If not specified, the preprocessing parameters are: 1024 complex data points of the whole spectrum were loaded (no spectral region selection), zero phase correction, 256 undersampled complex data were used in water signal extraction by MPM based method, lineshape transform was performed by dividing the original signal by extracted water signal and then multiplying either a Lorentzian or a Gaussian function corresponding to the normal linewidth of the unsuppressed water signal and 512 data points were used in the spectral fitting algorithm. Metabolite concentrations were determined using water signal as an internal standard and assuming, that 75% of tissue water content is NMR visible [MacK94] [Gide99] [Roon96] [Chri94]. No T_1 and T_2 corrections were performed for the estimated signal amplitudes in the concentration conversions. Concentration values were given in millimole (mM).

An example of spectral fitting is shown in Fig. 3.7.11. On the top of the figure is the measured spectrum after removing the water components by MPM, overlaid with the fitted spectrum. Due to good fitting, the overlaid spectra agreed very well and are difficult to distinguish. The second trace

from top is the estimated baseline as determined by the iteration procedure of wavelet baseline characterization and parametric spectral fitting. The baseline is highly structured and consists of a number of broad spectral lines contributed from macromolecules and lipids. The following are the decomposed metabolite spectra with their names on the left of them. The bottom trace shows the residue of the measured and the fitted spectra. In the following, extensive studies were carried out to evaluate the performances of the method.

- Intra-individual reproducibility

The signals were measured on rat #1 (Wistar, male, 600g) with the specific experimental parameters: TR = 6 s, TE = 20 ms, voxel = 4*4*4 mm^3, NA = 128, FWHM of unsuppressed water was 8.5 Hz. About 15 metabolites were involved in the spectral fitting, but only 12 metabolites were normally detected by the method. The others were not reliably detected because either their estimated amplitudes were close to zero or their frequencies and/or decay rates were oscillating between constraint values. 8 data sets acquired successively in the experiment were estimated and the estimated metabolite concentrations were shown in Table 3.7.12.

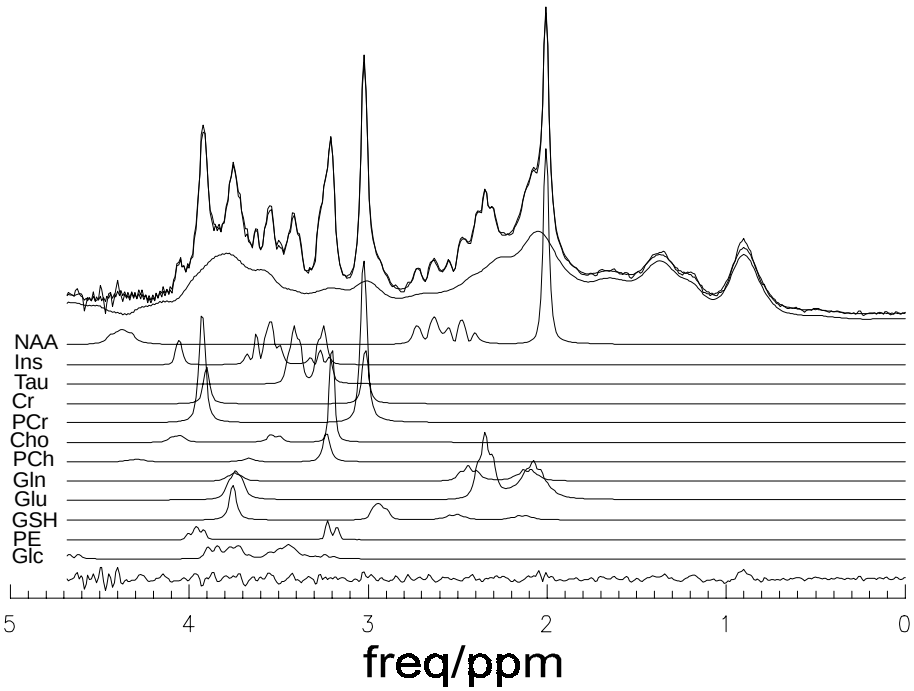

Fig.3.7-11 Spectral fitting of *in vivo* ^{1}H MRS measured on rat brain without WS. Water signal was removed by MPM in the post-processing. The main experimental parameters are: TE = 20 ms, TR = 6 s, voxel size = 4*4*4 mm^3. Spectral fitting was performed in time domain with 512 complex data points. From top to bottom are: the measured and fitted spectra overlaid, the estimated baseline, the estimated metabolite spectra reconstructed from the fitted parameters and the residue of subtracting the fitted spectrum from the measured spectrum.

Tab. 3.7.12 Metabolite concentrations (in mM) of rat #1.

Dataset	1	2	3	4	5	6	7	8
NAA	9.72	9.26	9.34	9.38	9.16	9.24	9.29	9.29
Ins	3.33	3.29	3.92	3.88	3.29	4.11	3.52	2.74
Tau	5.73	6.16	4.95	6.05	6.69	5.24	4.83	5.24
Cr	5.36	5.76	5.34	4.29	4.99	5.38	4.57	5.38
PCr	6.19	5.98	6.05	7.09	6.38	5.93	6.29	5.93
Cho	0.44	2.06	0.51	0.36	0.59	0.34	0.39	0.34
PCh	1.61	0.08	1.87	1.41	0.89	1.76	1.66	1.76
Gln	2.17	2.42	1.47	2.59	2.64	2.03	2.54	2.03
Glu	12.21	12.72	13.63	11.59	12.17	12.65	12.30	12.65
GSH	1.55	1.32	1.59	1.68	1.47	1.56	1.27	1.56
PE	0.67	0.84	1.28	1.09	1.56	1.24	1.22	1.25
Glc	1.50	1.92	0.76	1.25	1.72	1.38	1.66	1.83

To assess the accuracy and reproducibility of the method, the means and the standard deviations and the coefficients of the variation (CV) were calculated, and are shown in Table 3.7.13.

The table shows that the most prominent metabolite NAA was estimated with a mean value that is very close to the values given in the literature [Pfeu99] and with very small CV of 2%. Other metabolites with prominent spectral lines, such as Cr, PCr, Glu and GSH, were also estimated with concentrations that agree well with the literature values and with CVs within 10% of their estimated concentrations. Tau and Gln were estimated with CVs within 20%. For Ins, PE and Glc, the CV were within 27%.

It is noteworthy that the largest CVs occurred with the choline containing compounds, Cho and PCh, even though the two have prominent spectra. This is due to the fact that the choline containing compounds have similar spectral structure and their spectra are difficult to be resolved at 4.7 T. Despite this, the total concentration of the two agrees with the literature values and the CV of the two was within 20%. This indicates that individual values of the estimated concentrations of these compounds are not meaningful for this experimental condition and the total concentration of Cho and PCh are more reliable and therefore should be interpreted.

Although the CVs for Cr, PCr and Glu are within 10%, the spectral overlapping still caused problem. This is seen from the fact that the CVs of tCr and Glx are much smaller than their individual CVs , both being 2.3%.

Tab. 3.7.13 Estimated means and variations of the metabolite concentrations of Rat #1.

Metabolites	Concentrations (mM)		
	Mean	SD	CV%
NAA	9.36	0.19	2.0
Ins	3.35	0.62	27.5
Tau	5.77	0.70	12.1
Cr	5.18	0.54	10.4
PCr	6.14	0.47	7.6
Cho	0.74	0.61	82.4
PCh	1.13	0.47	65.4
Gln	2.32	0.41	17.7
Glu	12.38	0.63	5.1
GSH	1.49	0.11	7.4
PE	1.09	0.29	26.7
Glc	1.52	0.40	26.3
tCr	11.34	0.26	2.3
tCho	1.93	0.33	17.1
Glx	14.7	0.34	2.3

The CVs of the estimated concentrations of these metabolites with similar chemical and spectral structures increase with the linewidth of the spectra. Table 3.7.14 shows some results obtained from Rat #2. The sample is a female Wistar rat with 300g body weight. The FWHM of unsuppressed water is 10.5 Hz. Other experimental parameters were the same as for Rat #1.

As the linewidth is 2 Hz broader, the spectral overlapping is more severe in this case than that for Rat #1. Consequently, the CVs of all the three pairs of compounds, namely, Cr and PCr, Cho and PCh, Glu and Gln, increased dramatically as compared to those of Rat #1. The mean concentration of NAA is very close to that of Rat #1, and the CV increased by about 30%. The mean values of concentrations of tCr, tCho and Glx are also comparable to those of Rat #1 and the CVs of tCr increased by 100% and Glx by about 18%. This indicates the importance of excellent shimming for reliable concentration estimate of overlapping metabolites. However, the CV of tCho decreased by about 60%, even though their individual CVs are much larger than those with Rat #1.

Tab. 3.7.14 Estimated means and variations of the metabolite concentrations of Rat #2 (n = 8).

Metabolites	Concentrations(mM)		
	Mean	SD	CV(%)
NAA	9.15	0.24	2.6
Ins	3.53	0.30	8.4
Tau	4.97	0.93	18.9
Cr	1.41	0.64	45.4
PCr	9.96	1.11	11.1
Cho	1.02	0.51	50.0
PCh	0.54	0.53	98.1
Gln	2.68	0.60	22.4
Glu	10.44	0.75	7.18
tCr	11.38	0.52	4.6
tCho	1.57	0.12	7.6
Glx	13.12	0.84	6.4

- Comparison with results of signals with WS

Signals acquired with WS from the same experiment were submitted to the spectral estimation algorithm. The results are show in Table 3.7.15.

The concentrations of NAA, Tau, PCr, Cho Glu and GSH, and the concentrations of tCr, tCh and Glx were estimated accurately with CV less than 10%; Ins, Cr, Cln and Glc were estimated with CV within 20%. The CV for PCh was 50%, which is due to the spectral overlapping of PCh and Cho. Compared with the literature values and the values obtained from signals without WS, the individual values of Cr and PCr are not reliable because of the same reason as with Cho and PCh. The values of NAA, tCr, Glx, GSH, Glc and tCh are close to the values obtained from signals without WS. Despite this, student t-test results revealed that there are significant differences between most of the results for the two data sets, except for Glx, GSH and Glc. To find out the reason for the differences, the spectra acquired with WS and without WS were compared and it was found that there is significant differences between these original signals. The difference may stem

from the different experimental conditions with the two signals. The signals without WS were acquired without any spoiler gradients, while the signals with WS were acquired with spoiler gradients for the water suppression, activated after each CHESS water suppression pulses. The spoiler gradient pulses may have influences on the refocusing of the signals and the refocusing gradients should be trimmed to refocus the signals. Otherwise signal distortions may occur compared to the signals with well trimmed refocusing gradients. In the experiment, however, the refocusing gradients were the same for the two datasets, thus resulting in the spectral difference. Further experiments with specifically trimmed refocusing gradients need to be done to confirm this analysis.

Table 3.7.15. Metabolite concentrations estimated from datasets acquired with WS (rat #1). The preprocessing parameters and spectral estimation protocols are the same as those used with datasets acquired without WS.

Metabolites	***Concentrations***		
	Mean	***SD***	***CV (%)***
NAA	10.07	0.27	2.7
Ins	2.87	0.39	13.6
Tau	7.32	0.23	3.1
Cr	0.47	0.07	14.9
PCr	13.82	0.54	3.9
Cho	2.16	0.13	6
PCh	0.1	0.05	50
Gln	2.41	0.28	11.6
Glu	13.17	0.29	2.2
GSH	1.88	0.12	6.4
PE	0.22	0.22	100
Glc	1.58	0.17	10.8
tCr	14.29	0.48	3.4
tCh	2.26	0.12	5.3
Glx	15.58	0.38	2.4

- The “abnormal” situation

In the previous sections, the method was tested with data measured on healthy rats, i.e. on rat brain with normal metabolite concentrations. A quantification method needs to be validated with the abnormal subjects. However, in practice, one does not know, at least not in advance, which metabolite is normal or abnormal. Therefore, it is difficult to test quantitatively the performance of

a quantification method in estimating abnormal metabolites. In this section, an alternative approach is introduced to simulate the "abnormal" signal from normal signal, instead of using true abnormal subjects, to evaluate the presented method. This approach is described as follows. The original signal from a healthy rat brain is first estimated by the method for the signals of the metabolites. A portion (say 50%) of the estimated signal of a metabolite is subtracted from the original signal to obtain the abnormal signal with one metabolite of reduced concentration. The thus obtained abnormal signal is then estimated again by the method for the signals of the abnormal metabolite and the normal metabolites, and the corresponding concentrations are used as an estimator of the method. Such an approach was applied to *in vivo* data with focus on the estimated concentrations of both the abnormal (Table 3.7.16.) and the normal metabolites (Table 3.7.17.). One half of the normal signal of a metabolite was subtracted to form the abnormal signal and accordingly the theoretical concentration of the abnormal metabolite is one half of the normal case.

Table 3.7.16. Ratios of estimated metabolite concentrations of "abnormal" to estimated metabolite concentrations of "normal" brain. The theoretical ratio is 0.5 for all metabolites.

NAA	Ins	Tau	Gln	Glu	GSH	PE	Glc	tCr	tCho
0.48	0.51	0.53	0.52	0.56	0.40	0.33	0.66	0.56	0.53

Table 3.7.16 shows that five metabolites, namely, NAA, Ins, Tau , tCho, Gln, were estimated in the abnormal cases within 6% of error; Glu and tCr were estimated within 12%; GSH was within 20%; Glc and PE were within 35%. The large errors for GSH, Glc and PE are due to the fact that their contributions to the spectrum are relatively low and their spectra are strongly overlapping with predominant spectral components. Usually, small errors with predominant spectral components will cause larger errors for the minor spectral components overlapping with them. Another reason for the large errors is that the normal values for low concentration metabolites themselves suffer from larger errors than those for high concentration metabolites.

The next question is whether the "abnormal" metabolites concentration affect the estimation of other "normal" metabolite concentrations and to what extend. In practice, one does not know, at least not in advance, which metabolite is normal or abnormal. However, the answer to the question here will serve to validate the ability of the method to detect and estimate metabolite in a large dynamic range and to serve as a check of the reproducibility of the method. To this end, the influences of abnormal metabolite concentration on the estimation of other normal metabolite concentration were investigated and the results are given in Table 3.7.16. In the table, the means and SDs were calculated from the estimates of normal metabolites with only one "abnormal"

metabolite concentration, which was reduced by 50%, in the signal. The relative differences Δd% were obtained by subtracting the values estimated from the original signal from the means described above, and then divided by the values with all metabolites being normal. A positive value means that the mean is larger than the value obtained from the original signal.

Table 3.7.17. Influence of "abnormal" metabolite concentration on the estimations of other "normal" metabolite concentrations. The means and SDs were from the normal metabolite concentrations (n = 11). The Δd is the difference between the mean of a metabolite given in the table and the value obtained with all the metabolites having "normal" metabolite concentrations.

Metabolites	Estimated Concentrations in mM			Δd%
	Mean	SD	SD%	
NAA	9.33	0.14	1.52	0.27
Ins	3.15	0.14	4.40	-3.66
Tau	6.11	0.24	4.00	1.83
Gln	2.55	0.24	9.49	-1.20
Glu	12.25	0.29	2.35	0.29
GSH	1.38	0.08	5.79	3.44
PE	0.91	0.13	14.0	-11.1
Glc	2.07	0.16	7.73	2.98
tCr	11.30	0.15	1.32	0.89
tCh	1.62	0.20	12.6	19.1
Glx	14.80	0.18	1.20	0.01

As indicated in the table, the SDs are very small and all SDs are almost in the same order of magnitude. The CV as indicated by SD% of the major metabolites, such as NAA, Ins, Tau, tCr and Glu or Glx are within 5%. Gln, GSH and Glc are within 10%. The concentrations of PE were estimated with a relatively large CV of 14% and a difference of –11% respect to the value of normal case. However, the absolute variations of the estimate are still small (0.13), which is comparable to some of the predominant metabolites like NAA, Ins, Tau and so on. This shows that the large relative error with PE are mainly due to its low concentration level and small spectral contribution.

The last three data in the table show that if the overlapping Cr and PCr, Cho and PCh, Glu and Gln are accounted as tCr, tCho and Glx, their concentration can be estimated with high accuracy in the abnormal cases. The larger error for tCho is partly due to the relative lower concentration compared to the other two metabolites.

In conclusion, an approach to simulate *in vivo* signal with an abnormal metabolite concentration was used to test the performance of the method. The results show that (i) for most of the

metabolites, the quantification method is able to detect the concentration changes with high accuracy, and for some metabolites with low concentration levels, like PE, the accuracy is lower. (ii) The existence of abnormal metabolite concentration may have strong influences on the estimation of other metabolites with severe spectral overlapping but has only small influence on the estimation of prominent normal metabolite concentration itself. With the present method, the differences of the normal and abnormal signals are known, and whether the method can detect these differences or not can be used as a test of the performance of the method.

3.7.7 Comparisons with other methods

In this subsection, the present method, SPECFIT (metabolite **S**ignal **P**rior knowledge and **E**xperimental approaches **C**ombined spectral **F**itting **I**n the **T**ime domain), is compared with other *in vivo* ^{1}H MRS quantification methods. The comparison is classified into two categories: methods for data measured without WS and methods for data measured with WS.

3.7.7.1 Comparison with methods for data measured without WS

To the best of the author's knowledge, three methods to quantify *in vivo* ^{1}H MRS have been reported up to data, namely, the MPM based method [Dong00b], the SVD based method [Clay01] and the CWT based method [Serr01a].

The MPM based method was the first one to quantify *in vivo* ^{1}H MRS acquired without WS. The successes of the method is due to the fact that (i) it used the advantage of MPM for the signal decomposition to extract water signal from the raw signal; (ii) it introduced the lineshape transform using extracted water signal as reference to improve the accuracy of spectral parameter estimation. Due to the intrinsic properties of the MPM [Lin97], the MPM based scheme is accurate (with near-zero biases, low variances very close to the CRLBs), robust (with automatic signal recognition and lower "breakdown" SNR threshold) and automatic (user-independent). However, there is no build-in baseline correction mechanism and no prior knowledge incorporation in the scheme, therefore this method is not suitable to quantify short TE *in vivo* ^{1}H MRS where baseline distortion and spectral overlapping are severe. Only three singlets of NAA at 2.01, Cr at 3.04, and Cho at 3.24 ppm were estimated based on spectra at TE > 40 ms with T_2 corrections.

The main scheme of the SVD based method [Clay01] was the same as the MPM based one [Dong00a] and *in vivo* application results were reported only on the same three singlets as in [Dong00b], however from spectra using a very long echo time of 288 ms.

As for the CWT based method [Serr01a], the similar results as in [Clay01] were reported.

Therefore, the SPECFIT outplays all the existing methods for *in vivo* ^{1}H MRS acquired without WS.

3.7.7.2 Comparison with quantification methods for data measured with WS

Several methods have been developed to quantify short TE *in vivo* ^{1}H MRS [Prov93] [Bart99] [Vanh97]. The most popular and well established *in vivo* ^{1}H MRS quantification method is the LCModel [Prov93] [Prov01]. In the past decade, this method has been used by many research groups and clinical institutions all over the world for a variety of applications. It has been also widely tested and reviewed. Therefore, it is of significance to compare the presented method with LCModel. Table 3.7.17 summarizes a comparison of LCModel and SPECFIT.

Tab.3.7.18 A comparison of LCModel and SPECFIT.

	LCModel	SPECFIT
Prior knowledge	Full model spectra from phantom measurements(1)	Full model signals from spectral simulations
Phase correction	Zero and first order phase corrections are incorporated in the spectral fitting algorithm	First order phase errors are eliminated experimentally; Zero order phase error is corrected in the time domain and/or incorporated in the spectral fitting algorithm
FM artifacts elimination	N.A. (not necessary for spectra with WS)	Eliminated experimentally by gradient cycling and phase cycling
Baseline correction	Cubic B-spline fitting with equally spaced knots, incorporated in the spectral fitting.	Wavelet transform baseline characterization, combined with parametric spectral fitting iteratively.
Lineshape correction/transform	Lineshape correction involved in the model function.	Lineshape correction in time domain as a preprocessing and lineshape transform (optional).
Working domain	Frequency domain	Time domain spectral parametric fitting/frequency time baseline characterization

Model function	Accounts for zero and first order phases, baseline , lineshape and spectral parameters of the metabolites	Only accounts for spectral parameters of the metabolites.
Spectral fitting algorithm	Non-linear least squares with Marquardt-Levenberg algorithm.	Non-linear least squares with Marquardt-Levenberg algorithm.
Computing time	About 3 m for 18 metabolites on a 500 MHz computer.	About 30 s for 12 metabolites on a 1200MHz computer.
No. of metabolites estimated in *in vivo* ^{1}H data	Up to 18 for spectra acquired at 9.4 T.	About 12 presently for spectra acquired at 4.7 T.
Applications	Short TE *in vivo* ^{1}H MRS acquired with WS(2).	a. Short TE *in vivo* ^{1}H MRS acquired with WS ; b. Short TE *in vivo* ^{1}H MRS acquired without WS; c. Can be used for *in vivo* ^{1}H MRS with non-equidistant acquisition.
Performances	a. Fast, robust, and automatic; b. Standardized (Commercial); c. Widely tested, most widely and successfully used.	a. Fast, robust, automatic; b. Needs to be standardized; c. To be further tested, evaluated and applied;

(1) In principle, simulated model spectra can also be used;

(2) If Combined with RF sequence optimization and water extraction techniques, as those developed in this thesis, it can also be used to quantify spectra acquired without WS.

4 Summary

4.1 Discussions

The presented method, SPECFIT (metabolite **S**ignal **P**rior knowledge and **E**xperimental approaches **C**ombined spectral **F**itting **I**n the **T**ime domain), is a spectral quantification method combining spectral prior knowledge and experimental approaches to quantify *in vivo* ^{1}H magnetic resonance (MR) spectra acquired at short echo time (TE) without water suppression (WS) or with WS. The experimental and software approaches developed and employed in the scheme can efficiently deal with the common problems encountered in the *in vivo* ^{1}H MR spectra acquired with WS and some special difficulties associated with the *in vivo* ^{1}H MR spectra acquired without WS.

- The frequency modulation (FM) artifacts caused by gradient pulses constitute a special difficulty for the quantification of short TE *in vivo* ^{1}H MR spectra without WS. The experimental approaches developed in the present work to eliminate the FM artifacts surpass the existing software methods and result in spectra comparable to the intrinsic artifact-free spectra acquired with WS.

- First order phase errors must be corrected to allow accurate spectral evaluation. The experimental approach of optimizing the timing of RF pulses can efficiently eliminate first order phase errors. Long term observations showed that the first order phase errors can be limited well within 0.5 degree in the spectral region of interest. This experimental approach facilitates the present algorithm incorporating the entire model signal of each metabolite in the time domain spectral fitting.

- The Matrix Pencil Method (MPM) based parametric spectral fitting scheme was developed the first time as an independent method to quantify *in vivo* ^{1}H MR spectra acquired without WS. Three metabolites with prominent MR spectral singlets, namely NAA, Cr, and Cho, were quantified from spectra acquired without WS and at TE > 40 ms, using T_2 corrections. The

advantage of this scheme is not only due to the intrinsic properties of the MPM and its advantages over the conventional singular value decomposition (SVD) method, but also due to the water signal extraction and the lineshape transformation techniques. Spectral fitting results with phantom data showed that this method is able to fit very complicated spectra with high accuracy. The failure of this method in fitting short TE *in vivo* ^{1}H MR spectra acquired without WS or with WS is mainly due to the lack of a baseline correction procedure and not incorporating prior knowledge. The performance of this method could be improved in quantifying short TE *in vivo* ^{1}H MR spectra if combined with a baseline correction method and by incorporating prior knowledge into the spectral fitting.

In the present stage of MPM based method, its advantage in signal separation and reconstruction is employed as an important step in SPECFIT to extract water signal from the water unsuppressed raw signal, which is further used for the lineshape correction/transformation. In this respect, the MPM based method is used as an artifact-free filter to separate the water signal and the metabolite signals, ensuring accurate spectral fitting in the subsequent procedures.

- Discrete wavelet transformation (DWT) as a multiresolution analytical method was used for an iterative non-parametric baseline characterization and parametric spectral fitting scheme to extract broad baseline of the spectrum. The analyses and Monte Carlo studies showed that this technique surpasses the conventional methods, such as the spline or the polynomial methods, and can efficiently estimate well structured baselines in the short TE *in vivo* ^{1}H MR spectra.

- Incorporating model spectra of metabolites obtained from phantom measurements has been proven by other authors to be very successful in resolving the overlapping spectral lines and in improving the accuracy of the spectral quantification. In the present work, the approach of obtaining model spectra by spectral simulation using accurate prior knowledge of chemical shifts and J-coupling constants has been shown to be an efficient and equivalent alternative to phantom measurements. Compared to the *in vitro* measurements, the spectral simulation approach is time and cost saving, convenient and flexible.

- The entire simulated signal of each individual metabolite, instead of selected individual resonance lines, was used for the first time in the present work as a model signal. The advantages of this approach are that (i) full prior knowledge of the spectra is used, thereby, all

- the spectral contributions of the metabolites are accounted for; (ii) the complexity of metabolite spectra is no longer a difficulty in spectral fitting, but is beneficial for resolving the overlapping spectra, as no spectra of metabolites with complex spectral structure are completely the same; and (iii) employing the signals, $B_m(t)$, of the whole spectra in the model function of parametric spectral fitting reduces the number of parameters, and thus speeds up the algorithm and improves the accuracy.

- Integrated with the aforementioned experimental and software approaches, the model function of the spectral fitting can completely represent the metabolite spectra with a minimum number of parameters. For m metabolites, only 3m parameters account for the frequencies, amplitudes and Lorentzian decay rates of the metabolite signals and additional one or two parameters account for the global Gaussian decay rate and the zero order phase. As first order phase errors are eliminated experimentally and the lineshape is corrected in the time domain pre-processing step, only baseline characterization and parametric spectral fitting are performed in an iterative way, thus allowing fast and accurate estimation of the spectrum.

The SPECFIT method was tested with Monte Carlo studies, phantom and *in vivo* experimental data under various conditions and with different procedures. The results of these tests showed that,

- Short TE *in vivo* ^{1}H MR spectra acquired without WS can be quantified and the disadvantages of WS can thus be avoided.
- The model spectral fitting of SPECFIT has near-zero biases and small variations close to the Cramer Rao lower bounds.
- SPECFIT can estimate about 12 metabolites from short TE (20 ms) *in vivo* ^{1}H MR spectra acquired without or with WS on a 4.7 T spectrometer.
- The estimated concentrations of the prominent metabolites agree very well with the literature values and have very small standard deviations.
- The SPECFIT fitting is very fast, robust and requires very limited user interference.
- The SPECFIT scheme is easy to implement and can be realized in any modern spectrometer and computer systems.

4.2 Outlook

Although initial and encouraging results have been achieved by the SPECFIT, there is still the need of the improvements, evaluations, extensions and applications of the method. Some topics are listed as follows.

- Further testing, improving and evaluating the performance of the method, e.g., further comparing the effects of the lineshape and lineshape transformation with phantom and *in vivo* signals.
- Updating the model signals with improved prior knowledge of the metabolites.
- Exploiting the unique features of the method, for instance, applying the method to signals obtained by non-equidistant acquisition or massively truncated signals.
- Investigating the possibility and the performance of wavelet transform based baseline characterization in the time domain. If possible, the SPECFIT could be applied exclusively in the time domain, thus avoiding any possible side-effects caused by changing between the domains.
- Extending and applying SPECFIT to quantify low field spectra.
- Standardizing the program and improving the user interface of the method.
- Extending the present method of experimental elimination of frequency modulation artifacts to *in vivo* ^{1}H magnetic resonance spectroscopic imaging (MRSI) acquired without WS with a 4-step phase cycling.
- Extending SPECFIT to MRSI.

References

[Abra60] A. Abragam, Principles of nuclear magnetism. Clarendon, Oxford, 1960.

[Albe94] M. S. Albert, G. D. Cates, B. Driehuys, W. Happer, B. Saam, C. S. Springer, A. Wishnia, Biological Magnetic Resonance Imaging Using Laser-Polarized 129 Xe. Nature, 370, 199-201, 1994.

[Alth02] M. Althaus, W. Dreher, Z. Dong, D. Leibfritz, Fast NAA mapping using the Matrix Pencil Method on spectroscopic RARE data sets. Accepted by ESMRMB 2002.

[Ande95] E. Anderson, T. Bai, C. Bischof, J. Demmel, J. J. Dongarra, J. J. Du Droz, A. Greenbaum, S. Hammarling, A. MeKenney, S. Ostrouchov, D. Sorensen, LAPACK Users‘ Guide (2nd Ed.) SIAM, Philadelphia, 1995.

[Aldr96] A. Aldroubi, M. Unser (eds), Wavelet in Medicine and Biology. CRC Press, Boca Raton, FL, 1996.

[Anto01] J.-P. Antoine, C. Chauvin, A. Coren, Wavelet and related time-frequency techniques in magnetic resonance spectroscopy. NMR Biomed. 14:265-270, 2001.

[Bark85a] H. Barkhuijsen, R. de Beer W. M. Bovee, J. H. Creyghton, D. van Ormondt, Application of linear prediction and singular value decomposition (LPSVD) to determine NMR frequencies and intensities from the FID. Magn. Reson. Med. 61: 465-481, 1985

[Bark85b] H. Barkhuysen, R. de Beer, W. M. M. J. Bovee, D. van Ormondt, Retrieval of frequencies, amplitudes, damping factors, and phases from time domain signals using a linear least-squares procedure. J. Magn. Reson. 61: 465-481, 1985.

[Bark87] H. Barkhuysen, R. de Beer, D. van Ormondt, Improved algorithm for non-iterative time-domain model fitting to exponentially damped magnetic resonance signals. J. Magn. Reson. 73: 553-557, 1987.

[Bark93] P. B. Barker, B. J. Soher, S. J. Blackband, J. C. Chatham, V. P. Mattews, R. N. Bryan, Quantification of proton NMR spectra of the human brain using tissue water as an internal concentration reference. NMR Biome. 6: 89–94, 1993.

[Bart99] R. Bartha, D. J. Drost, P. C. Williamson, Factors affecting the quantification of short echo in vivo 1H MR spectra: prior knowledge, peak elimination, and filtering. NMR Biomed. 12: 205-216, 1999.

[Beer92] R. de Beer, D. van Ormondt, WWF Pijnappel, Quantification of 1D and 2D magnetic resonance time domain signals. Pure and Applied Chem. 64:815-823, 1992.

[Berg99] J. C. van den Berg, Wavelet in physics, Cambridge Univ. Press, Cambridge, 1999.

[Bess89] J. A. O. Besson, S. G. Greentree, M. A. Foster, J. E. Rimmington, Regional variation in rat brain proton relaxation times and water content. Magn. Res. Imag. 7: 141-143, 1989.

[Bloc46] F. Bloch, Nuclear induction. Physical Review; 70:460-474, 1946.

[Boog94] A. van den Boogaart, M. Ala-Korpela, J. Jokisaari, J. R. Griffiths, Time and frequency domain analysis of NMR data compared: an application to 1D ^{1}H spectra of lipoproteins. Magn. Reson. Med. 31, 347-358, 1994.

[Bos82] A. van den Bos, Handbook of measurement science, Wiley, New York, 1982.

[Bott81] P. A. Bottomley, W. A. Edelstein, Power deposition in whole body NMR imaging. Med. Phys. 8: 510-512, 1981.

[Bott84] P. A. Bottomley, Selective volume method for performing localized NMR spectroscopy. U. S. patent 4480228, 1984.

[Call93] P. T. Callaghan, Principle of nuclear magnetic resonance microscopy. Oxford University Press, Oxford,1993.

[Camp79] I. D. Campbell, C. M. Dobson, The application of high resolution nuclear magnetic resonance to biological systems. Methods Biochem. Anal. 25: 1 – 135, 1979.

[Cane96] D. Canet, Nuclear Magnetic Resonance – Concepts and Methods. John Wiley & Sons, Chichester, 1996.

[Cava97] S. Cavassila, B. Fenet, A. van den Boogaart, C. Remy, A. Brigue, D. Graveron-Demilly, ER-Filter: A preprocessing technique for frequency-selective time domain analysis. J. Magn. Reson. Anal. 3: 79-86, 1997.

[Cava01] S. Cavassila, S. Deval, C. Huegen, D. van Ormond, D. Graveron-Demilly, Cramer-Rao bounds: an evaluation tool for quantification. NMR Biomed. 14: 278-283, 2001.

[Ceci01] K. M. Cecil, B. V. Jones, Magnetic resonance spectroscopy of the pediatric brain. Topics in MR Imaging, 12: 435–452, 2001.

[Chri93] P. Christiansen, O. Henriksen, M. Stubgaard, P. Gideon, H. B. W. Larsson, *In vivo* quantification of brain metabolites by ^{1}H MRS using water as an internal standard. Magn. Reson. Imaging 11:107-118, 1993.

[Chri94] P. Christiansen, P.B. Toft, P. Gideon, E. R. Danielsen, P. Ring, O. Henriksen, MR-visible water content in human brain: a proton MRS study. Magn. Reson. Imaging, 12: 1237 – 1244, 1994.

[Clay99] D. B. Clayton, M. E. Elliott, R. E. Lenkinski, *In vivo* proton MRS of the human brain at 4T without solvent suppression. In: Proc. of the 6th Annual Meeting of ISMRM, Sydney, p1602, 1999.

[Clay01] D. B. Clayton, M. A. Elliott, J. S. Leigh, R. E. Lenkinski, Characterization of Gradient-induced signal modulations: implication for proton MR spectroscopic method. Proc. ISMRM. p1686, 2001.

[Corb95] R. J. T. Corbett, A. R. Öaptook, G. Tollefsbol, B. Kim, Validation of a non-invasive method to measure brain temperature *in vivo* using ^{1}H NMR spectroscopy. J. Neurochem., 64: 1224–1230, 1995.

[Cram46] H. Cramer, Mathematical methods of statistics, University Press, Princeton, NS, 1946.

[Daub88] I. Daubechies, Orthonormal Bases of Compactly Supported Wavelets. Comm. Pure Appl. Math. 41: 909-996, 1988.

[Daub92] I. Daubechies, Ten lectures on wavelets, CBMS-NSF Lecture Notes No. 61, SIAM, 1992.

[Dels86] M. A. Delsuc, J. Y. Lallemand, Improvement of dynamic range in NMR by oversampling. J. Magn: Reson. 69: 504-507, 1986.

[Dijk92] J. E. van Dijk, A. F. Mehlkopf, D. van Ormandt, W. M. J. Bovee, Determination of concentrations by time domain fitting of proton NMR echo signals using prior knowledge. Magn. Reson. Med. 27, 76-96, 1992.

[Clev79] W. S. Cleveland, Robust locally-weighted regression and smoothing scatter plots. J. Am. Stat. Assoc. 74: 829-836, 1979.

[Dodd86] D. Doddrell, G. Galloway, W. Brools, J. Field, J. Bulsing, M. Irving, H. Baddeley, Water signal elimination *in vivo*, using "suppression by mistimed echo and repetitive gradient episodes". J. Magn. Reson., 70: 176-180, 1986.

[Dong00a] Z. Dong, W. Dreher, D. Leibfritz, Quantification of proton MR spectroscopy without prior and post acquisition water suppression. Proc. 10th Intl. Soc. Magn. Reson. Med., Denver, p1954, 2000.

[Dong00b] Z. Dong, W. Dreher, D. Leibfritz, Quantification of metabolites by ^{1}H MRS in rat brain without water suppression: a preliminary study. MAGMA, 11: Suppl.1, 81, 2000.

[Dong02] Z. Dong, W. Dreher, D. Leibfritz, Experimental elimination of frequency modulation sidebands in localized ^{1}H MRS acquired without water suppression. Proc. 10th Intl. Soc. Magn. Reson. Med., Hawaii, 2198, 2002.

[Dono94] D.L. Donoho, I. M. Johnson, Ideal spatial adaptation by wavelet shrinkage, Biometrika, 81: 425-455, 1994.

[Dono95] D. Donoho, Denoising by soft-thresholding. IEEE Transaction on Information Theory. 613–627, 1995.

[Elli01] M., Elliott, D. Clayton, R. Lenkenski, ^{1}H spectroscopy without water suppression: removal of sideband modulation at short TE. Proc. 9th Intl. Soc. Magn. Reson. Med., Glasgow, p1688, 2001.

[Erns93] T. Ernst, R. Kreis, B. D. Ross, Absolute quantitation of water and metabolites in the human brain. I: Compartments and water. J. Magn. Reson. B 102, 1-8 1993.

[Erns87] R. R. Ernst, G. Bodenhausen, A. Wokaun, Principle of nuclear magnetic resonance in one and two dimensions, Clarendon Press, Oxford, 1987.

[Frah89] J. Frahm, H. Bruhn, M. L. Gyngell, K. D Merboldt, W. Haenicke, R. Sauter, Localized high resolution proton NMR spectroscopy in different regions of the human brain *in vivo*. Relaxation times and concentrations of cerebral metabolites. Magn. Reson. Med. 11: 47 – 63, 1989.

[Fuku81] E. Fukushima, S. B. W. Roeder, Experimental pulse NMR: A nuts and bolts approach. Addison-Wesley, Massachusetts, 1981.

[Gepp01] C. Geppert, W. Dreher, D. Leibfritz, PRESS sequence with very short echo times using asymmetric RF pulses. Application to the rat brain in vivo. Proc. 10th Intl. Soc. Magn. Reson. Med, Glasgow, 1022, 2001.

[Gesm88] H. Gesmar, J. J. Led, Spectral estimation of complex time domain NMR signal by linear prediction. J. Magn. Reson. 76: 183-192, 1988.

[Gide99] P. Gideon, S. Rosenbaum, B. Sperling, P. Petersen, MR-visible brain water content in human acute stroke. Magn. Reson. Imaging, 17: 301-304, 1999.

[Gill96] J. H. Gillard, P. B Barker, P. C. van Zijl, R. N. Bryan, S. M. Oppenheimer, Proton MR spectroscopy in acute middle cerebral artery stroke. AJNR Am J Neuroradiol. 17:873-86. 1996.

[Gold99] M. Goldman, Quantum description of high-resolution NMR in liquids. Oxford University Press, Oxford,1988.

[Gord80] R. E. Gorden, P. E. Hanley, D. Shaw, D. G. Gadian, G. K. Radda, P. Styles, P. J. Bore, L. Chan, Localization of metabolites in animals using 31P topical magnetic resonance. Nature, 287:736-738, 1980.

[Govi00] V. Govindaraju, K. Young, A. A. Maudsley, Proton NMR chemical shifts and coupling constants for brain metabolites. NMR Biomed 13:129-153, 2000.

[Graa90a] A. A. de Graaf, W. M. M. J. Bovee, Improved quantification of in vivo 1H NMR spectra by optimization of signal acquisition and processing and by incorporation of prior knowledge into the spectral fitting. Magn. Reson. Med. 15, 305-319, 1990.

[Graa90b] A. A. de Graaf, J. E. van Dijk, W. M. M. J. Bovee, QUALITY: Quantification improvement by converting lineshapes to the Lorentzian type. Magnetic Resonance in Medicine 13: 343-357, 1990.

[Graa97] M. van de Graaf, G. J. Jager, A. Heerschap, Removal of the outer lines of the citrate multiplets in proton magnetic resonance spectra of the prostatic gland by accurate timing of a point-resolved spectroscopy pulse sequence. MAGMA. 5: 65-69, 1997.

[Graa98] R. A. de Graaf, *In vivo* NMR spectroscopy: principles and techniques. John Wiley & Sons Ltd., 1998.

[Graa99] R. A. de Graaf, A. van Kranenburg, K. Nicolay, Off-resonance metabolite magnetization transfer measurements on rat brain in situ. Magn Reson Med. 41:1136-44, 1999.

[Graa01] R. A. de Graaf, D. L. Rothmans, *In vivo* detection and quantification of scalar coupled ^{1}H NMR resonances. Concepts in Magn. Reson. 13: 32–76, 2001.

[Grop95] A. Graps, An introduction to wavelets. IEEE Computational Sciences and Engineering, 2: 50-61, 1995.

[Grif80] J. R. Griffiths, A. N. Stevens, D. G. Gadian, R. A. Iles, R. Porteou, Hepatic fructose metabolite studied by 31 P nuclear magnetic resonance in the anaesthetized rat. Biochem Soc. Trans.8:641, 1980.

[Grue98] R. Gruetter, S, A. Weisdorf, V. Rajanayagan, M. Terpstra, H. Merkle, C. L. Truwit, M. Garwood, S. L. Nyberg, K. Ugurbil, Resolution improvements in *in vivo* ^{1}H NMR spectra with increased magnetic field strength. J. Magn. Reson. 135: 260–264, 1998.

[Gyng91] M. L. Gyngell, T. Michaelis, D. Hörstermann, H. Bruhn, W. Hänicke, K. D. Merboldt, J. Frahm, Cerebral Glucose is detectable by localized proton NMR spectroscopy in normal rat brain in vivo. Magn. Reson. Med. 19: 489–495, 1991.

[Haas85] A. Haase, J. Frahm, W. Hanicke, D. Mattaei, 1H NMR chemical shift selective (CHESS) imaging, Phys. Med. Biol. 30: 341-344, 1985.

[Haje00] M. Hajek, M. Burian, M. Dezortova, Application of LCModel for quality control and quantitative *in vivo* ^{1}H MR spectroscopy by short echo time STEAM sequence. MAGMA 10 6-17 2000.

[Henn92] J. Hennig, The application of phase rotation for localized *in vivo* proton spectroscopy with short echo times. J. Magn. Reson. 96, 40-49, 1992.

[Helm00] G.Helms, A precise and user-independent quantification technique for regional comparison of single volume proton MR spectroscopy of the human brain, NMR Biome, 13: 398-406, 2000.

[Henn99] F. Hennel F. Girard, T. Loenneker, Silent MRI with soft gradient pulses. Magn Reson. Med. 42: 6-19 1999.

[Henr95] O. Henriksen, *In vivo* quantification of metabolite concentrations in the brain by means of proton MRS. NMR Biomed. 8: 139–148, 1995.

[Hilt02] Y. Hiltunen, J. Kaartinen, J. Pulkkinen, A. M. Hakkinen, N. Lundbom, R. A. Kauppinen, Quantification of human brain metabolites from *in vivo* ^{1}H NMR magnitude spectra using automated artificial neural network analysis. J. Magn. Reson. 154: 1-5, 2002.

[Hore85] P. Hore, NMR data processing using the maximum entropy method. J. Magn. Reson., 62: 561-567, 1985.

[Hua90] Y. Hua, T. K. Sarkar, Matrix pencil method for estimating parameters of exponentially damped/undamped sinusoids in noise. IEEE Trans. Acoust. Speech Signal Processing. 38: 814–824, 1990.

[Hurd98] R. E. Hurd, D. Gurr, N. Sailasuta, Proton spectroscopy without water suppression: The oversampled J-resolved experiment. Magn. Reson. Med. 40:343-347, 1998.

[Joli91] M. Joliot, B. M. Mazoyer, R. H. Huesman, *In vivo* NMR spectral parameter estimation: a comparison between time and frequency domain methods. Magn. Reson. Med. 18: 358-370, 1991.

[Kama94] K. Kamada, K. Houkin, Y. Iwasaki, H. Abe, T. Kashiwaba, Localized proton spectroscopy of focal brain pathology in humans: significant effects of edema on spin-spin relaxation time. Magn. Reson. Med. 31:537-40. 1994.

[Klos90] U. Klose, *In vivo* proton spectroscopy in presence of eddy currents. Magn. Reson. Med. 14: 26 – 30, 1990.

[Knij92] A. Knijn, R. de Beer, D. van Ormondt. Frequency-selective quantification in the time domain. J. Magn. Reson. 97: 444–450, 1992.

[Kölb92] W. Kölbel, H. Schäfer, Improvement and automation of the LPSVD algorithm by continuous regularization of the singular values. J. Magn. Reson. 100: 598 – 603, 1992.

[Krei93] R. Kreis, T. Ernst, B. D. Ross, Absolute quantitation of water and metabolites in the human brain. II. metabolite concentrations. J. Magn. Reson. B 102, 9-19 1993.

[Krei97] R. Kreis, Quantitative localized ^{1}H MR spectroscopy for clinical use. J. Prog. in Nucl. Magn. Reson. Spectr. 31: 155 – 195, 1997.

[Kung83] S. Y. Kung, K. S. Arun, D. V. Bhaskar Rao, State-space and singular value decomposition-based

approximation methods for the harmonic retrieval problem. J. Opt. Soc. Am. 73: 1799 – 1811, 1983.

[Laut73] P. C. Lauterbur, Image formation by induced local interactions: Examples employing magnetic resonance. Nature, 242:190-191, 1973.

[Lenk01] R. E. Lenkinski, MR spectroscopy: clinical tool or research probe? Academic Radiology, 8: 567 – 570, 2001.

[Lent81] C. Lentner (Ed), Geigy Scientific Tables, Volume I. Units of measurement, Body fluids, Composition of the Body, Nutrition. Ciba-Geigy, Basel, 1981.

[Leun98] A. K. Leung, F. T. Chau, J. B. Gao, A review on application of wavelet transform techniques in chemical analysis: 1989 – 1997. Chemom. Intell. Lab. Syst. 43: 165 – 184, 1998.

[Lin97] Y-Y. Lin, P. Hodgkinson, M. Ernst, A. Pines, A novel detection-estimation scheme for noisy NMR signals: applications to delayed acquisition data. J. Magn. Reson. 128: 30 – 41, 1997.

[Lind80] J. C. Lindon, A. G. Ferringe, Digitalization and data processing in Fourier transform NMR. J. Prog. in Nucl. Magn. Reson. Spectr. 14:27-66, 1980.

[Lu97] Y. Lu, S. Joshi, J. M. Morris, Noise reduction for NMR FID signals via Gabor expansion. IEEE Trans. Biomed. Eng. 44: 512 – 528, 1997.

[Luri85] D. J. Lurie, A systematic design procedure for selective pulses in NMR imaging. Magn. Reson Imaging, 3: 235-243, 1985.

[MacK94] A. MacKaay, K. Whittall, J. Alder, D. Li, D. W. Patty, D. Graeb, *In vivo* visualization of myelin water in brain by magnetic resonance. Magn. Res. Med. 31: 673-677, 1994.

[Mans77] P. Mansfield, Multiplanar image formation using NMR spin echoes. J. Phys. C 10: L55-L58, 1977.

[Mans78] P. Mansfield, J. M. Pykett, cho-planar imaging. Biological and medical imaging by NMR. J. Magn. Reson. 29: 355-373, 1978.

[Mao88] J. Mao, T. H. Marcel, E. R. Andrew, Experimental study of optimal selective 180^{o} radio frequency pulses. J. Magn. Reson. 79: 1-10, 1988.

[Marq63] D. W. Marquardt, An algorithm for least squires estimation of nonlinear parameters, J. SIAM, 11: 431-441, 1963.

[Mars92] M. F. Marshman, I. M Brereton, R. E Rose, A. J O'Connor, D. M Doddrell, Application of self-refocusing band selective RF pulses for spectroscopic localization. Magn. Reson. Med. 25: 248-259, 1992.

[Maud95] A. A. Maudsley, Spectral lineshape determination by self-deconvolution. J. Magn. Reson. B 106: 47 – 57, 1995.

[Mesc96] M. Mescher, A. Tannus, M. O'Neil Johnson, M. Garwood, Solvent suppression using selective echo dephasing. J. Magn. Reson. A 123: 226-229, 1996.

[Mier98] S. Mierisova, A. van den Boogaart, I. Tkac, P. V. Hecke, L. Vanhamme, T. Liptaj, New approach for quantification of short echo time *in vivo* ^{1}H MR spectra of brain using AMARES. NMR Biomed. 11: 32 – 39, 1998.

[Mier01] S. Mierisova, M Ala-Korpela, MR spectroscopy: a review of frequency domain methods. NMR Biomed. 14:247-259, 2001.

[Moon90] C. Moonen, P. van Zijl, Highly effective water suppression for in vivo proton NMR spectroscopy. J. Magn. Reson. 88: 28 – 41, 1990.

[Nowa99] R. Nowak, Wavelet-based Rician noise removal from magnetic resonance imaging. IEEE Trans. Image Proc. 8:1408-1419, 1999.

[Ordi85] R. J. Ordidge, M.R. Bendall, R. E. Cordon, A. Connelly, in G. Govil, C. L. Khetrapal, A. Saran (Ed.)

Magnetic Resonance in Biology and Medicine, McGraw-Hill, New Delhi, pp. 387 – 397, 1985.

[Ordi86] R. J. Ordidge, A. Connelly, J. A. B. Lohman, Image-selected in vivo spectroscopy (ISIS). A new technique for spatially selective NMR spectroscopy, J Magn Reson 66: 283-294, 1986.

[Pfeu99] J. Pfeuffer, I. Tkac, S. W. Provencher, R. Gruetter, Toward an *in vivo* neurochemical profile: Quantification of 18 metabolites in short-echo-time ^{1}H NMR spectra of the rat brain. J. Magn. Reson. 141:104 – 120, 1999.

[Pijn92] W. W. F. Pijnappel, A. van den Boogaart, R. de Beer, D. van Ormondt, SVD-based quantification of magnetic resonance signals. J. Magn. Reson. 97, 122 – 134, 1992.

[Piot92] M. Piotto, V. Saudek, V. Sklenar, Gradient-tailored excitation for single-quantum NMR spectroscopy of aqueous solutions. J. Biomol. NMR 2: 661-665, 1992.

[Pres92] W. H Press, et al. Numerical recipes in C: The art of scientific computing. Cambridge University Press, 1992.

[Preu98] M. C. Preul, Z. Caramanos, R. Leblanc, J. G. Villemure, D. L. Arnold, Using pattern analysis of *in vivo* proton MRSI data to improve the diagnosis and surgical management of patients with brain tumor. NMR Biomed. 11: 192-200, 1998.

[Prie81] M. B. Priestley, Spectral Analysis and Time Series. Academic Press, London,1981.

[Prov93] S. W. Provencher, Estimation of metabolite concentration from localized *in vivo* proton NMR spectra. Magn. Reson. Med. 30: 672-679, 1993.

[Prov01] S. W. Provencher, Automatic quantitation of localized *in vivo* ^{1}H spectra with LCModel. NMR Biomed.14:260-4, 2001.
[Rao46] C. R. Rao, Minimum variance and the estimation of several parameters. Proc. Cambridge Phil. Soc. 43: 280-283, 1946.

[Riss87] J. Rissanen, Stochastic complexity. J. of Royal Statistical Society B 49:223-239, 1987.

[Röll01] S. Röll, Initial experience with an "Unspoiled" spin-echo sequence for short TE proton MR spectroscopy of the human brain. Proc. 9th Intl. Soc. Magn. Reson. Med. Glasgow, p.618, 2001.

[Roon96] W. D. Rooney, T. Ebisu, A. Mancuso, S. Graham, Metabolite ^{1}H relaxation in normal and hyponatremic brain. Magn. Reson. Med. 35: 688-696, 1996.

[Roth00] R. L. Rothman, Practical applications of spectral editing. In: ISMRM syllabus, 560, ISMRM, Berkeley, 2000.

[Sark02] T. K. Sarkar, M. Salazar-Palma, M. C. Wicks, Wavelet applications in engineering electromagnetics. Artech House. Norwood, MA. 2002.

[Serr97] H. Serrai, L Senhadji, J. D. de Certaines, J. L. Coatrieux, Time domain quantification of amplitude, chemical shift, apparent relaxation time T_2* and phase by wavelet transform analysis: application to biomedical magnetic resonance spectroscopy. J Magn Reson B 124: 20-34, 1997.

[Serr01a] H. Serrai, L. Senhadji, D. B. Clayton, C. Zuo, R. E. Lenkinski, Water modeled signal removal and data quantification in localized MR spectroscopy using a time-scale postacquisition method. J. Magnetic Reson. 149:45-51, 2001.

[Serr01b] H. Serrai, D. Clayton, L. Senhadji, C. Zuo, R. E. Lenkinski, Removal of gradient induced frequency modulation in localized proton spectroscopy. Proc. 10th Intl. Soc. Magn. Reson. Med. Glasgow, p1668, 2001.

[Slot98] J. Slotboom, C. Boesch, R. Kreis, Versatile frequency domain fitting using time domain models and prior knowledge. Magn. Reson. Med. 39: 899-911, 1998.

[Smit94] S. Smith, T. O. Levante, B. H. Meir, R. R. Ernst, Computer simulations in magnetic resonance. An object-oriented programming approach. J. Magn. Reson. A 106: 75 – 105, 1994.

[Smit02] I. C. P. Smith, L. C. Stewart, Magnetic resonance spectroscopy in medicine: clinical impact. Prog. in Nuclear Magn. Reson. Spectr. 40: 1 – 34, 2002.

[Sokó01] Maria Sokół, *In vivo* 1H MR spectra analysis by means of second derivative method. MAGMA 12, 177-183, 2001.

[Spie89] D. Spielman, P. Webb, A. Macovski, Water referencing for spectroscopic imaging. Magn. Reson. Med. 12: 38-49, 1989.

[Stan95] J. A. Stanly, D. J. Drost, P. C. Williamson, R. T. Thompson, The use of a prior knowledge to quantify short echo *in vivo* ^{1}H MR spectra. Magn. Reson. Med. 34, 17-24, 1995.

[Step88] D. S. Stephenson, Linear prediction and maximum entropy methods in NMR spectroscopy. Prog. in Nuclear Magn. Reson. Spectr. 20: 515-626, 1988.

[Stoy00] R. S. Stoyanova, T. R. Brown, Generalied application of principle component analysis for spectral analysis. Proc. 10th Intl. Soc. Magn. Reson. Med., Denver, p1953, 2000.

[Tang85] J. Tang, CP. Lin, M. K. Bowman, J. R. Norris, An alternative to Fourier Transform spectral analysis with improved resolution. J. Magn. Reson. 62: 167-171, 1985.

[Tasw99] C. Taswell, http//www.toolsmiths.com

[Torr97] C. Torrence, G. P. Compo, A practical guide to wavelet analysis. Bulletin of the American. Meteorological. Society. 79: 61-78, 1997.

[Vanh97] L. Vanhamme, A. van den Boogaart, S. Van Huffel, Improved method for accurate and efficient quantification of MRS data with use of prior knowledge. J. Magn. Reson. 129: 35-43, 1997.

[Vanh98] L. Vanhamme, R. Fierro, S. Van Huffel, R. de Beer, Fast removal of residual water in proton spectra. J. Magn. Reson. 132: 197-203, 1998.

[Vanh01] L. Vanhamme, T. Sundin, P. Van Hecke, S. Van Huffel, MR spectroscopy quantitation: a review of time-domain methods. NMR Biomed. 14: 233-246, 2001.

[Veen88] J. W. C. Van de Veen, R. de Beer, P. R. Luyten, D. van Ormondt, Accurate quantification of in vivo 31P NMR signals using the variable projection method and prior knowledge. Magn. Reson. Med. 6: 92-98, 1988.

[Veen99] J. W. C. van der Veen, D. R. Weinberger, J. A. Frank, and J. H. Duyn, Proton magnetic resonance spectroscopic imaging without water suppression. Proc 7th Intl. Soc. Magn. Reson. Med. Philadelphia, p.249 1999.

[Veen00] J. W. C. van der Veen, D. R. Weinberger, G. Tedeschi, J. A. Frank, J. H. Duyn, Proton MR spectroscopic Imaging without water suppression. Radiology, 217: 296 – 300, 2000.

[Widr96] B. Widrow, I. Kollar, M. Liu, Statistical theory of quantization. IEEE Trans. Instr. Meas. 45:353-361, 1996.

[Wu00] Y. Wu, B. A. Chronik, C. Bowen, C. K. Mechefske, B. K. Rutt, Gradient-induced acoustic and magnetic field fluctuations in a 4T whole-body MR imager. Magn. Reson. Med. 44:532-536, 2000.

.

[Zhu97] G. Zhu, D. Smith, Y. Hua, Post-acquisition solvent suppression by singular value decomposition. J. Magn. Reson. 124,: 286-289, 1997.

[Zhu98] G. Zhu, W. A. Choy, B. C. Sanctuary, Spectral parameter estimation by an iterative quadratic maximum likelihood method. J Magn Reson, 135: 37-43, 1998.

[Zijl97] P. C. M. Van Zijl, P. B. Barker, Magnetic resonance spectroscopy and spectroscopic imaging for the study of brain metabolism. In: Imaging brain structure and function. New York, 75 – 96, 1997

Appendix A

^{1}H Chemical shifts and J-coupling constants of major brain metabolites

Compounds	Groups	Chemical shift (ppm)	J-coupling (Hz)	Multiplicity
NAA	$^{1}CH_3$	2.0080		s
	^{2}CH	4.3817	2-3: 3.861	dd
	$^{3}CH_2$	2.6727	2-3‘:9.821	dd
		2.4863	3-3‘:-15.592	dd
	NH	7.8205	NH-2:6.400	d
GABA	$^{2}CH_2$	3.0128	2-3: 5.372, 2-3‘:7.127	m
	$^{3}CH_2$	1.8890	2‘-3:10.578, 2‘-3‘:6.982	qu
	$^{4}CH_2$	2.2840	3-4:7.755, 3-4‘:7.432	t
			3‘-4:6.173, 3‘-4:	
			7.933	
Cho	$N(CH_3)_3$	3.1850	1-2: 3.140, 1-2‘: 6.979	s
	$^{1}CH_2$	4.0540	1‘-2‘: 3.168, 1‘-2: 7.011	m
	$^{2}CH_2$	3.5010	1-N: 2.572, 1‘-N: 2.681	m
PCh	$N(CH_3)_3$	4.2805	1-2: 2.284, 1-2‘:7.231,	s
	$^{1}CH_2$	3.6410	1‘-2‘: 2.235, 1‘-2: 7.326	m
	$^{2}CH_2$	3.2080	1-N: 2.680, 1‘-N:2.772	m
			1-P: 6.298, 1‘-P: 6.249	
Cr	$N(CH_3)$	3.0270		s
	$^{2}CH_2$	3.9130		s
	NH	6.6490		s
PCr	$N(CH_3)$	3.0290		s
	$^{2}CH_2$	3.9300		s
	NH	6.5810		s
	NH	7.2960		
Glu	$^{2}CH_2$	3.7433	2-3: 7.331, 2-3‘: 4.651	dd
	$3CH_2$	2.0375	3-3‘: -14.849, 3-4‘: 8.406	m
	$^{4}CH_2$	2.1200	3‘-4‘: 6.875, 3-4: 6.413	m
		2.3378	3‘-4: 8.478, 4-4‘: -15.915	
		2.3520		
Gln	$^{2}CH_2$	3.7530	2-3:: 5.847, 2-3‘: 6.500	t
	$3CH_2$	2.1290	3-3‘: -14.504, 3-4: 9.165	m
		2.1090	3-4‘: 6.347, 3‘-4: 6.324	
	$^{4}CH_2$	2.4320	3‘-4‘: 9.209, 4-4‘: -15.371	m
		2.4540		
	NH_2	6.8160		s
		7.5290		s
Ins	^{1}CH	3.5217	1-2: 2.899, 1-6: 9.998	dd
	^{2}CH	4.0538	2-3: 3.006, 3-4: 9.997	t
	^{3}CH	3.5217	4-5: 9.485, 5-6: 9.482	dd
	^{4}CH	3.6144		t
	^{5}CH	3.2690		t
	^{6}CH	3.6144		t
Lac	2CH	4.0974	2-3: 6.933	q
	$^{3}CH_3$	1.3142		d
Tau	$^{1}CH_2$	3.4206	1-2: 6.742, 1‘-2: 6.403	t
	$^{2}CH_2$	3.2459	1-2‘:6.464, 1‘-2‘: 6.792	t
Asp	^{2}CH	3.1850	2-3: 3.647, 2-3‘: 9.107	dd
	$^{3}CH_2$	4.0540	3-3‘: -17.426	dd
		2.6533		dd
Ala	^{2}CH	3.7746	2-3: 7.234, 3-3‘: -14.366	q
	$^{3}CH_3$	1.4667	3-3‘‘: -14.366, 3‘-3‘‘: -14.366	d
PE	$^{1}CH_2$	3.9765	1-2: 3.182, 1‘-2: 7.204	m
	$^{2}CH_2$	3.2160	1-2‘: 6.716, 1‘-2‘: 2.980	m
			1-P: 7.288, 1‘-P: 7.088	
			1-N: 0.464, 1‘-N: 0.588	

Acknowledgement

As I finished this thesis, I feel a deep sense of indebtedness to those who kindly offered their invaluable help and support to my work in the past three years. It is my great pleasure to express my profound gratitude to all of them.

First of all, I am indebted to my supervisor, Prof. Dr. Dieter. Leibfritz, for taking me to his group, for his constant help, advice, support and encouragement in my research and in the writing of this thesis. I also owe him lots of gratitude for his kindness in helping my family joining me in Germany.

My special thanks go to Prof. Dr. Wolf-Dieter Stohrer for his readiness as the second referee, and to Prof. Dr. Franz-Peter Montforts for his readiness as a member of the examination committee.

I am especially grateful for Dr. Wolfgang Dreher for his guidance and instructions during my studies. His scientific insight and troubleshooting ability have been great beneficial for the development of the work in this thesis. His attitude toward high standards of science, his ideas of completeness, strictness and precision, and his “philosophy” about scientific experiments have deeply impressed me. His help to me and his influence on me are far beyond my academic life.

My former and present colleagues in the “Tomo” group, Dr. Kurt Bockhorst, Dr. Christian Meier, Dr. Dirk Mayer, Dr. Andreas Ebel, Dipl.-Phys. Volker Nebe, Dipl.-Phys. Christian Geppert and Dipl.-Phys. Matthias Althaus, and all the other colleagues in the AG Leibfritz have offered their precious help and support in many ways. I extend my sincere thanks to them all.

It is a long journey for me to travel from a small town in China to the free Hanseatic city of Bremen in Germany and from a coal mine worker to a Dr. rer. nat. The self-sacrificing love of my parents and my wife has been accompanying me wherever I am; and the whole family including my son and many friends have offered their support and encouragement during this long and hard journey. This dissertation is dedicated to them.